1990

Size Dependence Of Lateral Diffusion In Model Cell Membranes Using Fluorescently Labelled Probe Molecules

Bruce John Balcom

SIZE DEPENDENCE OF LATERAL DIFFUSION IN MODEL CELL MEMBRANES USING FLUORESCENTLY LABELLED PROBE MOLECULES

by

Bruce John Balcom

Department of Chemistry

Submitted in partial fulfillment
of the requirements for the degree of
Doctor of Philosophy

Faculty of Graduate Studies
The University of Western Ontario
Lon on, Ontario
July 1990

ISBN 0-315-59113-7

ABSTRACT

We have systematically investigated the probe size and shape dependence of lateral diffusion coefficients in model dimyristoylphosphatidylcholine membranes. This was achieved through synthesis of labelled probe molecules which differ systematically in both length and width. The diffusion measurements, both above and below the main phase transition, were performed using the technique of Fluorescence Photobleaching Recovery. The fluorescent label employed, NBD, was used to derivatize both alcohol and thiol bearing probe molecules.

Linear hydrophobic polymers, based on the isoprenoid alcohols citronellol, solanesol, and dolichol, spanned an order of magnitude in length and were used to explore hydrodynamic restrictions in the bilayer interior. Despite the order of magnitude difference in length we find these labelled molecules all diffuse at the rate of lipid self-diffusion ($5 \times 10^{-12} m^2 s^{-1}$) in the liquid crystal phase. Based on companion measurements in model systems and measurements below the phase transition, where the membrane interior is semi-crystalline, the results are interpreted to mean the NBD label itself determines the rate of diffusive motion. This occurs due to probe localization in the ordered hydrocarbon region of the host phospholipid near the glycerol backbone. Steady state fluorescence quenching experiments support, but do not confirm this contention. Thus lateral diffusion of these probes is likely controlled by free area fluctuations at the

bilayer/water interface and may be interpreted in terms of Free Area Theory.

The radial dependence of the probe molecule's diffusion coefficient, in the same phospholipid system, was explored using novel polymerizable surfactants based on triesters of *cis,cis*-1,3,5-cyclohexanetriol. Monomeric, dimeric, and tetrameric oriented polymers were synthesized, however, only monomers and dimers were amenable to NBD labelling. Labelled monomers and dimers diffuse once again at the rate of host lipid self-diffusion, in the liquid crystal phase. The projected area of the monomer in a bilayer is approximately that of the host lipid. Diffusion of the labelled dimer at rates comparable to that of the host lipid, suggests Free Area Theory's prediction of an inverse exponential dependence on radii is mistaken.

To Lesley

ACKNOWLEDGEMENTS

First and foremost I wish to thank Dr. Nils O. Petersen for supervising my work. He has allowed a fledgling scientist room to grow, yet his breadth of knowledge always ensured sound advice and guidance. My fellow graduate students Dave Bjarneson, Alison Paprica, Paul St. Pierre, and Paul Wiseman have been of immense aid and comfort. Their assistance was invaluable during the last few difficult months.

The nature of my work required a significant amount of organic syntheses. Vince Quiquero was unfailingly helpful in this regard. His suggestion lead directly to the NaSH reaction which proved crucial to our syntheses. I wish also to thank Harold Dick and Biswajit Choudhury for their help in performing the monolayer experiments.

The Canadian government, through NSERC, generously provided a graduate fellowship to support this work.

I am profoundly grateful to my wife Lesley for her continuing belief in the inherent worth of my studies. Her love and support help make the bad times less painful and the good times more memorable.

TABLE OF CONTENTS

Page

CHAPTER ONE

INTRODUCTION

Biological membranes are the milieu about which life swirls. These membranes, the enclosure defining a cell, provide a flexible and powerful host media for many, if not most, biochemical processes.

The lipids which make up such membranes vary to a remarkable degree.[1,2] They have in common a number of key structural features, the most important of which is that they are amphiphilic molecules. Amphiphiles possess a dual character. One portion of the molecule, the head group, is polar, or charged, and is hydrophilic. The other portion of the molecule, the tail group, is made up of long hydrocarbon chains and is hydrophobic.

In water-based media, amphiphilic molecules self-assemble into a variety of macromolecular assemblies.[3] The nature of these assemblies depends intimately on the amount of water and other solvents present, as well as the geometry of the amphiphilic molecule.[4-6] Phospholipids are common amphiphiles which have the molecular structure shown in Figure 1.1.

The driving force for the self-assembly of amphiphiles, or surfactants, appears to be the 'hydrophobic effect'.[7,8] The hydrophobic effect is an entropic effect. Exposure of a phospholipid's long hydrocarbon tails to water forces the water into a structural phase surrounding the hydrocarbon which is highly ordered. This structure is clearly unfavorable and can only be avoided by minimizing the surface area of contact between the water and hydrocarbon. Phospholipids, the most common membrane lipid, minimize

LIST OF FIGURES

LIST OF SYMBOLS

Symbol	Description
α	coefficient of thermal expansion
a	area per molecule
a^*	critical area for diffusion
a_v	Van der Walls area
a^o	free area per molecule
A^f	attenuation *or* area *or* dynamical variable
β	Taft's solvent parameter
B	Shorter's solvent parameter
C	concentration *or* correlation function
d	diameter *or* density
d'	dimensionality
D	diffusion coefficient
ε	extinction coefficient
Φ	quantum yield
f	relative fluorescence intensity *or* fraction
F	absolute fluorescence
γ	Euler's constant
g	signal losses
G	fluorescence anisotropy correction factor
h	height
I	intensity
I_a	rate of photon absorbance
J	diffusive flux
κ	isothermal compressibility
k	Boltzmann's constant *or* generic rate constant
K	bleaching parameter *or* equilibrium constant
λ	photobleaching rate constant
L	length
μ	solution viscosity
μ'	membrane viscosity
n	flux in the laboratory frame of reference
N	number
p	probability
P	power *or* probability
Q	emission coefficient
R	radius
r	radial distance *or* anisotropy
τ	lifetime
τ_d	characteristic time for recovery
t	time
t'	time
T_m	liquid crystal phase transition temperature
T	absolute temperature

Symbol	Description
v	velocity (vector)
v	velocity (scalar)
w	beam width
X	mole fraction
X_m	mobile fraction
z^m	distance along the z axis

LIST OF ABBREVIATIONS

Abbreviation	Description
A	Acid
$AA_{\bullet}$	Anhydride
AD	O-acylisourea
DCC	Dicyclohexylcarbodiimide
DMPC	Dimyristoylphosphatidylcholine
DMSO	Dimethyl Sulfoxide
FPR	Fluorescence Photobleaching Recovery
FRAP	Fluorescence Recovery After Photobleaching
GPC	Gel Permeation Chromatography
HPLC	High Performance Liquid Chromatography
IANBD	Iodo acetyl derivative of NBD
MS	Mass Spectroscopy
MS(CI)	Mass Spectroscopy (Chemical Ionization)
NA	N-acylurea
NBD	N-methyl-4-amino-7-nitrobenz-2-oxa-1,3-daizole
NBD-acid	Carboxylic acid derivative of NBD
NMR	Nuclear Magnetic Resonance
PC	Phosphatidylcholine
PE	Phosphatidylethanolamine
PMT	Photomultiplier Tube
PPG	Poly(propylene glycol)
RPTLC	Reverse Phase TLC
TEA	Triethyl amine
TLC	Thin Layer Chromatography
TRIS	[Tris(hydroxymethyl)aminomethane hydrochloride]
UV/VIS	Ultraviolet/visual

LIST OF APPENDICIES

CHAPTER ONE

INTRODUCTION

Biological membranes are the milieu about which life swirls. These membranes, the enclosure defining a cell, provide a flexible and powerful host media for many, if not most, biochemical processes.

The lipids which make up such membranes vary to a remarkable degree.[1,2] They have in common a number of key structural features, the most important of which is that they are amphiphilic molecules. Amphiphiles possess a dual character. One portion of the molecule, the head group, is polar, or charged, and is hydrophilic. The other portion of the molecule, the tail group, is made up of long hydrocarbon chains and is hydrophobic.

In water-based media, amphiphilic molecules self-assemble into a variety of macromolecular assemblies.[3] The nature of these assemblies depends intimately on the amount of water and other solvents present, as well as the geometry of the amphiphilic molecule.[4-6] Phospholipids are common amphiphiles which have the molecular structure shown in Figure 1.1.

The driving force for the self-assembly of amphiphiles, or surfactants, appears to be the 'hydrophobic effect'.[7,8] The hydrophobic effect is an entropic effect. Exposure of a phospholipid's long hydrocarbon tails to water forces the water into a structural phase surrounding the hydrocarbon which is highly ordered. This structure is clearly unfavorable and can only be avoided by minimizing the surface area of contact between the water and hydrocarbon. Phospholipids, the most common membrane lipid, minimize

Figure 1.1: Molecular structure of a phospholipid. The amphiphilic character of these molecules is determined by the long hydrocarbon chains and the charged phosphate and choline functions in the headgroup. Dimyristoylphosphatidylcholine, the lipid we commonly use, has n = 12.

In model membranes composed primarily of phospholipids, simple models exist which predict the size dependence of the lateral diffusion coefficient in two extremes of diffusant size.[16,32] The two extremes are: (1) diffusants which are much larger than the solvent lipids and (2) diffusants which are the same size as the host lipid solvent molecules.

The second regime, most appropriate for self diffusion of solvent lipids, is treated by what has become known as Free Area Theory.[16] This theory is a derivative of the analogous three-dimensional simple fluid theory known as Free Volume Theory.[33] Both are semi-empirical theories which proceed from statistical mechanical considerations of density fluctuations in the solvent. Voids which are opened by such density fluctuations are filled by the movement of neighboring molecules into the void. Since lipids in the Free Area Model are considered to be hard rods, and motion, by the nature of the membrane, is restricted to a plane, this is a two-dimensional problem. Free Area Theory predicts a strong dependence of the lateral diffusion coeffic ent on diffusant radii.

The first regime mentioned above is the most appropriate for diffusion of large proteins in model membranes composed of very much smaller phospholipids. The theory, introduced by Saffman and Delbruck,[32] treats the bilayer as a thin sheet of viscous fluid through which model cylinders diffuse. This approach treats the lipid sea as a continuum characterized by a certain viscosity. By contrast to the free area approach, it ignores the interaction and collision of individual solvent molecules. The Saffman-Delbruck Theory predicts a

this area by forming enclosed arrays of molecules. The bilayer membrane is the most important of these arrays for our purposes, and is the one which has been most intensely studied.

Phospholipids forming bilayers may be thought of as liquid crystals since they possess both a long range order and a short range disorder.[9] The long range order results from their orientation and localization in the bilayer. They possess a short range disorder because of the dynamic freedom individual phospholipids possess.

The 1972 Fluid Mosaic model of Singer and Nicolson[10] emphasized the dynamic nature of biological membranes. They proposed that a cell membrane (Figure 1.2) is a melange of oriented molecules comprising a variety of host lipids and proteins. The membrane is fluid because the hydrophobic portion of the host lipids have an appropriate mixture of saturated and unsaturated fatty acids which prevent solidification of the bilayer interior at physiological temperatures.[10] The fluid nature of this model means the constituent lipids are free to diffuse laterally in the plane of the membrane. They rotate about their long axis and indeed flip, albeit at a restricted rate, between the opposing leaflets of the bilayer. Embedded within these membranes to various extents are proteins which one might envision as icebergs floating in an ocean. These proteins are also free to rotate and diffuse in the membrane although, due to their larger size and cytoskeletal obstructions, they move at slower rates.

A dynamic picture of the bilayer membrane suggests there should exist a diffusive motion in the bilayer plane which will satisfy the time dependent diffusion equation (Equation 1.1).

Figure 1.2: Artist's rendering of a cell membrane in cross-section. This drawing illustrates the Fluid Mosaic model of Singer and Nicholson.[10] A large variety of oriented molecules make up the cell membrane. Reprinted with permission from *Biology: Principles, Patterns, and Processes* by Don Galbraith et. al. Copyright 1989 John Wiley and Sons Canada Ltd.

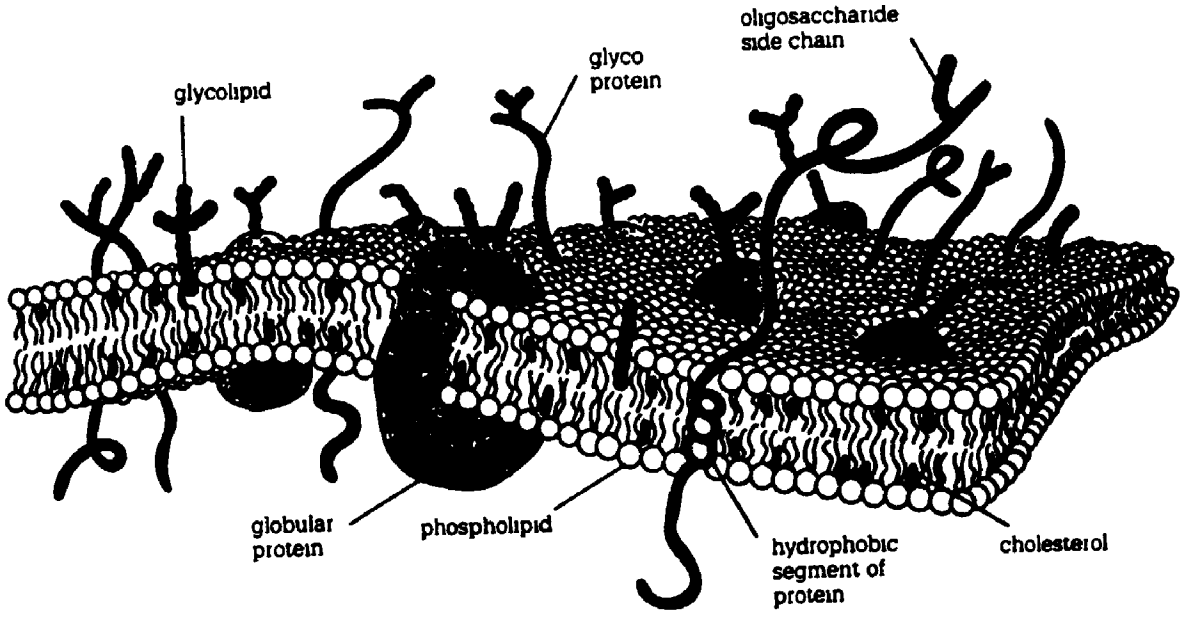
oligosaccharide
side chain
glyco
protein
glycolipid
globular
protein
phospholipid
hydrophobic
segment of
protein
cholesterol

$$\frac{\partial C(r,t)}{\partial t} = \left(\frac{D}{r}\right) \frac{\partial}{\partial r} \left(r \frac{\partial C(r,t)}{\partial r} \right) \qquad (1.1)$$

In Equation 1.1, D is the diffusion coefficient and C(r,t) is a spatially, r, and time, t, dependent concentration. Experimental evidence accumulated over the last twenty years suggests that lateral diffusion in the bilayer membrane does occur and is governed by the two-dimensional solution to the diffusion equation.[11-16] In the case of diffusion in two dimensions, the mean square displacement of a test particle with time is no longer 6Dt, as in three-dimensional motion, but is 4Dt as shown in Equation 1.2.

$$\langle r^2 \rangle = 4Dt \qquad (1.2)$$

The angled brackets of Equation 1.2 indicate an average. The variables r, D, and t have the same meaning as in Equation 1.1.

The ordered yet dynamic structure of the phospholipid bilayer has important implications for its function as a reaction environment. Membranes function, in part, to segregate substrates and the enzymes that act upon them into the same membrane-limited compartment. Apart from subdividing space, the bilayer membrane plays an important role in biochemical events as a reaction environment.[17,18] Diffusion within this environment takes on an added importance due to the reduction of dimensionality associated with the bilayer structure.

This reduction of dimensionality will enhance the rate of diffusion-controlled processes in the membrane.[19,20] Two reactants moving through the leaflets of a bilayer encounter one another far

more quickly than if they were moving through three-dimensional space. Many biochemical processes require lateral mobility of membrane proteins to trigger certain cellular responses and to form specialized structures at the cell surface. Receptor clustering,[21] ligand-receptor interactions,[22] and conventional chemical reactions[23] have the potential to be rate-limited by the two-dimensional dynamics of the cell surface.

Electron transfer reactions with their very low activation energy barriers are good candidates for diffusion controlled kinetics. Two important redox reactions in the cell membrane have been postulated to be diffusion controlled reactions.[24,25] Proof of these mechanisms is difficult without some understanding of the actual rates of diffusion of the molecules in question.

While there must clearly be some dependence of the rate of diffusion on molecular size, the nature of this dependence is uncertain. Aside from a long standing theoretical interest in the size dependence of the lateral diffusion coefficient, as noted above, there is an obvious interest from the point of view of biochemical kinetics. If one knew the two-dimensional diffusion coefficient of any of these molecules, one could more easily ascertain whether their reactions or interactions were diffusion controlled. The *a priori* prediction of lateral diffusion coefficients in cell membranes based on molecular size and orientation is almost impossible. The complications of lipid heterogeneity, large protein concentrations, phase segregation and cytoskeletal structure hamper the prediction of rates of lateral motion in cell membranes.[26,27] This is, however, a field of active endeavor.[28-31]

In model membranes composed primarily of phospholipids, simple models exist which predict the size dependence of the lateral diffusion coefficient in two extremes of diffusant size.[16,32] The two extremes are: (1) diffusants which are much larger than the solvent lipids and (2) diffusants which are the same size as the host lipid solvent molecules.

The second regime, most appropriate for self diffusion of solvent lipids, is treated by what has become known as Free Area Theory.[16] This theory is a derivative of the analogous three-dimensional simple fluid theory known as Free Volume Theory.[33] Both are semi-empirical theories which proceed from statistical mechanical considerations of density fluctuations in the solvent. Voids which are opened by such density fluctuations are filled by the movement of neighboring molecules into the void. Since lipids in the Free Area Model are considered to be hard rods, and motion, by the nature of the membrane, is restricted to a plane, this is a two-dimensional problem. Free Area Theory predicts a strong dependence of the lateral diffusion coeffic ent on diffusant radii.

The first regime mentioned above is the most appropriate for diffusion of large proteins in model membranes composed of very much smaller phospholipids. The theory, introduced by Saffman and Delbruck,[32] treats the bilayer as a thin sheet of viscous fluid through which model cylinders diffuse. This approach treats the lipid sea as a continuum characterized by a certain viscosity. By contrast to the free area approach, it ignores the interaction and collision of individual solvent molecules. The Saffman-Delbruck Theory predicts a

weak dependence of the lateral diffusion coefficient on diffusant radii.

The continuum model also has its roots in three-dimensional fluid theory. The Stokes-Einstein Equation for the three-dimensional diffusion coefficient of a sphere in a fluid is a continuum mechanics approach to a similar problem.

Recently a review article by Vaz et. al.[16] considered the body of evidence supporting the two theories and a possible reconciliation of the two. The conclusions of this review are threefold. (1) The individual theories provide an adequate description of the size dependence of the lateral diffusion coefficient in the two size extremes. (2) Neither theory works well in the other size regime. (3) The transition between the two size regimes is uncertain and there is a dearth of experimental work in the region where this transition should occur. Figure 1.3 illustrates the two size regimes and shows the area of theoretical uncertainty.

The area of uncertainty corresponds to the size of a large number of physiologically important molecules larger than phospholipids but smaller than proteins. Peptides and alkaloids, for example, could fall within this size range. The dependence of the diffusion coefficient on molecular radius has divergent predictions under these two theories in the transition region. The discontinuity in the theories, and the transition between continuum mechanics and molecular theories of diffusion, make this a particularly attractive region to explore.

The aim of this study has been to examine in more detail the size dependence of the lateral diffusion coefficient with a particular interest in trying to bridge the gap between the two theories.

Figure 1.3 Size dependence of lateral diffusion in model membranes. This figure illustrates the appropriate size regime for the Free Area and Continuum Theories. The diffusive behavior of particles with radii between 5 and 10 Å has an uncertain dependence on size. The shaded region corresponds to an estimated range of viscosities for the membrane. Diffusion measurements were performed at 36 °C in dimyristoylphosphatidylcholine bilayers. Reprinted by permission of the publisher from *FEBS Lett.* Vol. 174, No. 2, pp 199, 207.

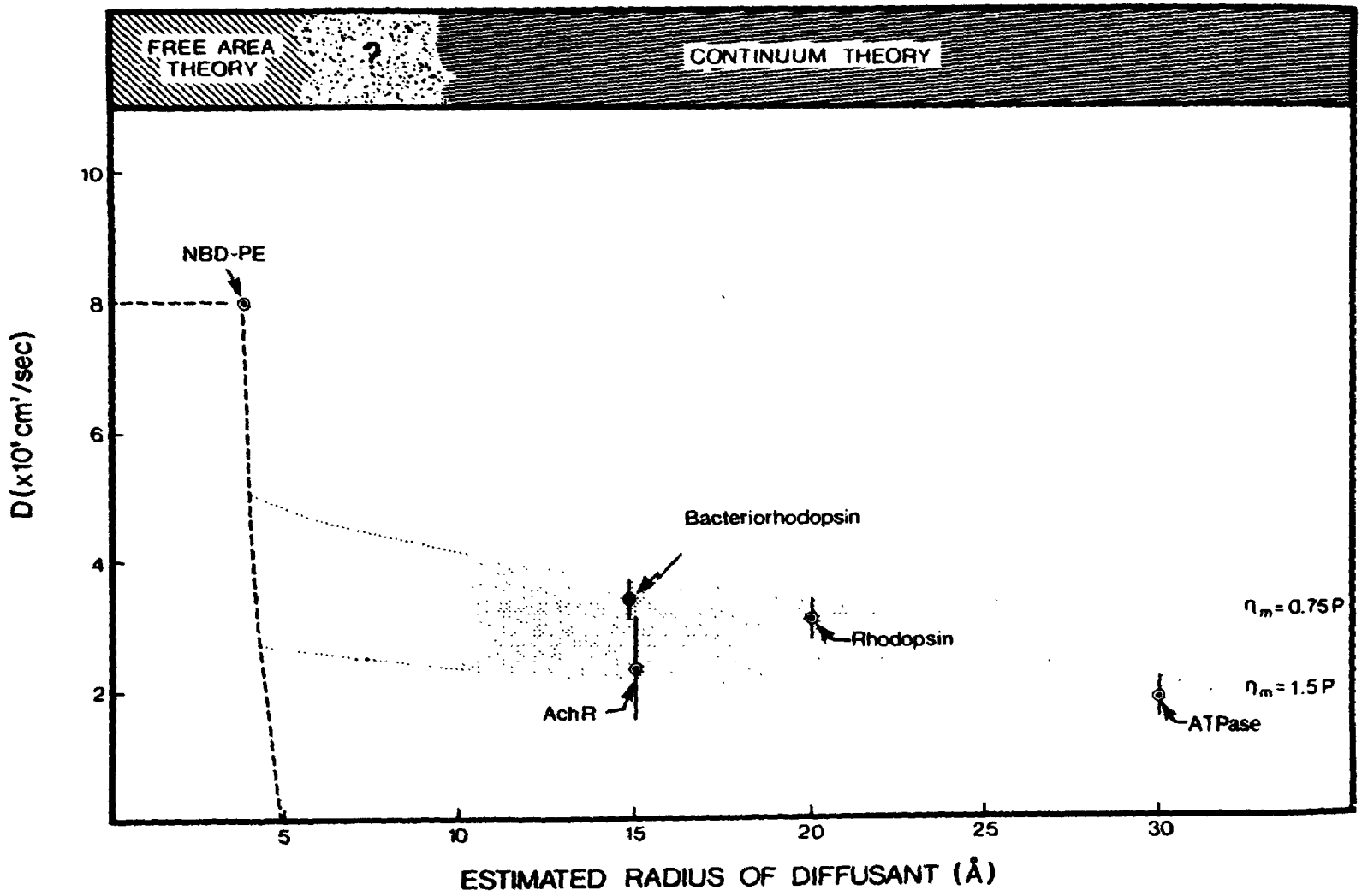
FREE AREA THEORY
?
CONTINUUM THEORY
D(x10⁷cm²/sec)
10
8
6
4
2
NBD-PE
Bacteriorhodopsin
Rhodopsin
AchR
ATPase
η_m = 0.75 P
η_m = 1.5 P
5
10
15
20
25
30
ESTIMATED RADIUS OF DIFFUSANT (Å)

The anisotropic geometry of the bilayer which results in a two-dimensional problem has potential to shed light on the analogous transition between theories of diffusive motion in three-dimensional fluids.

There is an added theoretical interest in a two-dimensional problem of this type. The diffusion coefficient has a precise mathematical definition in terms of the time integral of the velocity autocorrelation function (Equation 1.3).[34] This integral, however, may diverge in two dimensions.[35,36] The divergence of this integral has been used to argue that diffusive motion in two dimensions can not formally exist.[37]

$$D = \int_0^\infty \langle v(t)\, v(0) \rangle\, dt \qquad (1.3)$$

The brackets in Equation 1.3 indicate an ensemble average of the particle velocity, $v(t)$, as a function of time, t.

The seeming contradiction between the experimental observation of a constant D in the diffusion equation and its theoretical non-existence will be considered in the next chapter. Its immediate significance relates to the experimental method chosen to investigate the size dependence of the diffusion coefficient in two dimensions.

The simplest approach to the problem would be a two-dimensional molecular dynamics simulation[38] where one varied the radius of a test particle hard disk or rod in a sea of constant radii disks or rods. From the integral of the velocity autocorrelation function one could determine the size dependence of the diffusion coefficient in two

dimensions directly. Such an approach, however, is flawed by the non-analytic character of Equation 1.3.

Our approach, perforce, to the problem is experimental. The philosophy we have followed has been to assemble probe molecules that directly examine the physical phenomena in which we are interested. This approach has been followed with great success by, among others, Jean Marie Lehn[39] and Donald Cram[40] in examining macromolecular assemblies and complexation.

In our case we have synthesized a large number of fluorescently labelled probes which systematically differ in a chosen dimension so as to examine the size dependence of the lateral diffusion coefficient in model membrane systems. The fluorescence technique known as Fluorescence Photobleaching Recovery (FPR) was used to measure the tracer lateral diffusion coefficient of the labelled probe molecules sequestered in model phospholipid membranes.

FPR is often used as a qualitative or semi-quantitative measure of the overall mobility of a lipid or cell system under various stimuli or conditions. Fewer attempts have been made to use FPR in a truly quantitative manner.[26,41] Measuring the diffusion coefficient of trace amounts of a series of related probe molecules in a constant host system is more amenable to theoretical interpretation. Through this approach we hope to learn more about the fundamental process of diffusion in membranes. Systematic organic synthesis yielded an homologous series of probe molecules with defined structural differences (Figure 1.4) in two discrete dimensions.

The first series of probes resemble flexible cylinders with a constant cross-sectional area which differ in length, smallest to

Figure 1.4: Idealized series of probe molecules. Series A differs systematically in length. Series B differs systematically in radii. These variations are not to scale.

A

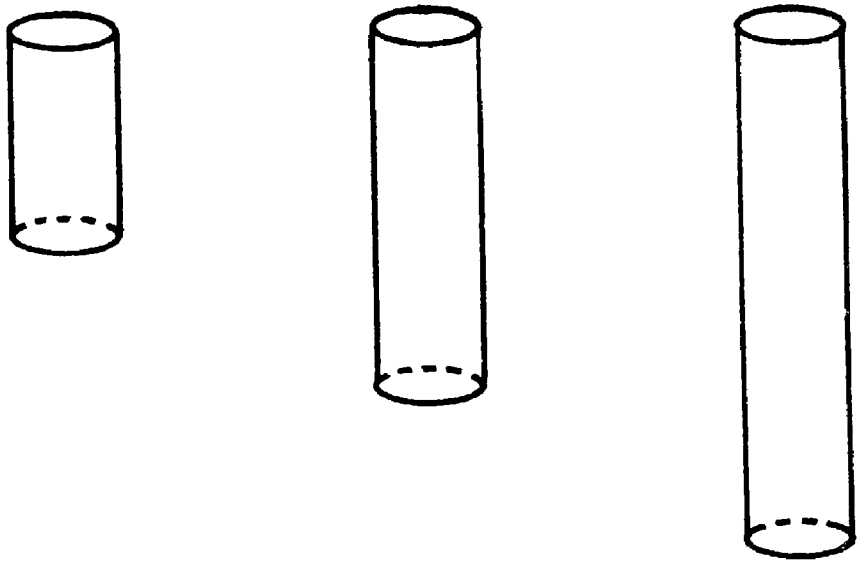

B

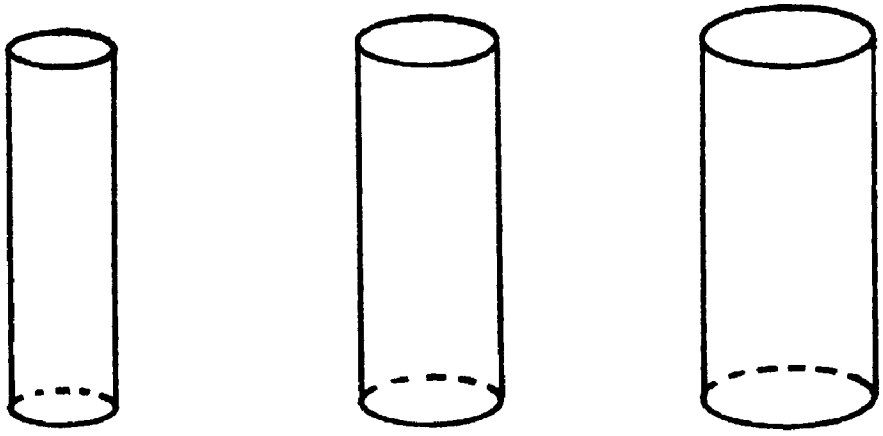

largest, by an order of magnitude. This series derives from naturally occurring isoprenoid alcohols. The smallest member of the series has approximately the same length as the host phospholipid used in our model membranes.

The second series of molecules we have synthesized possess a constant length but differ systematically in radii. This graded series results from the controlled polymerization of a novel thiol bearing surfactant based on *cis,cis*-1,3,5-cyclohexanetriol triesters.

Both series of compounds permit us to examine the size dependence of the lateral diffusion coefficient by systematically moving from the free area regime shown in Figure 1.3 towards the larger molecule regime governed by continuum mechanics and Saffmann-Delbruck Theory.

REFERENCES

(1) Houslay, M. D.; Stanley, K. K. *Dynamics of Biological Membranes*; Wiley: New York, 1982; pp 17, 24.

(2) Small, D. M. *The Physical Chemistry of Lipids*; Plenum: New York, 1986; pp 1, 20.

(3) Silver, B. R. *The Physical Chemistry of Membranes*; Solomon: New York, 1985; pp 57, 74.

(4) Israelachveli, J. N.; Mitchell, D. J.; Ninhaum, B. W. *Faraday Discuss. Chem. Soc.* **1976**, *72*, 1525.

(5) Small, D. M. *The Physical Chemistry of Lipids*; Plenum: New York, 1986; pp 43, 88.

(6) Small, D. M. *The Physical Chemistry of Lipids*; Plenum: New York, 1986; pp 89, 96.

(7) Tanford, C. *The Hydrophobic Effect*; Wiley: New York, 1973.

(8) Ben-Naim, A. *Hydrophobic Interactions*; Plenum: New York, 1980.

(9) Ringsdorf, H.; Schlarb, B.; Venzmer, J. *Angew. Chem. Int. Ed. Engl.* **1988**, *27*, 113.

(10) Singer, S. J.; Nicholson, G. L. *Science* **1972**, *175*, 720.

(11) Frye, C. D.; Edidin, M. *J. Cell Sci.* **1970**, *7*, 319.

(12) Poo, M. *Nature* **1982**, *295*, 332.

(13) Kornberg, R. D.; McConnell, H. M. *Proc. Natl. Acad. Sci.* **1971**, *68*, 2564.

(14) Vaz, W. L.; Derzko, Z. I.; Jacobson, K. A. *Cell Surface Rev.* **1982**, *8*, 83.

(15) Wade, C. G.; Kuo, A. L. *Biochemistry*, **1979**, *18*, 2300.

(16) Vaz, W. L.; Goodsaid-Zalduondo, F.; Jacobson, K. *FEBS Lett.* **1984**, *174*, 199.

(17) Harrison, R.; Lunt, G. G. *Biological Membranes, Their Structure and Function*; Halsted: New York, 1980.

(18) Weissmann, G.; Claiborne, R. *Cell Membranes: Biochemistry, Cell Biology, and Pathology*; H. P. Publishing: New York, 1975.

(19) Adam, G.; Delbruck, M. In *Structural Chemistry and Molecular Biology*; Rich, A.; Davidson, N., Eds.; Freeman: San Fransisco, 1968; pp 198, 215.

(20) Berg, H.; Purcell, E. M. *Biophys. J.* **1977**, *20*, 193.

(21) Schlessinger, J. *Trends Biochem. Sci.* **1980**, *5*, 210.

(22) Dower, S. K.; Titus, J. A.; Segal, D. M. In *Cell Surface Dynamics*; Perelson, A. S.; DeLisi, C.; Wiegel, F. W.; Eds., Marcel Dekker: New York, 1984; pp 277, 328.

(23) Keizer, J. *Acc. Chem. Res.* **1985**, *18*, 235.

(24) Strittmatter, P.; Rogers, M. J. *Proc. Natl. Acad. Sci.* **1975**, *72*, 2658.

(25) Gupte, S.; Wu, E. S.; Hoechli, L.; Hoechli, M.; Jacobson, K.; Sowers, A. E.; Hackenbrock, C. R. *Proc. Natl. Acad. Sci.* **1984**, *81*, 2606.

(26) Petersen, N. O. *Can. J. Biochem. Cell Biol.* **1984**, *62*, 1158.

(27) Elson, E. L. *Ann. Rev. Phys. Chem.* **1985**, *36*, 379.

(28) Saxton, M. J. *Biophys. J.* **1987**, *52*, 989.

(29) Abney, J. R.; Scaletter, B. A.; Owicki, J. C. *Biophys. J.* **1989**, *56*, 315.

(30) O'Leary, T. J. *Proc. Natl. Acad. Sci.* **1987**, *84*, 429.

(31) Minton, A. P. *Biophys. J.* **1989**, *55*, 805.

(32) Saffman, P. G.; Delbruck, M. *Proc. Natl. Acad. Sci.* **1975**, *72*, 3111.

(33) Cohen, M.H.; Turnbull, D. *J. Chem. Phys.* **1959**, *31*, 1164.

(34) McQuarrie, D. A. *Statistical Mechanics*; Harper and Row: New York, 1976; pp 512, 515.

(35) Alder, B. J.; Wainwright, T. E. *J. Phys. Soc. Japan Suppl.* **1968**, *26*, 267.

(36) Alder, B. J.; Wainwright, T. E. *Phys. Rev. A.* **1970**, *1*, 18.

(37) Berne, B. J.; Foster, D. *Ann. Rev. Phys. Chem.* **1971**, *22*, 563.

(38) Easteal, A. J.; Woolf, L. A. *Chem. Phys. Lett.* **1990**, *167*, 329.

(39) 3M University Lecture Series. Chemistry Department, The University of Western Ontario, 1986.

(40) 3M University Lecture Series. Chemistry Department, The University of Western Ontario, 1989.

(41) Tocanne, J. F.; Dupou-Cezanne, L.; Lopez, A.; Tournier, J. F. *FEBS Lett.* **1989**, *257*, 10.

CHAPTER TWO

THEORY OF DIFFUSION IN TWO DIMENSIONS

2.1 Velocity Autocorrelation Function

Time correlation functions are one of the most active and fruitful areas of research in nonequilibrium statistical mechanics. Green[1,2] and Kubo[3], in the 1950s, showed that the phenomenological coefficients describing many transport processes could be written as integrals over the appropriate time correlation functions.

A classical time correlation function, C(t), is defined as an ensemble average governed by Equation 2.1.

$$C(t) = \int \cdots \int dp\, dq\, A(p,q;0)\, A(p,q;t)\, f(p,q) \qquad (2.1)$$

In Equation 2.1, f(p,q) is the equilibrium phase space distribution function and dp, dq are the generalized momentum and position coordinates for the particles in the ensemble. A(p,q;t) could be any dynamical variable which is a function of position, momentum, and time. Force and velocity are frequently used. The complicated integral in Equation 2.1 is usually written in a shorthand notation using angular brackets which signify the ensemble average.

$$C(t) = \langle A(t)\, A(0) \rangle \qquad (2.2)$$

When the ensemble averaged variables are the same, C(t) is referred to as an autocorrelation function. If the physical system of

interest is Markovian, the ensemble average may be calculated as an average over time. The time average is shown in Equation 2.3.

$$\langle A(t)\, A(0)\rangle = \lim_{t' \to \infty} \frac{1}{t'} \int_0^{t'} A(t+\tau')\, A(\tau')\, d\tau' \qquad (2.3)$$

The diffusion coefficient, one of the phenomenological coefficients mentioned above, is the time integral of the velocity autocorrelation function.

$$D = \int_0^{\infty} \langle v(t)\, v(0)\rangle\, dt \qquad (2.4)$$

Molecular dynamics experiments on model systems of hard disks and hard spheres, performed by Alder and Wainwright,[4-6] showed that the velocity autocorrelation function decays asymptotically as $t^{-d'/2}$ where d' is the dimensionality of the system.

The unusual persistence of velocity implied by the long time tail of the autocorrelation function has been related to a vortex flow about the particle under study.[6] The effect of the vortex, at low densities, is to reduce the 'drag' on the particle resulting in a long lasting positive correlation in the velocity of the particle.

The long time tail causes the integral in Equation 2.4 to diverge in two dimensions. This has led to the conjecture that there are no hydrodynamics in two dimensions[7,8] and the notion of a two-dimensional diffusion coefficient is misleading.

Saxton[9] has argued against the invalidation of two-dimensional diffusion measurements based on molecular dynamics simulations. The vortex structure which causes the long time tail has an energy per particle in the vortex structure which is small compared to kT.[5] The

divergence of the velocity autocorrelation function has been demonstrated for model systems which have purely repulsive potential energy functions.[4-6,10,11] A real world system like our membranes, however, involves attractive potentials and internal degrees of freedom. A small amount of cohesive energy could destroy the vortex structure.

Of more significance, with respect to our work, is the fact that bilayer membranes are not two-dimensional structures Due to its anisotropic nature, the bilayer is frequently considered two-dimensional but it clearly is not. Not only is the bilayer itself three-dimensional, but lipids in the bilayer are coupled to the surrounding media by hydrogen bonding between the headgroups and water. True cells, seen in the light of the Singer Nicolson Fluid Mosaic model,[12] possess a great number of membrane constituents such as proteins and glycolipids which may project a great distance into the aqueous phase. The coupling between the bilayer and aqueous phase in fact is <u>required</u> for a continuum mechanics treatment of diffusion so as to avoid Stokes' Paradox.

2.2 Stokes' Paradox

In a three-dimensional system the application of a steady force per unit length perpendicular to an infinitely long cylinder gives rise to an infinitely large translational velocity. This is Stokes' Paradox.[13,14] It has its origin in the inability of the linearized Navier-Stokes Equation to simultaneously satisfy the boundary conditions for the flow at the particle surface and at infinity.

Stokes' Paradox also applies to the translational Brownian motion of particles in a two-dimensional sheet.[15] A cell, however, as pointed out above, is surrounded by a three-dimensional fluid medium which comprises the inside and outside of the cellular structure. Coupling of the two-dimensional motion of a membrane particle to the surrounding medium induces reaction forces on the membrane. These forces permit a solution to the Navier-Stokes Equation in the membrane which can satisfy all the boundary conditions simultaneously.[16]

2.3 Saffman-Delbruck Theory

Saffman and Delbruck[15] modelled the diffusion of proteins in membranes by coupling the external medium to the equation of motion for the fluid in the sheet. Their model treats the fluid as a continuum characterized by a viscosity, μ', through which a protein, regarded as a cylinder of diameter d and height h, diffuses with its axis perpendicular to the plane of the sheet under Brownian motion. The surrounding water, in the Saffman-Delbruck model, has a viscosity μ which must be much less than that of the thin fluid layer. Estimates of the viscosity of the membrane interior[17,18] suggest this is a reasonable approximation. Hughes et. al.[16] have examined the rigor of this assumption in detail. Figure 2.1 illustrates the hydrodynamic model of Saffman and Delbruck. The Saffman-Delbruck expression for the diffusion coefficient is given by Equation 2.5.

$$D = \frac{k\,T}{4\,\pi\,h\,\mu'}\left(\ln\frac{2\,\mu' h}{\mu\,d} - \gamma\right) \qquad (2.5)$$

Figure 2.1: Hydrodynamic model of Saffman and Delbruck. The protein is represented as a cylinder of height h and diameter d, diffusing in a thin sheet with viscosity μ'. The viscosity of the surrounding aqueous phase is μ.

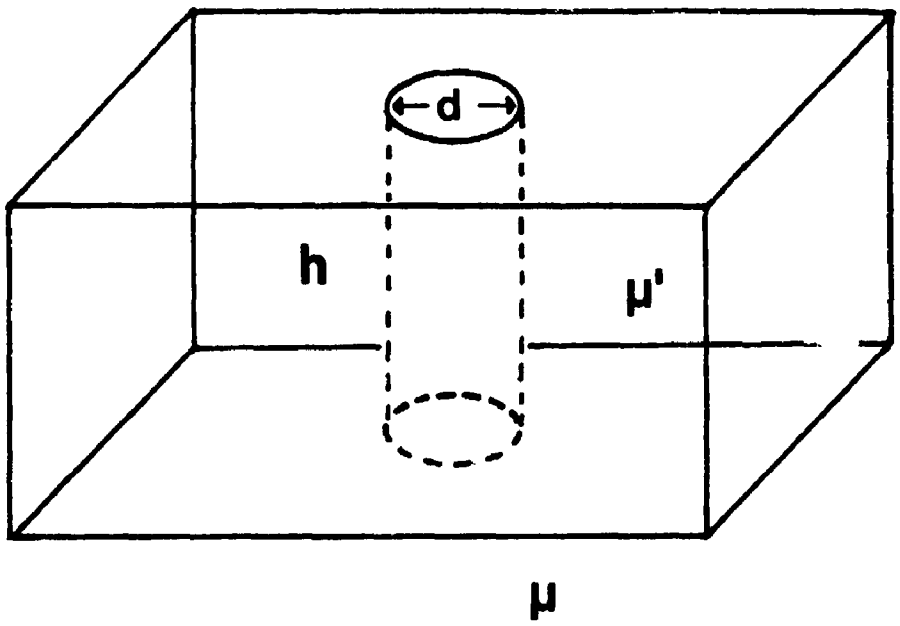
d
h
μ'
μ

Variables in Equation 2.5, not mentioned above, include Boltzmann's constant k, Euler's constant γ, and the absolute temperature T. Saffman and Delbruck have also developed a theoretical expression for the rotational diffusion coefficient using the same model.[15]

One should note that there is no dependence of the diffusion coefficient on particle mass in the Saffman-Delbruck Equation. This is a continuum mechanics approach to diffusion and so, in common with the Stokes-Einstein Equation, D is dominated by viscous forces not inertial forces. In terms of fluid dynamics one would say the fluid sheet has a low Reynold's number.[19]

Equation 2.5 has a functional form which is immediately amenable to experimental examination. In particular one should note the dependence of D on the cylinder radii is particularly weak. The weak dependence of D on particle radius has been examined in three publications from the early 1980's. Vaz et. al.[20] used FPR to measure tracer diffusion coefficients of three labelled integral membrane proteins in phospholipid membranes to show experimentally there was little change in D with size. The proteins rhodopsin, adenosinetriphosphatase, and acetylcholine receptor have molecular weights of 37 000 g/mol, 100 000 g/mol, and 250 000 g/mol respectively. Using radii provided by independent X-ray and neutron diffraction studies, the Saffman-Delbruck Equation gave absolute diffusion coefficients in good agreement with experimental values.

These studies were extended by Vaz et. al.[21] to monomers and covalently linked tetramers of the acetylcholine receptor protein. Fluorescently labelling these proteins permitted the measurement of D using FPR in bilayer membranes of soybean lipids. Once again there is

little difference in the observed lateral diffusion coefficient for the two species although their radii differ by approximately a factor of three. Based on Equation 2.5, one may calculate, for a membrane thickness of 10^{-9} m and a viscosity of 1 Poise, that changing the radii by a factor of three should result in a reduction of the diffusion coefficient by approximately twenty five percent. This calculation assumes a water viscosity of 0.01 Poise. While Vaz et. al[21] did not observe this great a reduction, twenty five percent also approaches the error associated with the FPR technique in membranes.

Peters and Cherry[22] evaluated the Saffman-Delbruck Equation by measuring the lateral and rotational diffusion in phosphatidylcholine membranes of a well characterized protein, bacteriorhodopsin. The ratio of the two diffusion coefficients yields, after a simple calculation, the hydrodynamic radii of bacteriorhodopsin. The value obtained is in reasonable agreement with the electron microscopy results of Henderson and Unwin.[23]

Peters and Cherry[22] also examined the dependence of the lateral diffusion coefficient for bacteriorhodopsin as a function of the water viscosity. Adding sucrose to the aqueous phase changed the viscosity from 0.76 to 9.54 centiPoise and resulted in an approximately two-fold decrease in the diffusion coefficient. This agrees very well with the prediction of Equation 2.5 and also suggests that the bulk viscosity of the aqueous phase is a faithful indication of the viscosity at the membrane surface.

There have been attempts to account for the lateral diffusion of the host lipid in a membrane using Saffman-Delbruck Theory.[20,22] Fundamentally this approach is wrong since the self diffusion of the

lipid cannot be considered a continuum mechanics - Brownian motion type problem since individual collisions and correlated motion of other lipids is important. In three dimensions, continuum theories are semi-quantitative when the diffusant is much larger than the solvent, but are poor when the diffusant size approaches that of the solvent.[24,25] Lipids diffuse faster than predicted by Equation 2.5 and their rates of motion are independent of the depth of penetration of the labelled lipid in the host membrane.[26] The independence of D on the depth of penetration is contrary to the Saffman-Delbruck model.

The Saffman-Delbruck Equation adequately describes the tracer diffusion of proteins in model lipid membranes above the phase transition. It does not work well in realistic cell systems[27,28] which have large and diverse protein concentrations, phase segregated regions, and cytoskeletal obstructions.

2.4 Free Area Theory

The self diffusion of lipids in a model membrane is best understood in terms of kinetic theories of diffusion. Free Volume Theory introduced in 1959 by Cohen and Turnbull[29] was a very successful early theory of diffusive motion in hard sphere systems. A two-dimensional analog was first applied to lateral diffusion in membrane systems by Galla, Hartmann, Theilen, and Sackmann[30] in 1979.

Phospholipids in the liquid crystal phase may be viewed as an array of closely packed rods. If one thinks of the two-dimensional projection of this system, one may treat it as a two-dimensional array of hard disks. An idealized array of hard disks, meant to represent

one surface of a bilayer membrane, is shown in Figure 2.2. Free Area Theory treats the diffusive motion within each leaflet of the bilayer membrane as distinct systems with little or no interaction.

The basic assumption of Free Area Theory is that each lipid in the bilayer array is confined to a cage formed by its immediate neighbors. The lipid will move within this cage until fluctuations in density open up a hole large enough to permit a substantial lateral displacement. Diffusion thus occurs as a result of the redistribution of free area in the lateral plane of the membrane.

Density fluctuations arise naturally from a consideration of equilibrium statistical mechanics. In a two-dimensional analog of the grand canonical ensemble, where area, temperature, and chemical potential are held constant, the standard deviation of the particle density is given by Equation 2.6.

$$\sigma_d = \bar{d} \left(\frac{k T \kappa}{A} \right) \tag{2.6}$$

In Equation 2.6, σ_d is the standard deviation of the density, $\bar{d}$ is the average density, k is Boltzmann's constant, T is the absolute temperature, κ is the isothermal compressibility in two dimensions, and A is the observation area.

The Free Area Theory[31,32] assumes that the large scale diffusion coefficient can be written as the convolution of a diffusion coefficient D(a) and the probability p(a) of a void of area a being formed.

$$D = \int_{a^*}^{\infty} D(a)\, p(a)\, da \tag{2.7}$$

Figure 2.2: Idealized array of hard disks. This array represents the the projected area of phospholipids comprising one side of a bilayer membrane. Free Area Theory considers diffusion in such a system to result from discrete jumps of individual molecules into voids opened by lateral density fluctuations.

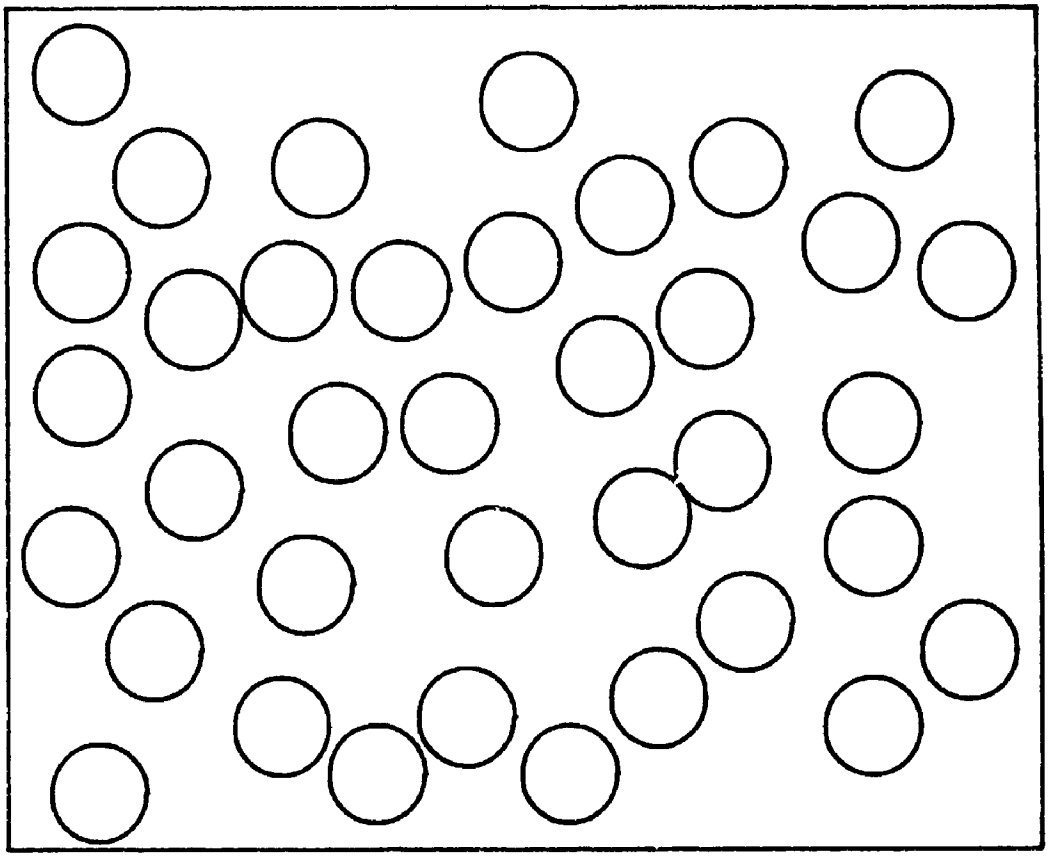

D(a) will be zero unless the free area is larger than a critical area, a^*, just large enough to permit another lipid to move in after the displacement.

The average distribution of free area, p(a), for a system of hard disks in which no energy change is associated with a redistribution of the free area may be derived, similarly to the Boltzmann distribution, using Lagrangian multipliers and information theory. The result is the probability as a function of a_f, the average free area, and ζ which is a numerical constant.

$$p(a) = \left(\zeta / a_f \right) \exp \left(-\zeta \, a / a_f \right) \tag{2.8}$$

The average free area, a_f, is the difference between the average area per molecule and the close packed area per molecule. Since D(a) varies little with a, it may be removed from the integral in Equation 2.7 and D is expressed according to Equation 2.9.

$$D = D(a^*) \, P(a^*) \tag{2.9}$$

$P(a^*)$ is the probability of finding a hole of area exceeding a^*.

$$P(a^*) = \int_{a^*}^{\infty} p(a) \, da \tag{2.10}$$

$$= \exp \left(- \zeta \, a^* / a_f \right)$$

Hence the final result is:

$$D = D(a^*) \exp\left(- \zeta a^* / a_f \right) \qquad (2.11)$$

$D(a^*)$ may be expressed in several different functional forms.[31]

The Free Area Theory predicts an extremely steep dependence on the critical area for diffusion a^*. The theory also predicts that molecules occupying less area than the solvent will diffuse at the same rate as the solvent since a diffusive step is only completed when a neighboring solvent molecule moves to occupy the void. The temperature dependence of D, as described by Equation 2.11, does not arise explicitly, however, both a_f and $D(a^*)$ must themselves be functions of temperature.

By analogy to Free Volume Theory, the average free area may be written in terms of the coefficient of thermal expansion α.[33]

$$a_f = a_0 \left[\beta + \alpha (T - T_m) \right] \qquad (2.12)$$

In Equation 2.12, a_0 is the van der Waals molecular area, α is the coefficient of thermal expansion in two dimensions, T_m is the temperature of the main phase transition for the host lipid, and $a_0\beta$ is the free area at the phase transition.

Equation 2.11 is not as amenable to experimental examination as the corresponding expression, Equation 2.6, derived using continuum mechanics. Nevertheless, Equation 2.11 has been the object of rather more scrutiny. Two groups have investigated directly the exponential dependence of D on the reciprocal free area. McCowan et. al.[34] were able to change the dilation of phospholipid multibilayers through

relative humidity changes. Changing the relative humidity altered the degree of hydration of the host phospholipids and thereby the intermolecular spacing. They were able to correlate the relative dilation of the membrane surface, through X-ray diffraction, with diffusion measurements of NBD labelled phosphatidylethanolamine lipids (NBD-PE) in the membrane. As predicted by Free Area Theory, a plot of their data as ln (D) versus $1/a_f$ is linear.

Peters and Beck,[35] in a particularly elegant experiment, measured the lateral diffusion of NBD-PE sequestered in monolayers of dilaurylphosphatidylcholine formed at the air-water interface of a Langmuir-Blodgett trough. They were able to directly measure and control the average free area per molecule by compression of the monolayer with a movable barrier. Their data plotted as ln (D) versus $1/a_f$ is also linear.

Nonnenmacher[36] has recently proposed a modification to the Free Area Theory. His renormalization group approach to the problem presumes that the fluctuations responsible for the creation of a hole within the context of the Free Area Theory do not operate on a single characteristic scale, but have many different length scales. Renormalization group theory is a mathematical strategy for dealing with problems of many different length scales. Nonnenmacher explained minor deviations from the ln (D) versus $1/a_f$ plot of Peters and Cherry using this approach. It should be emphasized the deviations were very small.

Surprisingly, the structure of the lipid analogs used to measure diffusion in phosphatidylcholine (PC) membranes, above the main phase transition, seem to have little effect on the measured diffusion

coefficient. Carbocyanine dyes with long alkyl chains from six to eighteen carbon atoms,[37] phospholipids labelled in one of the acyl chains,[37] phosphatidylethanolamine labelled in the head group,[37,38] cholesterol labelled at the end of the hydrocarbon tail,[38] and labelled phosphatidylethanolamine[37] with only one acyl chain all seem to move at the same rate. This rate, dependent on temperature, is approximately 5×10^{-12} $m^2 s^{-1}$.

The translational diffusion coefficient does not vary, in the liquid crystal phase, with the acyl chain length of the labelled lipid probe. While the differences in length for the NBD-PE used by Vaz et. al.[26,33] are not large (six carbons (1.13 nm) to eighteen carbons (1.53 nm)) if the viscosity of the membrane interior were at all important one might have expected some effect. This independence of diffusant depth is contrary to the expectations of continuum theory but supports the Free Area model where the headgroup limited area is the restricting feature.

Vaz et. al.[33] have also explored the effect on lipid diffusion of varying the host lipid. Such comparisons are complicated, however, by the varied phase transition temperatures of the lipid solvent. They showed that the longer the acyl chains of the lipid solvent, the faster the diffusion of NBD-PE at the same reduced temperature. The reduced temperature is $(T-T_m/T_m)$, where T_m is the main phase transition temperature. These results agree with Free Area Theory since experimentally it is known that the free area of the host lipids increase as their length increases, at the same reduced temperature.

Arrhenius plots of ln (D) versus 1/T of lipid probes in PC membranes are frequently non-linear.[33] Whether this non-linearity is

due solely to the form of a_f (Equation 2.12) or to a temperature dependence of the pre-exponential term $D(a^*)$ in Equation 2.11 is difficult to say *a priori*. $D(a^*)$, whatever its exact form, will have some temperature dependence. Apparent activation energies measured from plots of ln (D) versus 1/T generally range from four to eight kcal per mole.[39]

Despite the nearly universal acceptance of the Free Area model for lipid diffusion, there are several deficiencies. The intermolecular potential between particles is assumed to be a hard disk repulsion. There is, however, a significant attractive potential between phosphatidylcholine lipids in a bilayer. Modifications have been proposed to the Free Volume Theory to account for such attractive potentials in real fluids.[40] The Free Area Theory also has no dependence on particle mass. Molecular dynamics results on impurity diffusion in hard sphere fluids[41] show that light particles, smaller than the solvent, diffuse slowly since they lack the momentum to push their neighbors aside. Similar effects could be expected in two dimensions. Despite these limitations, as a model which reflects the gross physical characteristics of the system, the Free Area Theory has been remarkably successful.

There has been no attempt to test the model by measuring the diffusion coefficient of probe molecules which have alkyl chains <u>much</u> longer than the host lipid. Neither has there been any attempt to examine the effect of changing a^*, the critical area for diffusion, using probes systematically larger in the head group region than the host lipid. Equation 2.11 suggests the diffusion coefficient should be <u>very</u> sensitive to increasing a^*.

REFERENCES

(1) Green, H. S. *J. Chem. Phys.* **1952**, *20*, 1281.

(2) Green, H. S. *J. Chem. Phys.* **1954**, *22*, 1954.

(3) Kubo, R. *J. Phys. Soc. Japan* **1957**, *12*, 570.

(4) Alder, B. J.; Wainwright, T. E. *Phys. Rev. Lett.* **1967**, *18*, 988.

(5) Alder, B. J; Wainwright, T. E. *J. Phys. Soc. Japan Suppl.* **1968**, *26*, 267.

(6) Alder, B. J.; Wainwright, T. E. *Phys. Rev. A* **1970**, *1*, 18.

(7) Pomeau, Y.; Resibois, P. *Phys. Rep.* **1975**, *19*, 63.

(8) Berne, B. J.; Foster, D. *Ann. Rev. Phys. Chem.* **1971**, *22*, 563.

(9) Saxton, M. J. *Biophys. J.* **1982**, *39*, 165.

(10) Levesque, D.; Ashurst, W. T. *Phys. Rev. Lett.* **1974**, *33*, 277.

(11) Tresser, C.; Quentrec, B.; Brot, C. *J. Phys. (Paris)* **1977**, *38*, L267.

(12) Singer, S. J.; Nicholson, G. L. *Science* **1972**, *175*, 720.

(13) Lamb, H. *Hydrodynamics*; Cambridge: Cambridge, 1932; section 343.

(14) Landau, L. D.; Lifshitz, E. M.; *Fluid Mechanics*; Pergamon: New York, 1987; pp 61, 63.

(15) Saffman, P. G., Delbruc , M. *Proc. Natl. Acad. Sci.* **1975**, *72*, 3111.

(16) Hughes, B. D.; Pailthorpe, B. A.; White, L. R. *J. Fluid Mech.* **1981**, *110*, 349.

(17) Shinitzky, M.; Inbar, M. *Biochim. Biophys. Acta* **1976**, *433*, 133.

(18) Kinosita, K.; Kawato, S.; Ikegami, A.; Yoshida, S.; Orii, Y. *Biochim. Biophys. Acta* **1981**, *647*, 7.

(19) Tritton, D. J. *Physical Fluid Dynamics*; Oxford: New York, 1984; pp 97, 100.

(20) Vaz, W. L.; Criado, M.; Madeira, V. M.; Schoellmann, G.; Jovin, T. M. *Biochemistry* **1982**, *21*, 5608.

(21) Vaz, W. L.; Criado, M. *Biochim. Biophys. Acta* **1985**, *819*, 18.

(22) Peters, R.; Cherry, R. J. *Proc. Natl. Acad. Sci.* **1982**, *79*, 4317.

(23) Henderson, R.; Unwin, P. N. *Nature* **1975**, *257*, 28.

(24) Evans, D. F.; Tominaga, T.; Davis, H. T. *J. Chem. Phys.* **1981**, *74*, 1298.

(25) Chen, S. H.; Davis, H. T.; Evans, D. F. *J. Chem. Phys.* **1981**, *75*, 1422.

(26) Vaz, W. L.; Hallmann, D. *FEBS Lett.* **1983**, *152*, 287.

(27) Petersen, N. O. *Can. J. Biochem. Cell Biol.* **1984**, *62*, 1158.

(28) Peters, R. In *Structure and Properties of Cell Membranes*; Benga, G., Ed.; CRC Press: Boca Raton, FL, 1985; Vol.1, pp 35, 50.

(29) Cohen, M. H.; Turnbull, D. *J. Chem. Phys.* **1959**, *31*, 1164.

(30) Galla, H. J.; Hartmann, W.; Theilen, U.; Sackmann, E. *J. Membrane Biol.* **1979**, *48*, 215.

(31) Vaz, W. L.; Goodsaid-Zalduondo, F.; Jacobson, K. *FEBS Lett.* **1984**, *174*, 199.

(32) Shin, Y. K.; Moscicki, J. K.; Freed, J. H. *Biophys. J.* **1990**, *57*, 445.

(33) Vaz, W. L.; Clegg, R. M.; Hallmann, D. *Biochemistry* **1985**, *24*, 781.

(34) McCowan, J. T.; Evans, E.; Diehl, S.; Wiles, H. C. *Biochemistry* **1981**, *20*, 3134.

(35) Peters, R.; Beck, K. *Proc. Natl. Acad. Sci.* **1983**, *80*, 7183.

(36) Nonnenmacher, T. F. *Eur. Biophys. J.* **1989**, *16*, 375.

(37) Derzko, Z.; Jacobson, K. *Biochemistry* **1980**, *19*, 6050.

(38) Alecio, M. R.; Golan, D. E.; Veatch, W. R.; Rando, R. R. *Proc. Natl. Acad. Sci.* **1982**, *79*, 5172.

(39) Wade, C. G. In *Structure and Properties of Cell Membranes*; Benga, G., Ed.; CRC Press: Boca Raton, FL, 1985; Vol. 1, pp 51, 76.

(40) Ricci, F. P.; Rocca, D. In *Molecular Liquids - Dynamics and Interactions*; Barnes, A. J.; Orville-Thomas, W. J.; Yarwood, J., Eds.; Reidel: New York, 1984; pp 35, 58.

(41) Alder, B. J.; Alley, W. E.; Dymond, J. H. *J. Chem. Phys.* **1974**, *61*, 1415.

CHAPTER THREE

METHODS

3.1 Fluorescence Photobleaching Recovery - General Theory

Fluorescence Photobleaching Recovery (FPR) is a microscopy-based technique which has been applied with great success to mobility measurements of fluorescently labelled, or natively fluorescent, biological molecules in cells and model membranes.[1,2] While the technique is not limited to biological samples, its development occurred within the cell biology community and its applications have focused, for the most part, on questions relevant to this community.

Fluorescence is, from a number of respects, an ideal phenomena on which to base mobility measurements. The sensitivity of fluorescence is virtually unparalleled. Microscopic detection of <u>single</u> molecules using fluorescence is within the grasp of today's technology.[3] The organic chemistry of fluorescent labelling is well developed, and a large variety of fluorophores specific for a range of common and uncommon functional groups are commercially available.[4,5] Most fluorophores irreversibly photolyze under prolonged or intense irradiation. This photolysis, or photobleaching, renders the molecule non-fluorescent. It is usually an inconvenience to the experimentalist; however, it may be exploited to create macroscopic concentration gradients of bleached and unbleached fluorophores in a sample under study. The relaxation of these gradients is governed by the diffusion equation. The combinations of sensitivity (inherent to fluorescence) and specificity (through the labelling reaction) plus

the ease of photochemically imposing concentration gradients on the system, means that tracer diffusion coefficients of a large range of biological molecules may be measured using the FPR technique.

Poo and Cone[6], in 1974, first used these principles to make a measurement of the lateral diffusion coefficient of the fluorescent protein rhodopsin in the retinal disk membrane. Their work was closely followed by Liebman and Entine[7] on the same system and by Peters et. al.[8] who measured the lateral diffusion coefficient of labelled proteins in erythrocyte membranes. Since 1976, a large number of laboratories in the world, although only one in Canada, have acquired the capability of making such diffusion measurements. The methodology for making these measurements differs little from laboratory to laboratory and will be outlined below.

The technique, which is also known as FRAP (Fluorescence Recovery after Photobleaching), is conceptually very simple. A focused laser beam of low intensity, irradiates a surface or region of interest, frequently a cell, chosen by manipulating the sample mounted in the image plane of a fluorescence microscope. Within this irradiated region, molecules with an attached or native fluorophore will fluoresce. The intensity of the fluorescence, which is an indicator of concentration, is measured.

Photobleaching the same region of space with a brief, very intense pulse of light results in the irreversible photolysis of an intensity dependent fraction of the fluorophores. This photolysis macroscopically imposes a concentration gradient on the system which will relax according to Fick's Laws.

The recovery of the fluorescence signal after photobleaching

occurs as unbleached fluorophores diffuse into the observation region (Figure 3.1). This recovery is measured as a function of time using the original weak observation beam and may be characterized, knowing the geometry of the system, by a lateral diffusion coefficient extracted from the exponential recovery of the signal.

The various groups world-wide have diverged in the geometry employed to bleach and observe the fluorescence.[9-11] The discussion which follows is specific to the so-called spot photobleaching technique which is conceptually among the simplest variants and is the most commonly used. It is also the method used in this work.

3.2 Spot Photobleaching Technique[1,2]

The spot photobleaching method requires a cylindrically symmetric laser beam with a Gaussian radial intensity. The bleach and monitor beams are extracted from the source beam by a pair of beam splitters as shown in Figure 3.2. The result of the two beam splitters is two discrete, yet concentric, beams of vastly different intensity. The intensities usually differ by a factor of three to four orders of magnitude.

The fluorescence intensity, measured as a photocurrent f(t), as a function of time t depends on the concentration of fluorophore C(r,t) at position r. The position r is measured radially in the plane of focus from the optic axis.

$$f(t) = (g \varepsilon Q / A) \int_0^\infty I(r)\, C(r,t)\, d^2r \qquad (3.1)$$

Figure 3.1: FPR bleach/recovery sequence. Fluorophore (o) is irradiated by the monitor beam and an initial fluorescence level F(-) measured. At time zero the sample is exposed to the bleach beam and a portion of the fluorophore in the beam destroyed (●). The observed intensity at this point will be F(0). Lateral diffusion results in a time dependent increase in the observed fluorescence, F(t), as the concentration gradient decays. An infinite time later, or an approximation thereto, the fluorescence intensity F(∞) will have recovered to a maximum level. Frequently this recovery is complete.

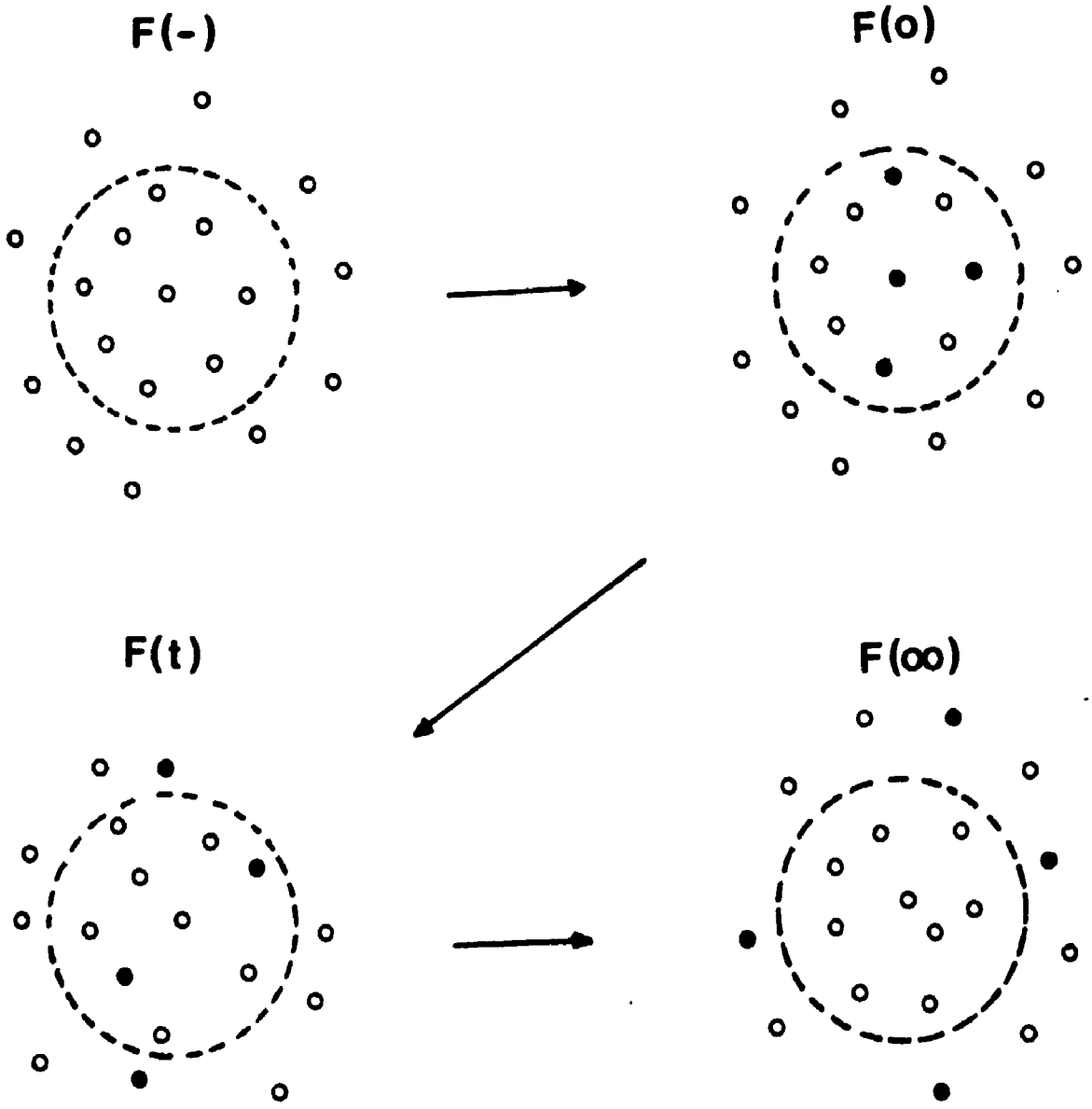
F(-)
F(o)
F(t)
F(oo)

Figure 3.2: Beam splitters. The beam splitters, B1 and B2, shown as inset a) yield a pair of concentric gaussian beams with intensities that differ by three or four orders of magnitude. The path of the stronger beam is indicated by the thick line. The dotted, thick line shows the path of the bleach beam when shutter S2 is open. Mirrors M1, M2, and M3 direct the beam, while shutter S1 limits the incident beam.

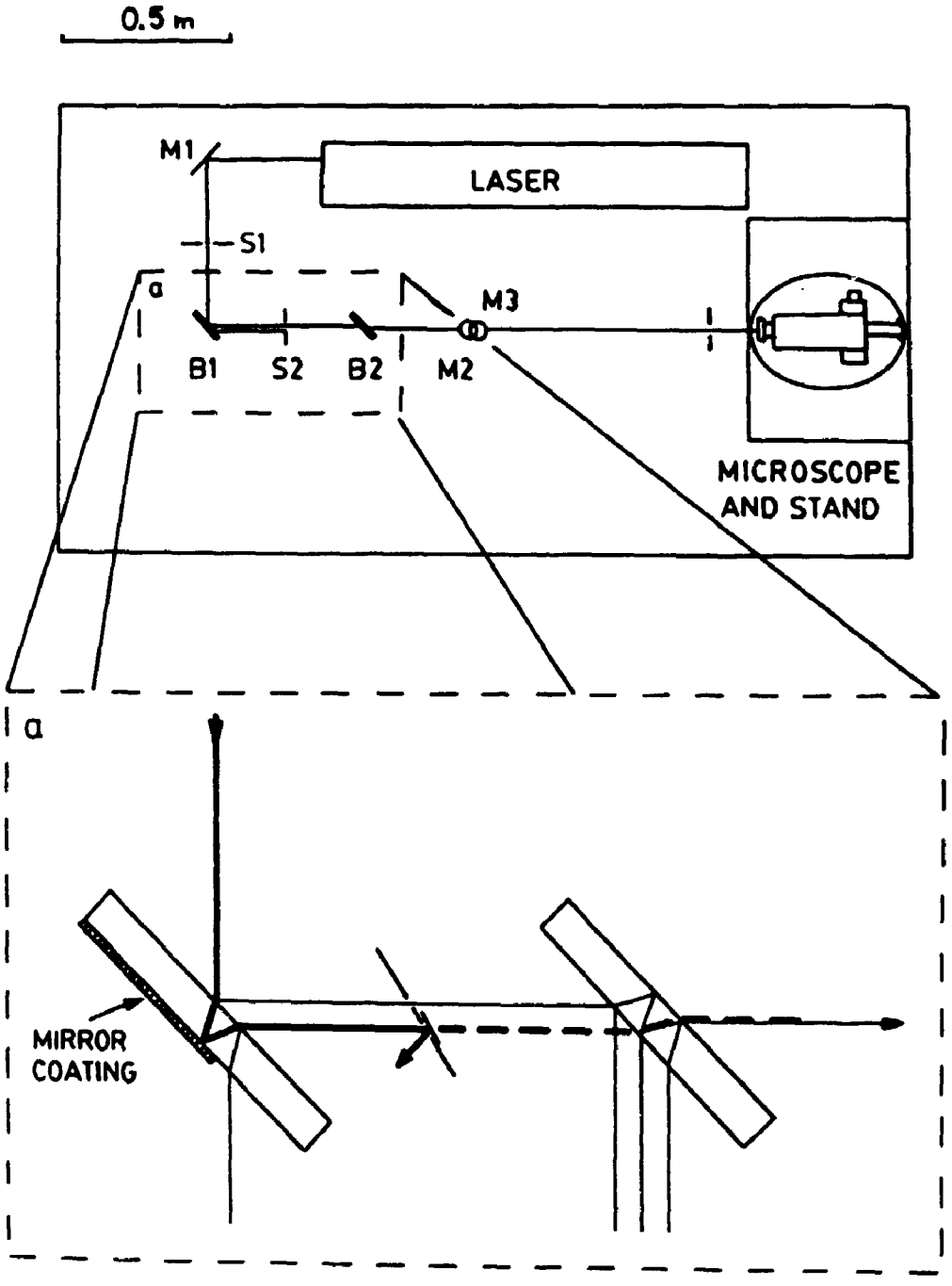
0.5 m
M1
LASER
S1
a
M3
B1
S2
B2
M2
MICROSCOPE
AND STAND
a
MIRROR
COATING

Equation 3.1 expresses this fluorescence intensity as a convolution of the concentration and incident laser intensity. The variables ε and Q respectively are the fluorescence excitation and emission coefficients of the fluorophore, and g accounts for the other signal losses. The integration limits may be extended to infinity without contradicting the experiment since the integrand decays quickly to zero. The quantity A is the attenuation of the beam in the observation, or monitor, phase of an experiment relative to the bleaching intensity. As mentioned above, A will be three or four orders of magnitude.

The integration in Equation 3.1 extends over the plane of the membrane. Since the laser is operated in TEM_{00} mode, the laser intensity is Gaussian when projected into two dimensions and is given by Equation 3.2.

$$I(r) = I_0 \exp (- 2 r^2 / w^2) \qquad (3.2)$$

$$= (2 P / \pi w^2) \exp (- 2 r^2 / w^2)$$

In Equation 3.2, P is the laser power incident on the surface and w is the radius of the beam. The radius w is the r value at which the intensity falls to exp(-2) of its maximum value. The width w may be calculated but is usually measured experimentally.[1]

Exposure of the sample to a brief pulse of the intense bleach beam results in the irreversible destruction of fluorophore in the observation area. If the bleaching is a first order process, as is usually assumed, then the rate of photobleaching is given by Equation 3.3.

$$\frac{d\,C(r,t)}{dt} = -\Phi_d\, I(r)\, C(r,t) \qquad (3.3)$$

In Equation 3.3, Φ_d is the quantum yield of photodestruction. Integrating Equation 3.3 yields the fluorophore distribution immediately after the bleach pulse.

$$C(r,0) = \bar{C} \exp\left(-\Phi_d\, I(r)\, t' \right) \qquad (3.3)$$

In Equation 3.4, $\bar{C}$ is the initial average fluorophore concentration and t' is the length of the bleach pulse. If $K = \lambda\, I_0\, t'$ is used as a measure of the extent of bleaching, then the post bleach concentration as a function of r will be the exponential of a Gaussian. The variable λ is the photobleaching rate constant. Hence C(r,0) is given by Equation 3.5 in terms of K.

$$C(r,0) = \bar{C} \exp\left\{ -K \exp\left(-2\, r^2 / w^2 \right) \right\} \qquad (3.5)$$

The post bleach concentration distribution C(r,0) is considered time zero because it is the initial boundary equation used to solve the two-dimensional time dependent diffusion equation, Equation 3.6.

$$\frac{\partial\, C(r,t)}{\partial t} = \left(\frac{D}{r} \right) \frac{\partial}{\partial r} \left(r\, \frac{\partial\, C(r,t)}{\partial r} \right) \qquad (3.6)$$

The solution to Equation 3.6, C(r,t), is used in Equation 3.1 to characterize f(t), the observed fluorescence signal. The recovery of f(t) is given by the series solution, Equation 3.7.[12]

$$f(t) = \left(\frac{g\,\varepsilon\,Q\,P\,C}{A}\right) \sum_{n=0}^{\infty} \frac{(-K)^n}{n!} \left\{ 1 + n\,(\,1 + 2t/\tau_d)\right\}^{-1} \qquad (3.7)$$

The characteristic time for diffusion, in Equation 3.7, is $\tau_d = w^2/4D$. This analysis presumes that photobleaching by the monitor beam is negligible during the recovery and that diffusion is the only physical process contributing to the recovery.

Operationally one extracts diffus' coefficients from the measured recovery using Equation 3.8, which allows for the fact that not all the fluorophore may be free to diffuse.[1]

$$F(t) = X_m\,F(-)\,f(t) + (1-X_m)\,F(0) \qquad (3.8)$$

In Equation 3.8, F(t) is the absolute fluorescence measured as a function of time after the bleach, F(-) is the intensity immediately before the bleach, and f(t) is the relative fluorescence due to mobile fluorophore according to Equation 3.7. The fraction of fluorophore mobile on the time scale of the experiment is X_m and F(0) is the absolute fluorescence immediately after the bleach pulse.

The mobile fraction X_m is defined according to Equation 3.9 where $F(\infty)$ is the fluorescence intensity reached an infinite time, or an approximation thereto, after the bleach.[1]

$$X_m = \frac{[F(\infty) - F(0)]}{[F(-) - F(0)]} \qquad (3.9)$$

The experimental fluorescence recovery is fit to three parameters using Equation 3.8. The three parameters are the characteristic time for recovery τ_d, the bleaching parameter K, and the mobile

fraction, X_m. The fitting procedure[13] uses the series solution of Equation 3.7 (truncated where possible) and fits iteratively to all three parameters. Prior to fitting, the data is piece-wise smoothed using linear least squares smoothing to third order polynomials.[14,15] Thirty representative data points are used in the fitting procedure. Their distribution is not uniform through the whole recovery curve but is skewed toward the early, steeply rising, portion of the recovery. The effect of this bias is to increase the precision in the τ_d fit at the expense of X_m and K. This is desirable, however, since τ_d is inherently the more difficult parameter to fit, as well as being the parameter of the most physical interest.

3.3 Experimental Artifacts in FPR

Objections have been raised to the FPR technique on a number of fronts. Experimental artifacts caused by the photobleaching chemistry are of the greatest concern. While singlet oxygen is believed to be involved in the photobleaching process,[16] the evidence is circumstantial and the mechanism is essentially unknown. The potential exists for serious collateral damage to the membrane. Concern is, of course, heightened when dealing with the complicated morphology of a cell membrane. The gravity of this problem has attracted the attention of many research groups.[17-21] The consensus appears to be that brief exposure of the system probably does not induce widespread damage to the membrane and its constituents.

The uncertain photochemistry of the photobleaching reaction means that the presumption of a first order irreversible reaction is

difficult to prove. That the photolysis occurs is unquestioned. Of greater concern than the actual kinetics is the question of irreversibility. This is easy to test experimentally. Bleaching the entire vesicle should result in the total destruction of resident fluorophore. Any recovery of fluorescence in the vesicle means the reaction is, at least to certain extent, reversible. Such does not appear to be the case.

Thermal artifacts have the potential to disrupt the diffusion measurement as well. If the bleaching pulse (or the monitor beam) produced substantial local heating, the resultant measurement would be suspect. The relative scarcity of fluorophore in the membrane for a typical application and the high specific heat of the water in an aqueous membrane environment conspire to produce a negligible local temperature jump.[22]

The FPR technique yields a two-dimensional measurement because of the restrictive geometry of the membrane. The incident laser beam must, however, traverse three-dimensional space before reaching the focal plane. Fluorophores above and below the plane of focus will be irradiated by the out of focus beam and may contribute to the observed fluorescence signal. Detection of the out of focus fluorescence is minimized by an image plane pinhole (Figure 3.3) installed in front of the detector. The pinhole reduces the background fluorescence by defining a depth of focus compatible with the beam size.[23] A pinhole size of 0.4 mm, convoluted with a beam of 1.1 μm width in the focal plane, results in a sensitive volume of roughly cylindrical shape which has a long axis extending approximately 6 μm above and below the plane of focus. The 6 μm height corresponds to an intensity which,

Figure 3.3: Image plane pinhole. Fluorescence, collected by the objective lens, traverses the dichroic mirror and is focused on the aperture of an image plane pinhole. Only fluorescence originating in the objective plane of focus, or a small region surrounding it, will pass through the image pinhole. The thick incident line is the monitor laser beam.

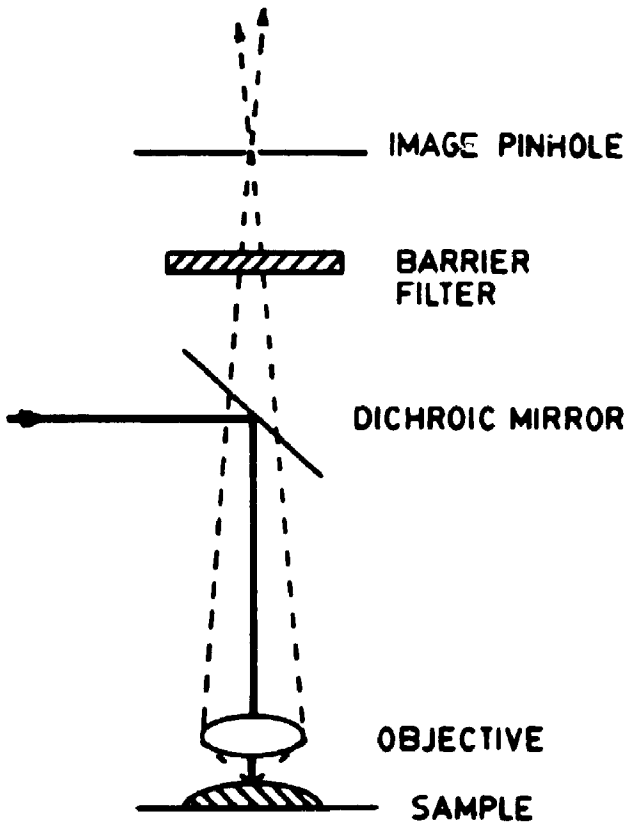
IMAGE PINHOLE
BARRIER
FILTER
DICHROIC MIRROR
OBJECTIVE
SAMPLE

relative to the central intensity, is exp(-4) less.

The image pinhole cannot discriminate against fluorescence which originates from a series of closely spaced, multilamellar membranes. These multilamellar systems result from the method we use to form model membranes. The spacing is so close (less than 1 μm) that if one focuses on the surface of a hollow multilamellar assembly, there is little divergence of the laser beam over their thickness and little effect of the image pinhole. Since the multibilayers are discrete layers, they have the same diffusion coefficient. The effective intensity observable is higher, however, which makes the multibilayer assembly attractive to work with.

3.4 FPR Hardware

The laser used in this work is a Coherent Inc. Innova 70 Four Watt Argon ion laser. The laser operates at 476.5 nm in light regulation mode at 100 mW. Timing of the bleach and monitor beams is controlled by a Digital Equipment Corporation Minc 23 microcomputer with a VT 105 display terminal. The intensity of the bleach and monitor beams is attenuated by placing neutral density filters in the optical path of the microscope, before the sample. In a typical experiment the neutral density filter is 1.5 O.D. and the bleach and observation beams are approximately 3 mWatts and 1 μWatt respectively at the sample. The fluorescence intensity incident on the detector is lowered as required by placing a second neutral density filter in the optical path after the sample.

The fluorescence microscope used in our FPR instrument is a Zeiss

Universal model fitted for epi illumination. A dry ice cooled RCA 31034A photo multiplier tube (PMT) is fitted to the top of the optical column. The output of the PMT, fed through an amplifier/discriminator, also feeds to the Minc microcomputer. A 140 mm focusing lens is installed on the optical bench behind the microscope to focus the laser beam onto the image plane of the microscope. The objective lens used was a x40 power water immersion lens with a numerical aperture of 0.75. The combination of the 140 mm focusing lens and x40 objective lens produce a beam with $w = 1.1\ \mu m$ in the focal plane.

Altering the time base of the experiment through the Minc computer and adjusting the laser intensity with neutral density filters permits the measurement of diffusion coefficients which range over six orders of magnitude, from $10^{-17}\ m^2s^{-1}$ to $10^{-11}\ m^2s^{-1}$.

Computer control of the fluorescence acquisition permits an immediate reconstruction of the experimental recovery on the VT 105 terminal. If desired, the file is saved onto a floppy disk, then uploaded on completion of the day's experiments to the University of Western Ontario's Vax 6330, as a batch job, for fitting and plotting. Plots, for example Figure 3.4, may be produced using a Dataproduct's 2600 laser printer or a Calcomp 1044 flat bed plotter located in the university's computer center. Plotting is controlled by a customized DI-3000 graphics program.

3.5 FPR Measurements on Model Membranes

The bulk of the diffusion measurements in this work were made using dimyristoylphosphatidylcholine (DMPC) as the host lipid in model

Figure 3.4: Sample FPR experiment. Average of three bleach/recovery cycles measured with 3° NBD 11C monomer in a DMPC model membrane at 29 °C. The bleach pulse lasted 4 msec, each channel in the figure is 10 msec. The diffusion coefficient is 5.5×10^{-12} $m^2 s^{-1}$ and the mobile fraction 0.99. The fluorescence intensities F(-), F(0), F(t), and F(∞) correspond to those of Figure 3.1.

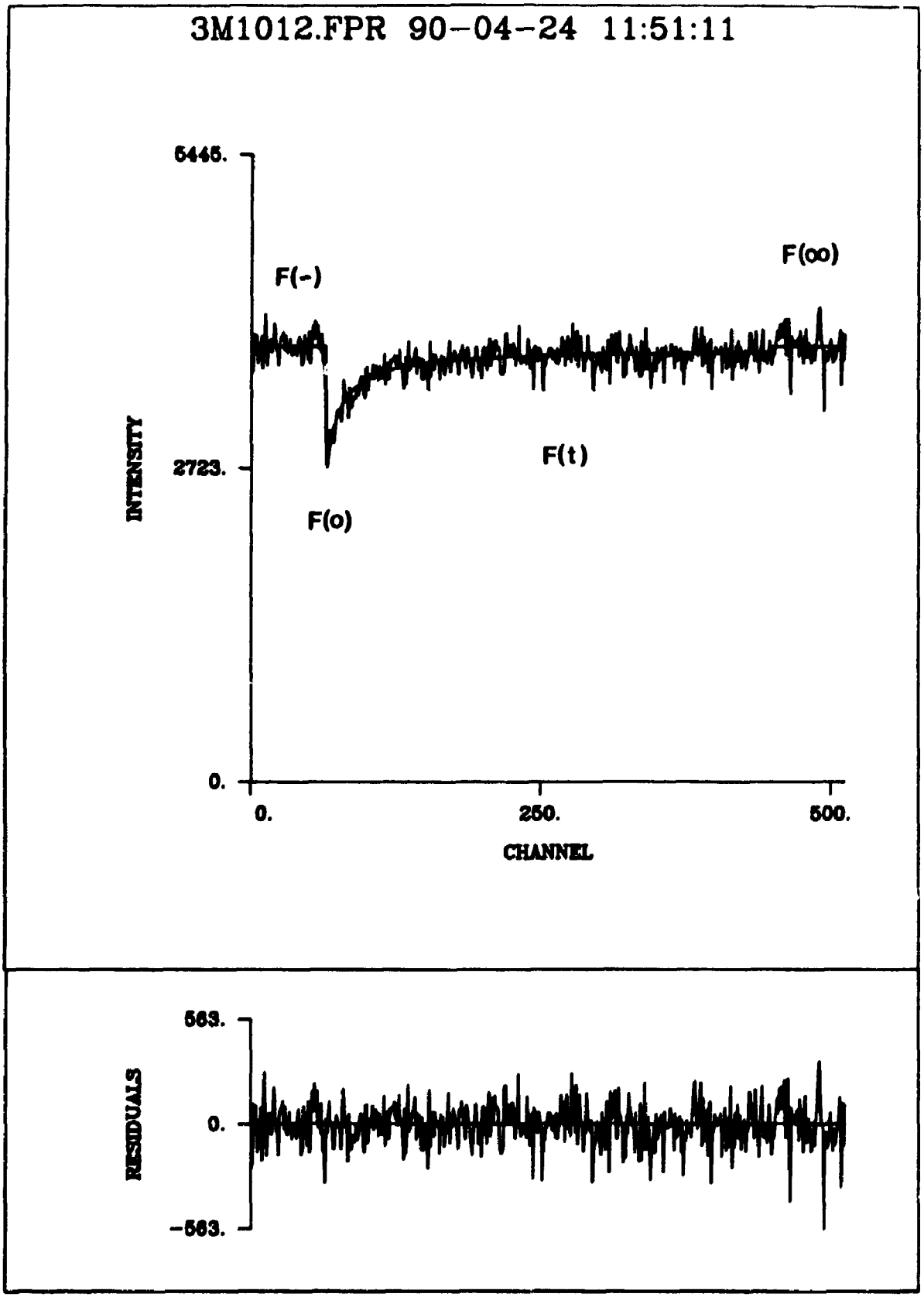
3M1012.FPR 90-04-24 11:51:11
5445.
F(-)
F(oo)
INTENSITY
2723.
F(t)
F(o)
0.
0.
250.
500.
CHANNEL
563.
RESIDUALS
0.
-563.

membranes. Myristic acid, the fatty acid in DMPC, has fourteen carbon atoms in the long hydrocarbon tail. DMPC was chosen for this work since its phase transition temperature, T_m, is 23 °C. This is a convenient temperature to work with since it permits one to work both above and below this phase transition with relative ease. By contrast, dipalmitoylphosphatidylcholine (sixteen carbons) undergoes the same phase transition at T_m = 41 °C, while for dilaurylphosphatidylcholine (twelve carbons) T_m = 0 °C. DMPC, (Fluka) was used without further purification.

Temperature control of the hydrated DMPC vesicles was achieved with a Cambion Bipolar temperature controller with a microscope stage sub-assembly. The nominal temperature range of the controller is from 0 °C to 50 °C. Temperature measurements were made by dipping a small 100 kΩ thermistor (YSI 44011) into the water surrounding the sample near the point of measurement. Translation of the resistance reading, with the manufacturer's (Yellow Springs Instrument Co.) calibration table, led directly to a temperature reading in degrees Celsius.

Samples were prepared using the conventional technique, with some modifications, of Kapitza et. al.[24] Generally 0.5 μmol of lipid and a small amount (less than 0.1% on a molar basis) of NBD labelled material were applied as a 50 μL droplet in a 2/1 chloroform/methanol solution to the surface of a clean, dry circular glass coverslip of 18 mm diameter. The slide was heated to 40 °C and the lipid film dried under a weak flow of nitrogen. The coverslip and film were put under high vacuum for eight hours, then lowered slowly (lipid film down) onto a clean 22 mm diameter glass coverslip with a 300 or 400 μL droplet of doubly distilled deionized water on its surface. The two slides, forming a

lipid/water sandwich, were sealed together with hot wax and stored overnight in the dark at 40 ^{0}C.

The samples were inverted and mounted in a hollow disk of copper preparatory to FPR measurements. An axially symmetric hole in the bottom of the disk was covered with a glass coverslip to permit light transmission. The disk was filled with water, covering the sample, and a light film of thermally conducting grease (Wakefield Engineering) was applied to the bottom of the disk.

The hydrated lipid film swells spontaneously (over several hours) to form large multibilayers. Many of the multibilayers so formed were greater than sixty μm in diameter. The multibilayers were examined and the laser beam positioned using phase contrast optics. The laser beam was focused on the top surface of the multibilayers under study by adjusting the microscope's fine focus until a bright spot of fluorescence was observed through the microscope eyepiece.

Vesicles made using this method were exceptionally plentiful. Those chosen for experiments were generally large and multilamellar but with a hollow core. Large vesicles were preferred since their curvature is less than small vesicles and their surface is much larger than the beam size. Equation 3.1 is derived for a flat surface of infinite size. Large vesicles are a close approximation to this idealized system. Control experiments showed no systematic difference in diffusion coefficients measured on true unilamellar bilayer membranes and the more plentiful multibilayers. Multibilayers were preferred due to their ease of detection with the phase contrast optics and, as mentioned above, their stronger fluorescence

Diffusion measurements on vesicles in the liquid crystal phase

were made at 29 ^{0}C ± 1 ^{0}C. For any one sample, typically five measurements on each of four or five vesicles were made. Each of the five measurements is an average of three bleach/recovery sequences. The multiple bleach/recovery sequence improves the signal to noise ratio and is permissible since samples in the liquid crystal phase have mobile fractions of one. Standard deviations were calculated, based on the discrete diffusion measurements, assuming a normally distributed population. This protocol was followed for all samples.

Diffusion measurements in the lipid gel phase frequently followed measurements on the same sample in the liquid crystal phase. Gel phase measurements were performed at 19 ^{0}C ± 1 ^{0}C. The slow diffusion in this regime, and mobile fractions less than one, required substantial attenuation of the bleach and monitor beams, longer observation times and single bleach/recovery sequences. The long time required for these measurements usually meant only one experiment per vesicle although frequently more than five vesicles were measured.

Diffusion measurements, similar to those described above, were performed using the fluorescent polyaromatic hydrocarbons tetracene (Aldrich) and rubrene (Aldrich) sequestered in DMPC multibilayers. The bilayers were formed by the conventional method.

3.6 Diffusion Measurements in Poly(propylene glycol) Polymers

Diffusion measurements of the NBD labelled polyisoprenoid alcohols were made in a series of poly(propylene glycol) (PPG) polymers. Polymers of average gram molecular weights 425, 725, 1000, 2000, 3000,

and 4000 were purchased from Aldrich. These polymers have viscosities, reported by Aldrich, of 80, 115, 150, 300, 600, and 930 centiPoise at 25 ^{o}C.

Samples for diffusion measurements in PPG matrices were prepared as follows. Small aliquots of the stock NBD alcohol solutions were added to a small glass one dram sample vial. The solvent was removed under high vacuum yielding 1.4 nmol of the labelled alcohol as a dry film. To these vials, 400 µL of warm (40 ^{o}C) neat PPG was added. The labelled alcohols dissolved readily in all the polymers.

Portions of the NBD containing polymer solutions were drawn into small rectangular glass tubes by capillary action after dipping one end into the warm polymer solution. The capillary microslides, purchased from Vitro Dynamics Inc., were sealed on filling by hot wax at each end. The microslides took from two to fifteen minutes to fill, depending on the viscosity of the warm polymer solution. The microslides had inside dimensions of 2 mm (width), 5 cm (length), and 100 µm (depth).

The sample holder was a thin hollow disk of copper with three shallow parallel grooves 2.5 mm in width, extending from one side of the disk to the other. A glass coverslip fit into the bottom of the sample holder to transmit light and permit the disk to be filled with water. Once again, thermal grease was applied to the bottom of the disk and the assembly maintained at 25 ^{o}C ± 1 ^{o}C with the Cambion temperature controller. Temperature measurements were made as described for membrane studies.

Diffusion measurements on each of the three microslides (with different samples) in the sample holder were made at two discrete

locations where five measurements were undertaken. Each of the five measurements was an average of three individual bleach/recovery sequences. Mobile fractions were, once again, unity. The laser beam was focused at the midpoint of the capillary tube in both depth and width. The laser and optics settings were the same as those used for vesicle measurements with two exceptions. A neutral density filter of 1.08 O.D. was used to attenuate the bleach and monitor beams, and the image pinhole was decreased to 0.25 mm for these measurements.

Diffusion measurements in isotropic solution were also made using parrafin oil (heavy, white, Fisher) and glycerol/water media. The same NBD labelled probes were investigated and the samples prepared as described above.

3.7 High Performance Liquid Chromatography

A major challenge of this work was the preparation and handling of small quantities of fluorescently labelled compounds. The purity and identity of these compounds were a constant source of concern. Reverse Phase High Performance Liquid Chromatography (HPLC) proved to be an exceptionally useful quantitative means of monitoring the NBD labelled compounds prepared.

The HPLC system comprised two Waters 510 pumps controlled by a Waters automated gradient controller. A Gilson 231 programmable sample injector and diluter were interfaced to the Waters system. A Rheodyne model 7125 injector with a 20 μL sample loop was used for manual sample injections. The detector was a Waters 490 multiwavelength detector. Output from the Waters detector was

recorded on a Goerz SE 120 analog chart recorder (two channels) and a Waters 740 integrator (one channel). Fluorophores were observed at 480 nm.

All HPLC analyses used Waters C_{18} reverse phase radial compression columns. The solvents used were isopropyl alcohol, methanol, acetonitrile (all purchased from BDH) and water. All were HPLC or spectroscopic grade. They were filtered and degassed before use. Solvent compositions and retention times for individual compounds are included with the details of their syntheses in the next chapter.

3.8 Steady State Fluorescence Measurements

Steady state fluorescence measurements in solution and in vesicles were performed using an LS-1 fluorimeter manufactured by Photon Technology International Flucrescence anisotropy measurements, in the steady state, were made with the addition of the proper polarizing optics.

Fluorescence emission measurements were performed by exciting the NBD chromophore at 480 nm and measuring the emission intensity in 2 nm intervals between 500 nm and 650 nm. Individual intensities at each wavelength were the average of fifty discrete lamp flashes. The entire emission was measured and averaged twenty-five times. Numerical integration of the area[13] under the emission curve from 500 nm to 650 nm gave the total emission intensity. The excitation, emission, and PMT monochromator slits were set for a 4 nm bandwidth. The sample chamber of the fluorimeter was temperature controlled (31 $^{0}C \pm 1\ ^{0}C$) with a circulating constant temperature bath.

Fluorescence intensity measurements were made using NBD adducts of undecanol, solanesol, and citronellol (synthesis described in Chapter Four). Fluorescence measurements were also made with NBD labelled cholesterol (NBD-cholesterol), palmitoylphosphatidylcholine (NBD-PC), and phosphatidylethanolamine (NBD-PE). The phosphatidylcholine analog (Figure 3.5b), labelled in the two-position was purchased from Avanti Polar Lipids. Phosphatidylethanolamine, labelled at the headgroup (Figure 3.5c) was also purchased from Avanti Polar Lipids. Cholesterol labelled at the end of the hydrocarbon tail (Figure 3.5a) was purchased from Molecular Probes.

Small unilamellar vesicles were formed by the ethanol injection technique[25] from DMPC doped with the NBD labelled molecules mentioned above. The small unilamellar vesicles were formed by rapidly injecting 40 μL of ethanol solution, containing 0.5 μmol of DMPC and less than 2.5 nmol of NBD labelled material, into 2 mLs of rapidly stirred 60 ^{0}C aqueous solution. The aqueous solution was pH 7 TRIS buffer with 150 mmolar sodium chloride. Vesicles formed by this method are typically between 150 and 500 Angstroms in diameter.

Stern-Volmer fluorescence quenching experiments were performed with aqueous Co^{2+} as the quencher.[26] Cobalt chloride hexahydrate was purchased from Fluka. Vesicles for quenching experiments were formed by injection (previous conditions) into solutions containing the appropriate cobalt ion concentration (0 - 20 mmolar). Correction was made for the internal filter effect of the cobalt ion in solution.

Figure 3.5: a) NBD-cholesterol. Cholesterol labelled in the tail group with NBD as a fluorescence probe (P). The NBD probe is described in Chapter Four.

a

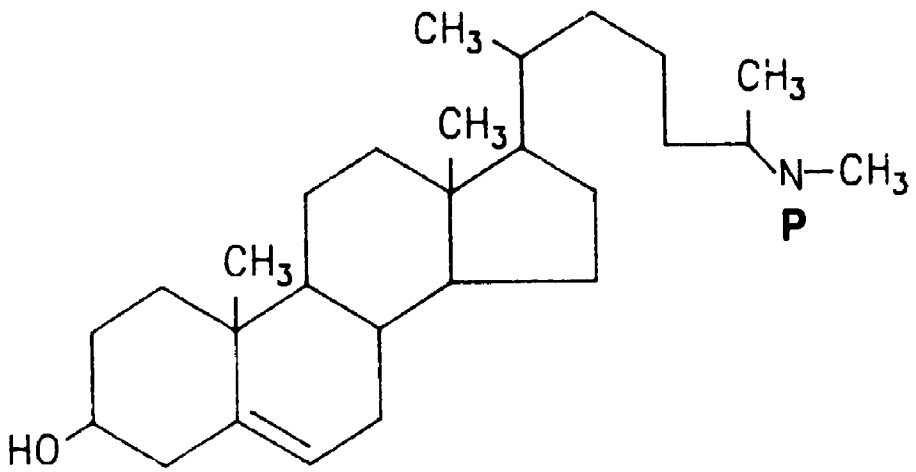

P =

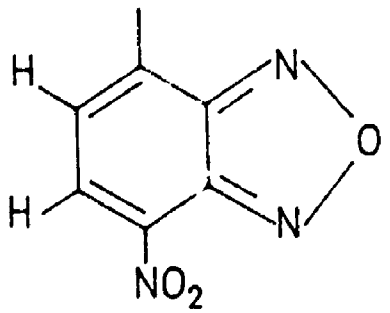

Figure 3.5: b) NBD-PC. Palmitoylphosphatidylcholine labelled in an acyl chain with NBD as a fluorescence probe (P). The NBD probe is described in Chapter Four.

c) NBD-PE. Dipalmitoylphosphatidylethanolamine labelled in the head group with NBD as a fluorescence probe (P). The NBD probe is described in Chapter Four.

b

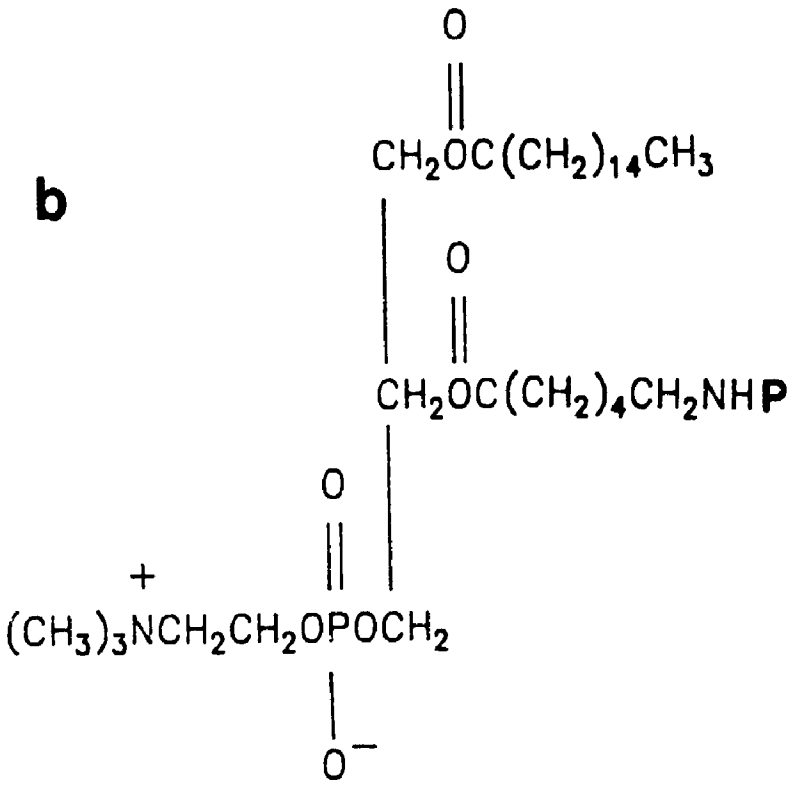

c

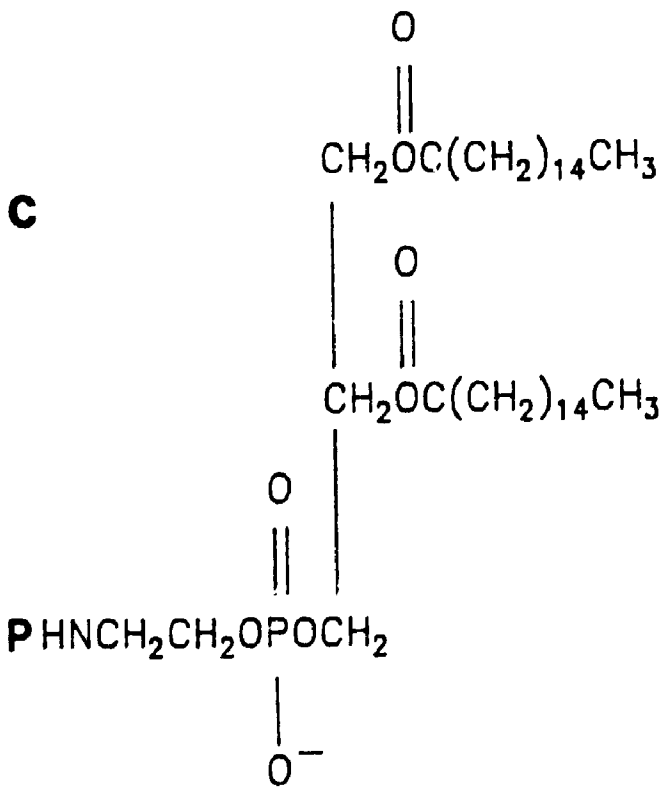

REFERENCES

(1) Petersen, N. O.; Felder, S.; Elson, E. L. In *Handbook of Experimental Immunology*; Weir, D. M., Ed.; Blackwell: Edinburgh, 1986; Vol. 1, pp 24.1, 24.23.

(2) Petersen, N. O.; Elson, E. L. In *Methods in Enzymology*; Hirs, G. H.; Timasheff, S. N., Eds.; Academic: New York, 1986; Vol. 130, pp 454, 484.

(3) Mathies, R. A.; Stryer, L. In *Application of Fluorescence in the Biomedical Sciences*; Taylor, D. L., Ed.; Liss: New York, 1986; pp 129, 140.

(4) Haugland, R. P. In *Excited States of Biopolymers*; Steiner, R. F., Ed.; Plenum: New York, 1983; pp 29, 58.

(5) Haugland, R. P. *Handbook of Fluorescent Probes*; Molecular Probes: Eugene, Or., 1989. References found therein.

(6) Poo, M.; Cone, R. *Nature* **1974**, *247*, 438.

(7) Liebman, P. A.; Entine, G. *Science* **1974**, *185*, 457.

(8) Peters, R.; Peters, J.; Tews, K. H.; Bahr, W. *Biochim. Biophys. Acta* **1974**, *367*, 282.

(9) Koppel, D. E. *Biophys. J.* **1979**, *28*, 281.

(10) Smith, B. A.; McConnell, H. M *Proc. Natl. Acad. Sci.* **1978**, *75*, 2759.

(11) Lanni, F.; Ware, B. A. *Rev. Scient. Instrum.* **1982**, *53*, 905.

(12) Axelrod, D.; Koppel, D. E.; Schlessinger, J.; Elson, E.; Webb, W. W. *Biophys. J.* **1976**, *16*, 1976.

(13) Bevington, P. R. *Data Reduction and Error Analysis For the Physical Sciences*; McGraw-Hill: New York, 1969.

(14) Savitzky, A.; Golay, M. J. *Analyt. Chem.* **1964**, *36*, 1627.

(15) Steinier, J.; Termonia, Y.; Deltour, J. *Analyt. Chem.* **1972**, *44*, 1906.

(16) Picciolo, G. L.; Kaplan, D. S. *Adv. Appl. Microbiol.* **1984**, *30*, 197.

(17) Lepock, J. R.; Thompson, J. E.; Kruuv, J.; Wallach, D. F. *Biochem. Biophys. Res. Commun.* **1978**, *85*, 344.

(18) Sheetz, M. P.; Koppel, D. E. *Proc. Natl. Acad. Sci.* **1979**, *76*, 3314.

(19) Wolf, D. E.; Edidin, M.; Dragsten, P. R. *Proc. Natl. Acad. Sci.* **1980**, *77*, 2043.

(20) Wey, C. L.; Cone, R. A.; Edidin, M. A. *Biophys. J.* **1981**, *33*, 225.

(21) Koppel, D. E.; Sheetz, M. P. *Nature* **1981**, *293*, 159.

(22) Axelrod, D. *Biophys. J.* **1977**, *18*, 129.

(23) Koppel, D. E.; Axelrod, D.; Schlessinger, J.; Elson, E. L.; Webb, W. W. *Biophys. J.* **1976**, *16*, 1315.

(24) Kapitza, H. G.; Ruppel, D. A.; Galla, H. J.; Sackmann, E. *Biophys. J.* **1984**, *45*, 577.

(25) Fung, B. K.; Stryer, L. *Biochemistry* **1978**, 17, 5241.

(26) Chattopadhyay, A.; London, E. *Biochim. Biophys. Acta* **1988**, *938*, 24.

CHAPTER FOUR

SYNTHETIC STRATEGY

4.1 Overview

The purpose of this thesis is to examine the effect of size and shape on the lateral diffusion coefficient of probe molecules in model membranes. As discussed in Chapter One, our approach to the problem is experimental. The design of suitable probes was of critical importance to the success of this endeavor. A synthetic strategy was therefore developed which produced a comprehensive series of probes that explore the size and shape dependence of the lateral diffusion coefficient. Since the logic is complex, it is best to first outline the strategy and the reasons for the choices of the molecules used. This chapter is intended only to provide the gross features, the rationales and to introduce the nomenclature associated with the variety of molecules used. The next chapter provides the details of the synthesis, the checks on identity and purity, and the various characterizations of the molecules.

4.2 Fluorophore

While other methods exist to measure diffusion coefficients in model membranes[1], FPR is without equal in membrane studies due to its ability to measure tracer diffusion coefficients of specific compounds. Paradoxically, the strength of FPR is also, in many cases, its greatest weakness. The sensitivity and specificity of the

measurements accrue from the fact the fluorescence originates from a labelled compound. The requirement for labelling, except for the few cases where the probe is natively fluorescent, is the weakness of FPR. Frequently, with large macromolecules like proteins, it is possible to add fluorophore without concern as to the extent or nature of the labelling.[2] Fluorescently labelled antibodies are also commercially available which permit indirect labelling of defined species through non-covalent interactions.

The molecules we have synthesized are small on the scale of biological macromolecules such as proteins. The nature and mode of the attachment is thus of more importance with regard to alteration of the labelled molecules properties. The label we have chosen to use is based on N-methyl-4-amino-7-nitrobenz-2-oxa-1,3-diazole (NBD). NBD (Figure 4.1) is very commonly used in FPR for two reasons. (1) It is relatively small, and therefore hopefully minimally perturbing. (2) NBD has favorable optical properties. It absorbs in close proximity to the 476.5 nm line of an argon ion laser with an extinction coefficient greater than 20,000 cm^{-1} $mol^{-1}L$.[3,4] The Stokes' shift of NBD yields an emission maximum at approximately 535 nm.[3,4] NBD bleaches with relative ease and its fluorescence is readily quenched by water.[4]

The polarity of the NBD moiety is uncertain, but must depend to some extent on the nature of the linkage (R in Figure 4.1) used in the labelling protocol. NBD itself seems to be sufficiently polar that it partitions, when sequestered in a membrane, towards the aqueous interface of the bilayer.[5,6]

Figure 4.1: NBD label. N-methyl-4-amino-7-nitrobenz-2-oxa-1,3-diazole. This fragment is the predominant fluorophore used in this thesis. Our organic syntheses utilized two derivatives of the basic NBD unit. a) NBD-acid. NBD-acid was used to label alcohol substrates. b) IANBD. The haloacetyl, IANBD was used to label thiol bearing molecules.

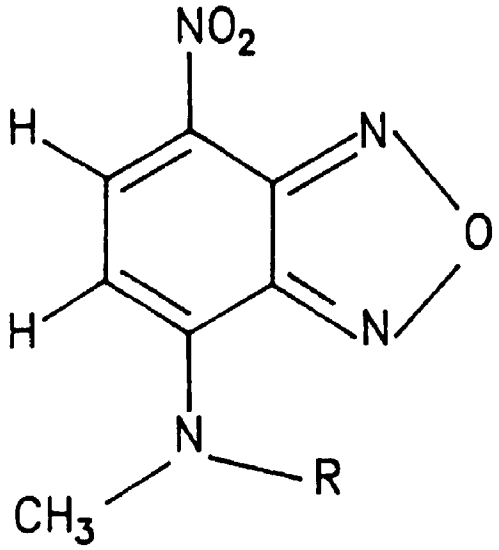

a R = $(CH_2)_5CO_2H$

b R = $CH_2CH_2O_2CCH_2I$

4.3 Linear Hydrophobic Polymers - Variation in L

The first series of compounds synthesized were intended to explore the effect of hydrocarbon interactions in the membrane interior as a retardant to lateral motion. To investigate this behavior, the ideal substrate should form an homologous series of well-defined hydrophobic polymers that possess a ready means of derivitization.

Fortunately, a naturally occurring hydrocarbon polymer satisfies these criteria. The polyisoprenoid alcohols, ubiquitous in nature, are monohydric alcohols composed of isoprene residues linked together in head-to-tail fashion through ordinary carbon - carbon single bonds (Figure 4.2). Short chain isoprenes are most prevalent in plants. Molecules such as citronellol[7] (2), nerol (2), farnesol (3), and geranyl geraniol (4) are common constituents of fragrant essential oils such as citronella, rose, and musk oil.[8] Solanesol[9] (9) is the major lipid component of tobacco leaves. Long chain polyprenols are more common in mammals. Dolichol[10] in rat liver, for example, is polydisperse with alcohols which range from fourteen to twenty-four isoprenes in length.

Despite the common linear architecture, two major structural differences occur in these polymers. The first is the extent of unsaturation and the second is the stereochemistry about the double bonds. Saturated isoprenes, when present, typically occur as the α sub-unit. This is the case for citronellol and dolichol used in our studies (Figure 4.2). Solanesol, the other isoprenoid alcohol we used, has a partially unsaturated α-subunit. Solanesol also has all

Figure 4.2: Isoprenoid alcohols. The isoprenoid alcohols citronellol, solanesol, and dolichol are naturally occuring hydrophobic polymers amenable to derivatization with NBD-acid.

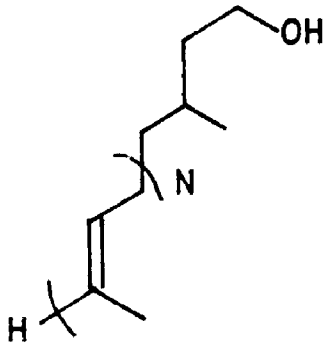

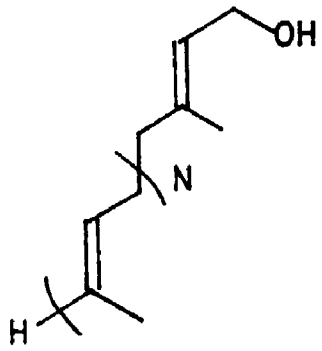

N = 1 Citronellol

N = 8

N = 13–24 Dolichol

Solanesol

trans stereochemistry about its nine double bonds.[11] Dolichol is poly cis with only the three terminal isoprenes possessing trans double bonds.[12]

Citroneliol (2), solanesol (9), and dolichol (average 20) provide the homologous, hydrophobic linear polymer series we need to investigate dynamic interactions in the membrane interior. Their one functional group, an alcohol, immediately suggests an esterification as the mode of fluorophore attachment. N-methyl-N-(7-nitrobenz-2-oxa-1,3-diazol-4-yl)-6-amino hexanoic acid, (NBD-acid) is an acid version of NBD (Figure 4.1a, [R = $(CH_2)_5CO_2H$]) suitable for esterification.

The best esterification reaction proved, after considerable difficulty, to be a dicyclohexylcarbodiimide (DCC) mediated acid condensation reaction with an alkyl aminopyridine catalyst (Figure 4.3).[13,14] This reaction has a significant by-product, N-acylurea, production of which is very solvent dependent (Appendix One).[15] The concomitant wastage of NBD-acid necessitates excess NBD-acid in the reaction. Esters synthesized from NBD-acid are named, in this work, by appending the alcohol name to NBD. For example, NBD-acid conjugated with solanesol forms the ester product NBD-solanesol.

Great effort went into model reactions using simple alcohols such as undecanol. Model reactions were necessary in order to: (1) elucidate the products of the DCC reaction; (2) ensure complete understanding of the mechanism before the rare (harvested from human liver on autopsy) dolichol was risked; (3) examine the light stability of the resulting ester. The undecanol ester was used, by analogy, to spectroscopically (MS, NMR) identify the other esters

Figure 4.3: DCC mediated NBD-acid esterification reaction. Sample reaction scheme illustrating the labelling reaction used with all our isoprenoid alcohols. In this case, NBD-acid (1) combines with DCC to form the acid anhydride (2) and the unwanted N-acylurea (5). An akyl aminopyridine catalyst assists the esterification of, in this case, undecanol (3). NBD-undecanol (4) is the resultant product.

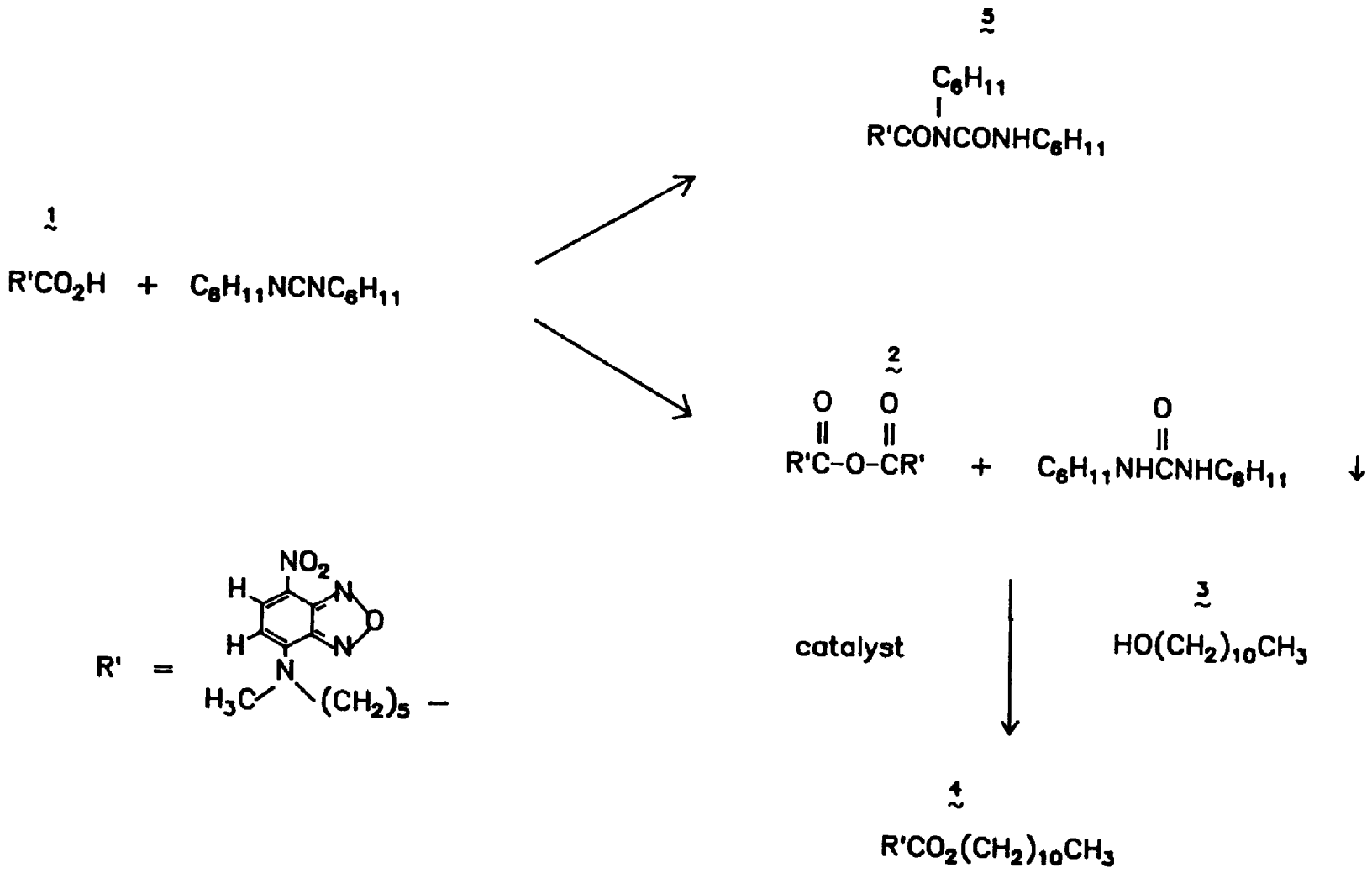
5
C6H11
R'CONCONHC6H11
1
R'CO2H + C6H11NCNC6H11
2
R'C–O–CR' + C6H11NHCNHC6H11
R' = NO2 H N O H N N CH3 (CH2)5 –
catalyst
3
HO(CH2)10CH3
4
R'CO2(CH2)10CH3

because of an unexpected instability of the product esters containing double bonds.

This instability (Appendix Two) results from a NBD sensitized, intramolecular, singlet oxygen 'ene' reaction. On exposure to intense light, in solvents where $^1O_2$ is long lived, double bonds in the isoprene structure are degraded by singlet oxygen which results in the production of hydroperoxides. Substrates such as NBD derivatives of solanesol and dolichol were particularly sensitive to the singlet oxygen 'ene' reaction, probably because of their greater number of reactive sites.

4.4 Radial Surfactant Polymers - Variation in R

The second series of compounds synthesized were intended to explore the effect on the lateral diffusion coefficient of increasing the probe molecule's area at the bilayer/water interface.

The obvious manner to assemble such a series of test molecules is to polymerize oriented surfactant molecules. The polymerization, however, must be controlled in such a manner that individual homologues (monomers, dimers, trimers etc.,) may be recovered and fluorescently labelled. Polymers such as these are readily available, and indeed extensively utilized, in nature.[16] These assemblies, however, are primarily cross-linked proteins. This methodology was used by Vaz et. al.[17], as discussed in Chapter Two, to explore the dependence of the diffusion coefficient on diffusant radii in the continuum regime. The starting point of his polymer series is too large to permit examination of the region of theoretical uncertainty

shown in Figure 1.3. Our purpose is best served by polymerizing oriented molecules the size of the host lipid.

Polymerized surfactant assemblies are the subject of intense scrutiny.[18-23] The industrial applications possible with a functionalized, oriented assembly are legion. The most popular approach to surfactant polymerization, in this context, has been UV induced, free radical cross-linking of butadienes,[24] diacetylenes[25] or carbon-carbon double bonds[26]. Another approach, introduced by Regen et. al.,[18] involves polymerizing phosphatidylcholines (Figure 1.1) which have thiols in the terminal position of both alkyl chains. Using hydrogen peroxide as an oxidizing agent, they were able to form reversible disulfide linkages between thiol containing phospholipids in small bilayers.

These approaches, in common with most overtures in this area, have significant drawbacks. (1) It is difficult, or impossible, to control the extent of polymerization. In many cases, it is impossible even to measure the extent of polymerization. (2) Polymers formed in this manner do not form a comprehensive network. Each individual surfactant can be joined covalently to, at most, two neighboring surfactants. A polymerized assembly formed in this manner will consist of many, mutually exclusive, two-dimensional sheets oriented perpendicular to the surfactant/water surface.

Both these limitations frustrated our attempts to assemble polymerized surfactant arrays with limited extents of polymerization and some degree of radial symmetry. The ideal surfactant, to satisfy these criteria, must have a high order symmetry axis in order to provide three or more points of attachment. An idealized scheme

showing three coordinate polymerization on a surface is shown in Figure 4.4. Carbon (graphite)[27] and boric acid[28] adopt this type of hexagonal lattice in their natural crystalline form.

Consider the monomer in Figure 4.5a, if one could control the reactivity of the three arms by some means of activation/deactivation, then one would have an ideal means to control the extent of polymerization. Cross-linking monomers, each with one arm 'activated' (1°), would produce dimers (Figure 4.5b). Cross-linking a mixture containing a large excess of 1° activated monomers and some monomers with all three arms activated (3°), would produce a mixture of dimers and tetramers (Figure 4.5c).

The challenge is to synthesize a surfactant molecule that has a C_3 rotation axis about its long axis and can be selectively activated to the first or third degree. Triesters of *cis,cis*-1,3,5-cyclohexanetriol have the required C_3 symmetry (Figure 4.6). Three closely spaced esters in combination with long alkyl R groups give these molecules sufficient amphiphilic character to make them surfactants (vide infra). Surfactants based on Figure 4.6 resemble triglycerides. In fact, they could be described as methylene interrupted cyclic triglycerides.

Nature's cross-linking agent is the disulfide bond.[29] We have chosen disulfide linkages as our means of polymerization for the same reasons they are so common in nature. The thiol to disulfide oxidation proceeds under very mild conditions, is easily reversible, and does not require or produce toxic functional groups.[30] Triesters assembled from cyclohexanetriol and terminal bromine fatty acids provide the means to selectively activate one or all of the triester

Figure 4.4: Three coordinate polymerization. An ideal crosslinking system should be based on a monomer unit with a high order rotational axis. Three coordinate polymerization results in an hexagonal lattice.

2

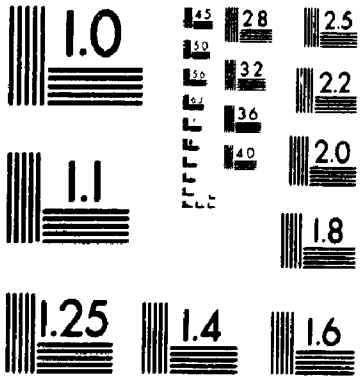

Figure 4.5: Small aggregates in three coordinate polymerization. Controlling the extent of three coordinate polymerization results in small aggregates. Optimizing the initial conditions of the polymerization will bias the product distribution in favour of the desired materials. In our case the a) monomer, b) dimer, and c) tetramer are the products of interest.

a

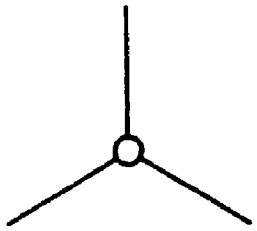

b

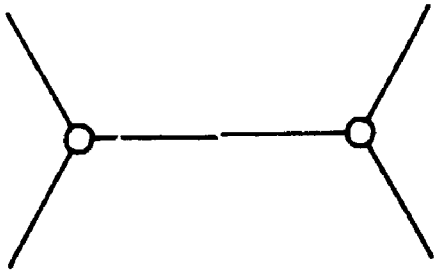

c

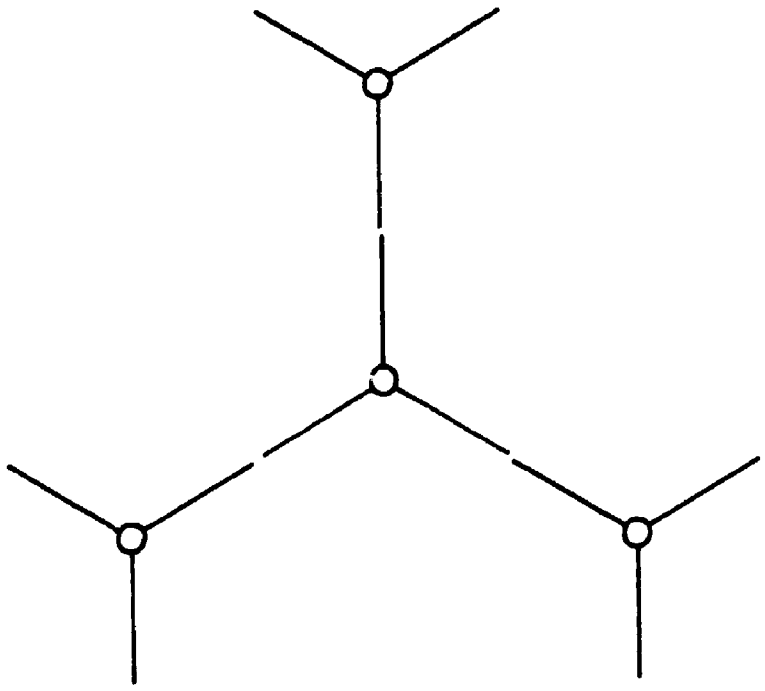

Figure 4.6: 8C Monomer. The polymerizable, three coordinate surfactants on which we have chosen to base our radial polymers are triesters of *cis,cis*-1,3,5-cyclohexanetriol. The 8C monomer shown here is illustrative of this type of molecule. The terminal bromines are converted to thiols to facilitate the polymerization.

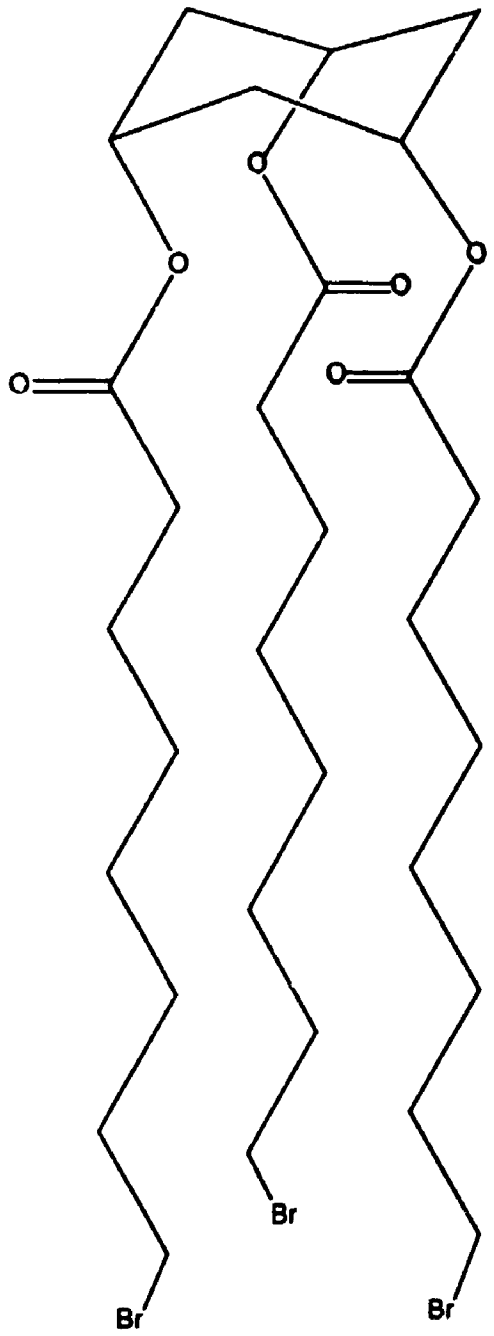
O
O
O
O
O
O
Br
Br
Br

arms. The terminal bromines may be converted quantitatively to terminal thiols using sodium hydrogen sulfide (NaSH) in dimethyl sulfoxide (DMSO).[31] Iodine oxidation cleanly and rapidly forms the disulfide.[32]

We did not anticipate the power of the sodium hydrogen sulfide reaction. Its success, however, was the key step in the synthesis of our labelled polymers. Direct, high yield reaction of the bromine substituents in the presence of ester and disulfide linkages voided any necessity for protection/deprotection schemes to produce a thiol bearing surfactant. The direct reaction of sodium hydrogen sulfide with halides has fallen out of favor due to the poor yields and hazardous products (H_2S) of the reaction.[33] The reaction in DMSO, however, proceeds quickly and quantitatively (^1H NMR) without harming esters or disulfide functionalities in the target molecule. The low polarity and poor hydrogen bonding of the thiol and disulfide moieties result in surfactant assemblies which will insert into a phospholipid bilayer with the headgroup ring at or near the bilayer/water interface and the sulfur functionalities residing in the hydrocarbon interior.

The thiol function is also useful in the fluorescence labelling reaction. Fluorescent haloacetyl derivatives are a common means of labelling thiol bearing biological molecules.[4] N-(((2-iodo acetoxy)ethyl)-N-methyl)-amino-7-nitrobenz-2-oxa-1,3-diazole, shown in Figure 4.1b (R = $CH_2CH_2O_2CCH_2I$) is the fluorophore we use. This haloacetyl derivative (IANBD) is employed to label thiol bearing monomers, dimers, and tetramers.

The great variety of compounds which result from cross-linking and labelling the monomers just described require a systematic

shorthand nomenclature. The shorthand convention we have adopted has four parts: 1) degree of substitution, if any; 2) substituent, if any; 3) fatty acid chain length; 4) aggregation state. For example a triester based on 8-bromooctanoic acid with one of the three bromines converted to a thiol would be called 1° SH 8C monomer. First degree indicates how many of the chains are derivatized, SH describes what it has been converted to and 8C denotes the length of the fatty acid chain. Monomer indicates there is only one triester unit. 1° NBD 11C dimer indicates one NBD label on a dimer comprised of two triesters with eleven carbon fatty acid chains. The simple terminal bromine triesters omit the first two descriptors and are known simply as 6C monomer, 8C monomer, and 11C monomer.

Figure 4.7 outlines the synthetic pathway followed to produce labelled, polymerized surfactants based on the cyclohexanetriol triester. Figure 4.7 uses the previously discussed nomenclature system based on the 11C monomer. This synthetic scheme has been followed for each of the three fundamental triesters. Three different triesters are used as the fundamental building blocks to explore the effect of attachment depth on the diffusion coefficient. No major alterations in the synthetic procedures are necessary whether working with the triester based on 6-bromohexanoic acid, 8-bromooctanoic acid or 11-bromoundecanoic acid.

The extent of polymerization in our system is controlled by limiting the number of bromines per monomer which are converted to thiol. The overall stoichiometry of the reaction, however, does not represent the product distribution on a molecular scale. The three equivalent sites in a monomer cause difficulties when attempting to

Figure 4.7: Synthetic pathway for labelled, radial, surfactant polymers. The pathway for the 11C monomer is shown here. Four NBD labelled products are desired. These products are highlighted by the rectangular enclosures.

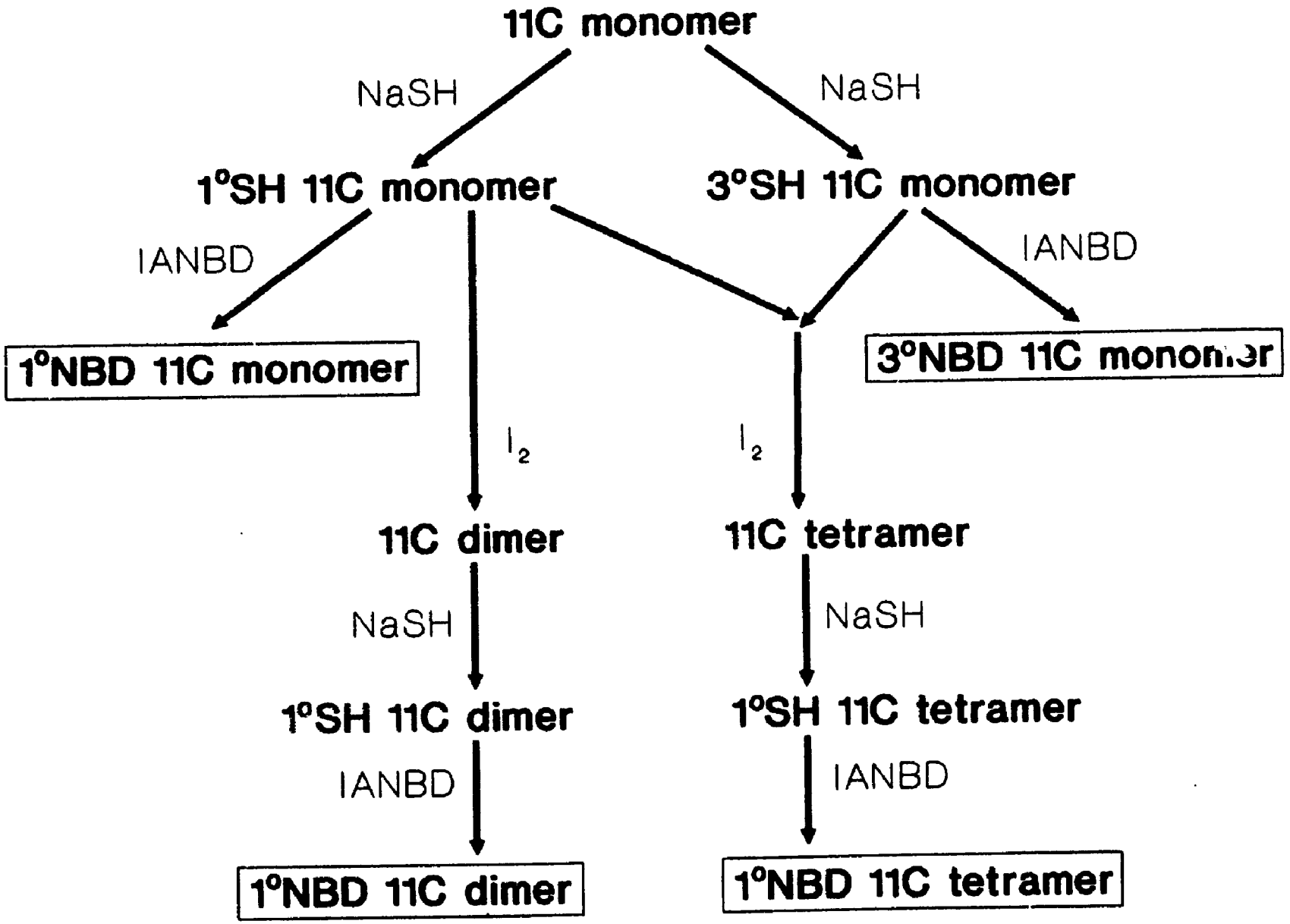
11C monomer
NaSH
NaSH
1°SH 11C monomer
3°SH 11C monomer
IANBD
IANBD
1°NBD 11C monomer
3°NBD 11C monomer
I2
I2
11C dimer
11C tetramer
NaSH
NaSH
1°SH 11C dimer
1°SH 11C tetramer
IANBD
IANBD
1°NBD 11C dimer
1°NBD 11C tetramer

produce monomers which have only one thiol per monomer. The product distribution is described by the binomial distribution if all three sites are independent. If the overall extent of conversion (bromine to thiol) is thirty-three percent, or an average of one per molecule, then a simple calculation shows that thirty percent of the monomers will have no thiols, fourty-four percent will have one thiol, twenty-two percent will have two thiols and four percent will have three thiols. This statistical distribution is the deficit engendered by the symmetry required of these molecules. Overall conversion rates of less than one third are necessary to reduce the number of large oligomers produced during the iodine oxidation.

Consider the case of an oxidation intended to produce 8C dimer. Each 2° SH 8C monomer present will remove two 1° SH 8C monomers from solution and produce a trimer. Similarly, each 3° SH 8C monomer present will remove three 1° SH 8C monomers producing a tetramer. This does not allow for cross-linking between higher order species, 3° + 2° for example, which will produce even larger oligomers. Decreasing the <u>overall</u> extent of thiol conversion to produce fewer multiply substituted monomers will simultaneously reduce the yield of the dimer since there will be fewer mono substituted species as well. Thus a delicate balance must be struck between the two inefficiencies. A simple calculus max/min calculation[34] of dimer yield versus extent of bromine conversion to thiol shows the optimum conversion is fourteen percent. This calculation assumes the second and third degree thiol bearing species react only with first degree thiol triesters.

The surfactant nature of these triesters caused great difficulty in their extraction and chromatography. Emulsion problems were devastating in solvents other than ether and separation of oligomers was impossible on silica based media due to the severe streaking behaviour of the surfactants. Model triesters were synthesized from both very short, acetic, and very long, stearic, acids to aid in understanding their physico-chemical behavior.

The chemical stability of the ester linkages was monitored by NMR examination of the ring protons located on the 1, 3, and 5 ring carbons. These protons have a large chemical shift and, due to the symmetry of the ring and its chair conformation in solution, an extremely symmetrical triplet of triplets splitting pattern. Any disruption in the symmetry of the headgroup is readily apparent in this splitting pattern. Harmful synthetic or chromatographic conditions were thus avoided. The splitting of this proton signal, from the acetic acid triester derivative mentioned above, is shown in Figure 4.8.

The large size of the polymerized surfactants and the difficulties associated with handling and purifying them necessitated a model system to develop the thiol oxidation reaction. The model thiol compound, 11-mercapto-(undecanoyl methyl ester), proved ideal in this respect.

Figure 4.8: Ring proton triplet of triplets. The symmetry of the triester ring results in a splitting of the protons on the ring carbons 1, 3, and 5 into a triplet of triplets. The coupling constants, 11 Hz and 4 Hz, show this triester has all three substituents in the equatorial positions. The ^{1}H NMR spectrum shown here was acquired from the triacetate derivative of the cyclohexanetriol (Chapter 5.3.1). The exceptional resolution of this triplet of triplets is not observed for triesters with longer hydrocarbon chains. The overall symmetry of the splitting, however, is maintained.

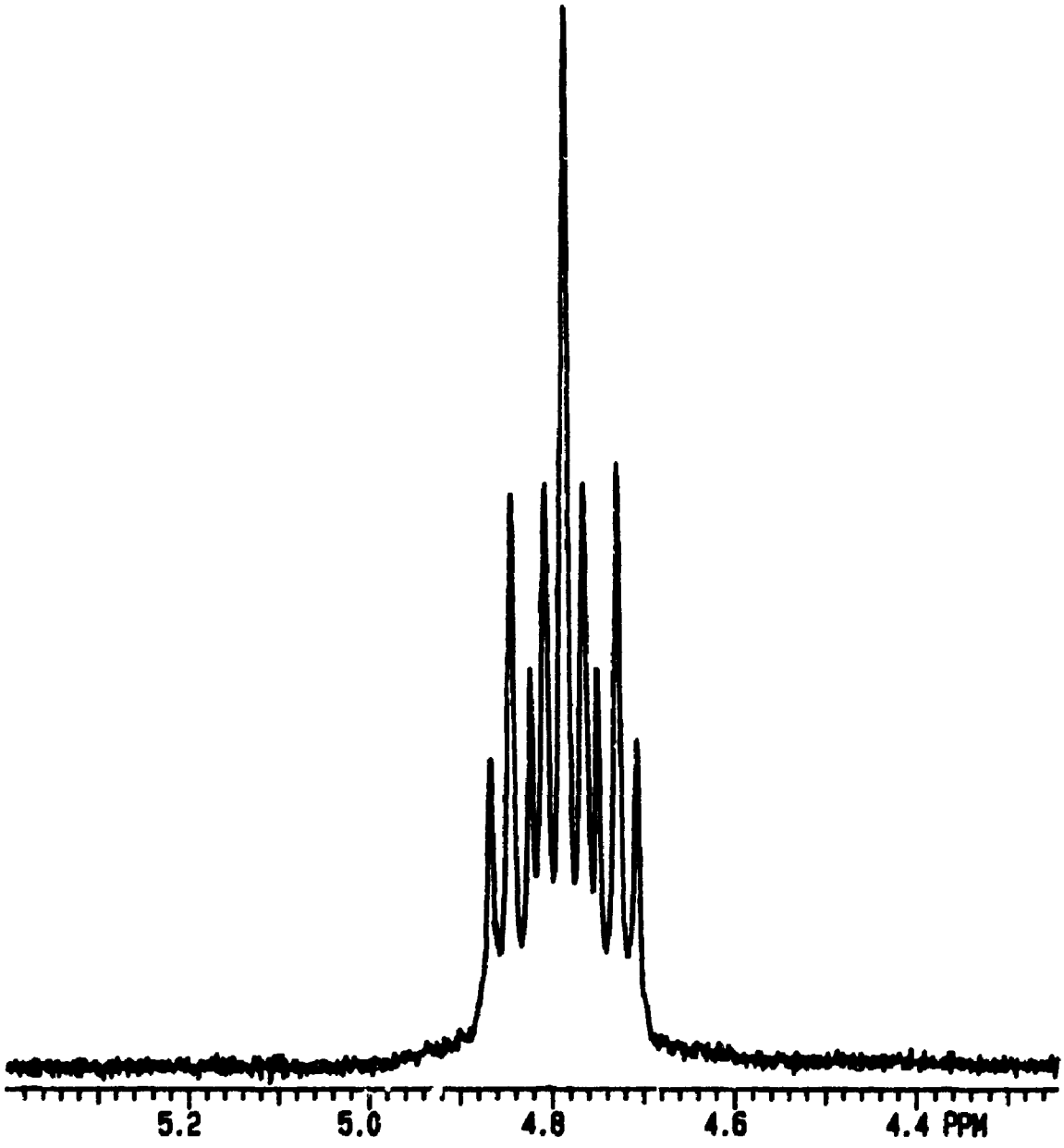
5.2
5.0
4.8
4.6
4.4 PPM

REFERENCES

(1) Wade, C. G. In *Structure and Properties of Cell Membranes*; CRC Press: Boca Raton, FL, 1985; Vol. 1, pp 51, 76.

(2) Haugland, R. P. In *Excited States of Biopolymers*; Plenum: New York, 1983; pp 29, 58.

(3) Petersen, N. O. *Can. J. Chem.* **1985**, *63*, 77.

(4) Haugland, R. P. *Handbook of Fluorescent Probes*; Molecular Probes: Eugene, OR, 1989.

(5) Chattopadhyay, A.; London, E. *Biochim. Biophys. Acta* **1988**, *938*, 24.

(6) Chattopadhyay, A.; London, E. *Biochemistry* **1987**, *26*, 39.

(7) The number following each species indicates the number of isoprene units it possess.

(8) Glasby, J. S. Ed. *Encyclopaedia of the Terpenoids*; Wiley: New York, 1982; Vol. 1, Vol. 2.

(9) Severson, R. F.; Ellington, J. J.; Schlotzhauer, P. F.; Arrendale, R. F.; Schepartz, A. I. *J. Chromatogr.* **1977**, *139*, 269.

(10) Rip, J. W.; Chaudhary, N.; Carroll, K. K. *Can. J. Biochem. Cell Biol.* **1983**, *61*, 1025.

(11) Erickson, R. E; Shunk, C. H.; Trenner, N. R.; Arison, B. H.; Folkers, K. *J. Am. Chem. Soc.*, **1959**, *81*, 4999.

(12) Jaenicki, L.; Siegmund, H. U. *Chem. Phys. Lipids* **1989**, *51* 159.

(13) Neises, B.; Stegleich, W. *Org. Synth.* **1985**, *63*, 183.

(14) Hassner, A.; Alexanian, V. *Tetrahedron Lett.* **1978**, 4475.

(15) Balcom, B. J.; Petersen, N. O. *J. Org. Chem.* **1989**, *54*, 1922.

(16) Ralston, G. B. In *Structure and Properties of Cell Membranes*; CRC Press: Boca Raton, FL, 1985; Vol. 1, pp 13, 33. References found therein.

(17) Vaz, W. L.; Criado, M. *Biochim. Biophys. Acta* **1985**, *819*, 18.

(18) Samuel, N. K.; Singh, M.; Yamaguchi, K.; Regen, S. L. *J. Am. Chem. Soc.* **1985**, *107*, 42.

(19) Chapman, D.; Lee, D. C.; Hayward, J. A. *Faraday Discuss. Chem. Soc.* **1986**, *81*, 107.

(20) Fendler, J. H. *Science* **1984**, *223*, 888.

(21) Markowitz, M. A.; Janout, V.; Castner, D. G.; Regen, S. L. *J. Am. Chem. Soc.* **1989**, *111*, 8192.

(22) Ringsdorf, H.; Schlarb, B.; Venzmer, J. *Angew. Chem. Int. Ed. Engl.* **1988**, *27*, 113.

(23) Ariga, K.; Okahato, Y. *J. Am. Chem. Soc.* **1989**, *111*, 5168.

(24) Ringsdorf, H.; Schupp, H. *J. Macromol. Sci. Chem.* **1981**, *A15*, 1015.

(25) O'Brien, D. F.; Whitesides, T. H.; Klingbiel, R. T. *J. Polym. Sci. Polym. Lett.* **1981**, *19*, 95.

(26) Uchida, M.; Tanizaki, T.; Kunitake, T.; Kajiyama, T. *Macromolecules* **1989**, *22*, 2381.

(27) Kotz, J. C.; Purcell, K. F. *Chemistry and Chemical Reactivity*; CBS College: New York, 1987; p 409.

(28) Kotz, J. C.; Purcell, K. F. *Chemistry and Chemical Reactivity*; CBS College: New York, 1987, p 789.

(29) Jocelyn, P. C. In *Biochemistry of the SH Group*; Academic: London, 1972; pp 94, 115.

(30) Capozzi, G.; Modena. G. In *The Chemistry of the Thiol Group*; Wiley: New York, 1974; Pt. 2, pp 785, 839.

(31) Vasil'tov, A. M.; Trofimov, B. A.; Amosova, S. V. *J. Org. Chem. USSR* **1983**, *19*, 1197.

(32) Vogel, A. *Textbook of Practical Organic Chemistry*; Longman: London, 1979; pp 585, 586.

(33) Streitwieser, A.; Heathcock, C. *Introduction to Organic Chemistry*; MacMillan: New York, 1985; p 758.

(34) The calculation is based on the following equations.

$$\text{Dimer Yield} = \text{Total Material } [X_1 - 2X_2 - 3X_3]$$

X_1, X_2, and X_3 are the mole fractions of 1^0, 2^0, and 3^0 thiol substituted triesters. The mole fractions, in terms of f, the overall conversion fraction, are expressed by the binomial distribution. The dimer yield may thus be expressed in terms of the overall thiol conversion.

$$\text{Dimer Yield} = \text{Total Material } [3f - 12f^2 + 6f^3]$$

Solve for f under the condition that $\frac{d\,[\text{dimer yield}]}{df} = 0.$

CHAPTER FIVE

DETAILED SYNTHESES

5.1 General

All solvents and chemicals used were BDH analytical grade, unless otherwise noted. Water used in our syntheses was doubly distilled and deionized. Diethyl ether (BDH) used in acid chloride reactions, for both work up and chromatography, was anhydrous and ethanol free. DCC reactions were run in spectroscopic grade methylene chloride (Caledon). Dimethyl sulfoxide (DMSO), required for sodium hydrogen sulfide reactions, was spectroscopic grade (BDH). Iodine oxidations were run in spectroscopic grade chloroform (BDH). Solvent mixtures are reported as volume/volume ratios. All reactions were carried out at room temperature unless otherwise specified. NBD-acid[1] was synthesized according to a published procedure.

Proton NMR spectra were recorded with a Varian XL-200 or Gemini 200 MHz Spectrometer. Carbon-13 NMR spectra were acquired with a Varian XL-300 spectrometer. Tetramethylsilane was used as an internal standard in all cases.

Silica thin layer chromatography (TLC) was performed on plastic backed Silica gel 60 UV/254 plates (Merck). Chromatograms were visualized by sample color, iodine staining, or an iodine/sodium azide spray.[2] The spray reagent was prepared by combining equal volumes of two reagent solutions. The first solution was 1 g of iodine in 100 mL of ethanol, the second solution was 2.5 g sodium azide in 100 mL 3/1

ethanol/water. Silica TLC of NBD-acid conjugates employed a solvent system which was 75/25 methylene chloride/ethyl acetate. Mallinckrodt 60-200 mesh silica gel, grade 62 special, was used for column chromatography. NBD-acid conjugates were eluted from a silica gel column with a 75/25 mixture of methylene chloride and ethyl acetate. Fatty acid triesters of *cis,cis*-1,3,5-cyclohexanetriol were eluted from silica gel with a 2.5 % triethyl amine (TEA) solution in ether.

Reverse phase thin layer chromatography (RPTLC) analyses were run on microscope slide $KC_{18}F$ plates (Whatman). Chromatograms were visualized by sample color or iodine staining. Gel permeation chromatography (GPC) in organic solvents necessitated Sephadex LH-20 gel (Pharmacia). The effective fractionation range for this gel is from 1000 to 5000 g/mol. Gel permeation chromatography separates components based on size. Small molecules penetrate the gel network readily, and therefore elute slowly, while large molecules do not penetrate the gel and elute quickly. GPC in chloroform required a SR-25 column (Pharmacia) fitted for upward elution. The flow rate through 50 g of gel, swollen in chloroform, was 0.5 mL/min. Preparative reverse phase chromatography (8C tetramer) was performed with a SEP-PAK C_{18} cartridge (Waters). HPLC equipment is described in Chapter Three.

Ellman's Reagent[3] was used as a qualitative test for thiols. The reagent, 5,5'-dithiobis-(2-nitrobenzoic acid) (Aldrich), reacts specifically with thiols by a disulfide exchange reaction to give the yellow/orange anion of 2-nitro-5-mercaptobenzoate. The reagent solution was 0.5 % 5,5'-dithiobis-(2-nitrobenzoic acid) in 50/50

pH 8 borate buffer/ethanol. Thiol-bearing compounds in solution develop a deep yellow/orange color within five minutes.

Fluorescently labelled compounds were handled in subdued light. Compounds labelled with NBD-acid were stored, as ethanol solutions under nitrogen in the dark at 4 °C. Compounds labelled with IANBD were stored as dry films under nitrogen at -15 °C in the dark . IANBD labelled compounds were used for FPR experiments within two days of isolation due to a long term instability of the thioether/ester linkage.[4]

Optical spectra were recorded using either a Cary 219 or Shidmadzu UV-160. NBD-acid[5] has $\varepsilon = 3.4 \times 10^4$ mol^{-1} L cm^{-1} at 476 nm, measured in ethanol. IANBD[6] has $\varepsilon = 2.6 \times 10^4$ mol^{-1} L cm^{-1} at 472 nm, measured in methanol. Mass spectroscopy analyses were performed on a Finnigan MAT 8230. Melting points, uncorrected, were measured on a Gallenkamp melting point apparatus.

5.2 Linear Hydrophobic Polymers - Variation in L

5.2.1 NBD-undecanol

NBD-acid (196 mg, 0.64 mmol) and 68 mg (0.33 mmol) dicyclohexylcarbodiimide (DCC), purchased from Kodak, were added to 10 mL of methylene chloride. The stirred mixture was allowed to react for five hours. The orange NBD-acid dissolved gradually as the anhydride was produced. Dicyclohexylurea precipitated as a fluffy white powder. Undecanol (Aldrich) was added to the mixture by syringe

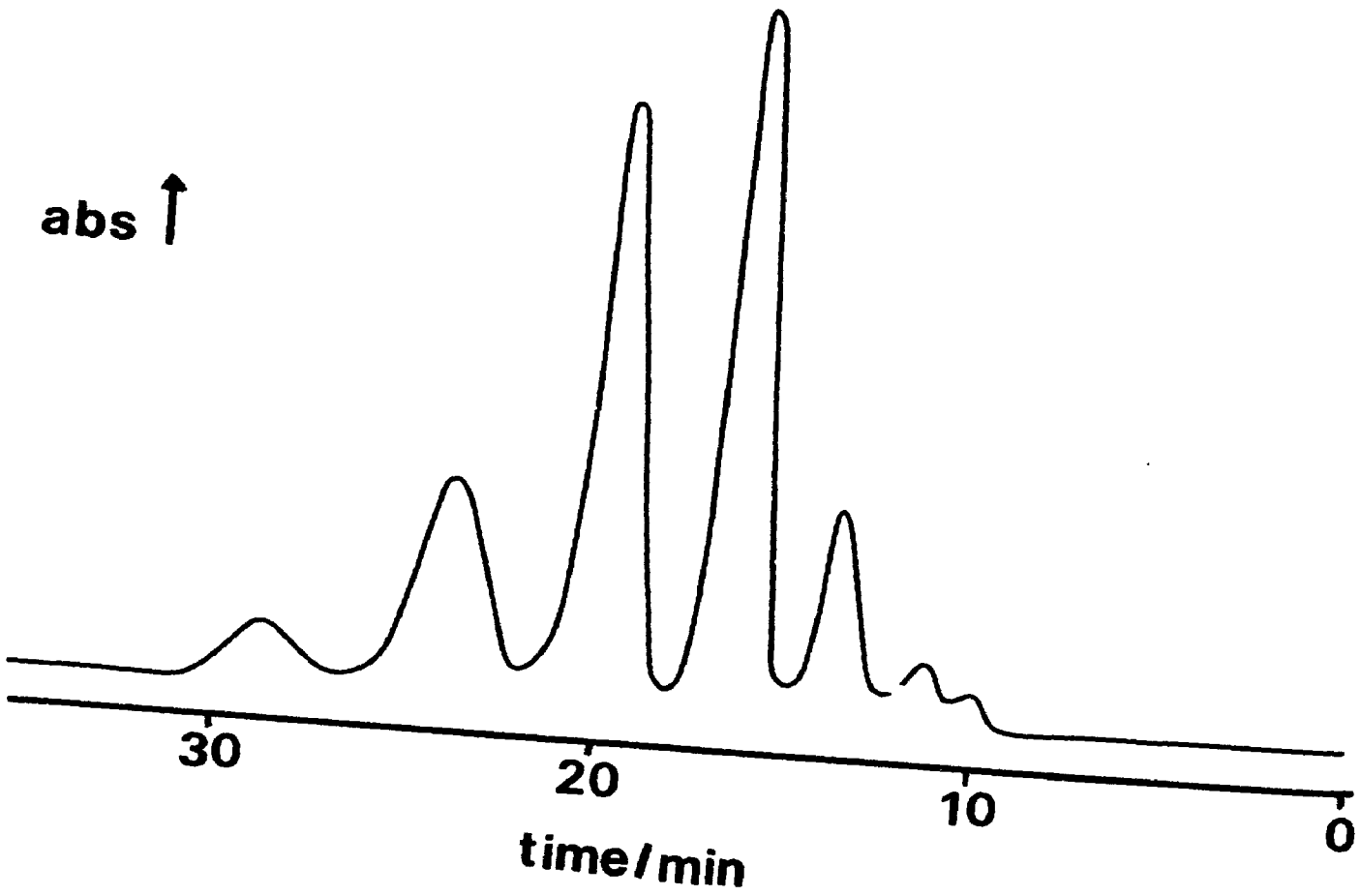
abs
30
20
10
0
time/min

3.47 (3H, broad singlet, NCH_3), 2.34 (2H, triplet, O_2CCH_2), 1.9-1.4 (8H, four overlapping partially resolved methylenes, $C\underline{H}_2CH_2O_2CCH_2C\underline{H}_2C\underline{H}_2C\underline{H}_2$), 1.26 (16H, broad singlet, eight methylenes interior of the undecanol chain), 0.88 (3H, triplet, CH_3). Carbon-13 NMR showed that the isolated product incorporated peaks characteristic of the two reactants, NBD-acid and undecanol. High resolution MS showed a molecular ion m/e = 462.2842, expected m/e = 462.2842.

NBD-undecanol, stored in ethanol, was stable for at least two years. The stability analysis was performed by reverse phase HPLC (480 nm).

5.2.2 NBD-methanol

The title compound was prepared using the procedure described for NBD-undecanol. NBD-acid (140 mg, 0.45 mmol) and 68 mg of DCC (033 mmol) reacted with 5 μL of methanol (BDH), 0.12 mmol, in the presence of 1.7 μmol of the catalyst. NBD-methanol (R_f = 0.66) was isolated by column chromatography as described above. Isolated NBD-methanol, 25 mg (sixty-six percent yield based on methanol), was an orange/red solid. HPLC analysis of NBD-methanol required a solvent mixture of 60/40 acetonitrile/water. Reverse phase HPLC (480 nm), showed one large peak at 4.5 min. ^1H NMR [$CDCl_3$, 200 MHz, δ(ppm)]: 8.45 (1H, doublet, ring proton α to nitro group), 6.09 (1H, doublet, ring proton β to nitro group), 4.08 (2H, triplet, CH_2N), 3.68 (3H, singlet, OCH_3), 3.48 (3H, broad singlet, NCH_3), 2.36 (2H, triplet, O_2CCH_2), 1.9-1.4 (6H, partially resolved multiplets, three methylenes interior acid

chain). High resolution MS m/e = 322.1271, expected m/e = 322.1277.

5.2.3 NBD-citronellol

NBD-citronellol was prepared using the procedure described for NBD-undecanol. NBD-acid (145 mg, 0.47 mmol) and 108 mg of DCC (0.52 mmol) were reacted with 15 μL of citronellol (Aldrich), 0.082 mmol, in the presence of 25 μmol of the catalyst. NBD-citronellol (R_f = 0.87) was isolated by column chromatography as described above. Isolated NBD-citronellol, 35 mg (ninety-three percent yield based on citronellol), was an orange/red oil. HPLC analysis of NBD-citronellol used the solvent conditions described for NBD-undecanol. Reverse phase HPLC (480 nm), showed one large peak at 14.3 min. A small labelled impurity (less than five percent) eluted at a slightly shorter time. The impurity was due to an alcohol, similar in size to citronellol, found in the commercial reagent. Elution at 2.0 mL/min with a 70/30 mixture of isopropyl alcohol/methanol changed the NBD-citronellol retention time to 1.8 min.

Exposure of NBD-citronellol to light and oxygen results in oxidation of the isoprene double bond yielding an oxidized product with R_f = 0.75 on silica gel (Appendix Two). Singlet oxygen, the oxidizing species, has a very long lifetime in chlorinated and deuterated solvents.[7] This makes ^{1}H NMR particularly difficult. Samples submitted for ^{1}H NMR invariably oxidized to some extent before acquisition. ^{1}H NMR [$CDCl_3$, 200 MHz, δ(ppm)]: 8.41 (1H, doublet, ring protor α to nitro group), 6.09 (1H, doublet, ring proton β to nitro

group), 5.06 (1H, triplet, CH=C), 4.12 (4H, triplet, CH_2O_2C; unresolved multiplet, CH_2N by analogy to NBD-acid), 3.48 (3H, broad singlet, NCH_3), 2.34 (2H, triplet, O_2CCH_2), 2.00 (2H, unresolved multiplet, $CO_2CH_2C\underline{H}_2$), 1.80 (3H, singlet, terminal methyl), 1.60 (3H, singlet, terminal methyl), 1.9-1.1 (11H, partially resolved multiplets, three methylenes interior acid chain, two methylenes and one methine interior citronellol chain), 0.91 (3H, doublet, CH_3). High resolution MS m/e = 446.2529, expected m/e = 446.2529.

NBD-citronellol stored in the dark, under nitrogen, was stable for at least one year in ethanol solution. The stability analysis was performed by reverse phase HPLC (480 nm).

5.2.4 NBD-solanesol

NBD-solanesol was prepared according to the procedure described for NBD-undecanol. NBD-acid (196 mg, 0.64 mmol) and 68 mg of DCC (0.33 mmol) reacted with 13 mg of crystalline solanesol (Sigma), 0.021 mmol, in the presence of 20 μmol of the catalyst. NBD-solanesol (R_f = 0.87) was isolated by column chromatography as described above. NBD-solanesol, 9 mg (fifty percent yield based on solanesol), was an orange/red tar. The yield was determined spectroscopically by the absorbance of the NBD chromophore. Reverse phase HPLC, (70/30 isopropyl alcohol/methanol, 2.0 mL/min) showed one peak (480 nm) at 4.0 min. NBD-solanesol is less stable than NBD-citronellol due to a larger number of isoprene units.

5.2.5 NBD-dolichol

NBD-dolichol was prepared according to the procedure described for NBD-undecanol. NBD-acid (71 mg, 0.23 mmol) and 24 mg of DCC (0.12 mmol) reacted with 18 mg of dolichol (0.013 mmol) in the presence of 5 μmol of the catalyst. Dolichol was a mixture of homologs between sixteen and twenty-two isoprenes in length (average nineteen). Dolichol, recovered from human liver upon autopsy, was a kind gift of Professor Ken Carroll, Department of Biochemistry, The University of Western Ontario. NBD-dolichol (R_f = 0.91) was isolated by column chromatography as previously described for NBD-undecanol. NBD-dolichol, 1 mg (six percent yield based on dolichol), was an orange/red tar. The yield was determined spectroscopically by the absorbance of the NBD chromophore.

Reverse phase HPLC (65/35 isopropyl alcohol/methanol, 2.0 mL/min) resolves the individual labelled (480 nm) dolichol species. The same distribution is observed prior to labelling, by observation at 210 nm. The unlabelled species (same elution conditions) have shorter retention times. Exposure of NBD-dolichol to light and oxygen in methylene chloride results in oxidation of the double bonds and a shift back to shorter elution times. NBD-dolichol is less stable in solution than NBD-citronellol due to a larger number of isoprene units.

The NBD-dolichol distribution is shown in the HPLC trace reproduced as Figure 5.1. Labelled homologs with sixteen, seventeen, eighteen, nineteen, twenty, twenty-one and twenty-two isoprenes had retention times of 10.7 min, 12.0 min, 14.4 min, 17.7 min, 20.5 min,

Figure 5.1: HPLC trace NBD-dolichol. Labelled homologs with from sixteen to twenty-two isoprenes are observable. This is the same distribution observed for the unlabelled homologs. The NBD-dolichol distribution was detected at 480 nm with elution by a 65/35 mixture of isopropanol and methanol at 2 mL/min.

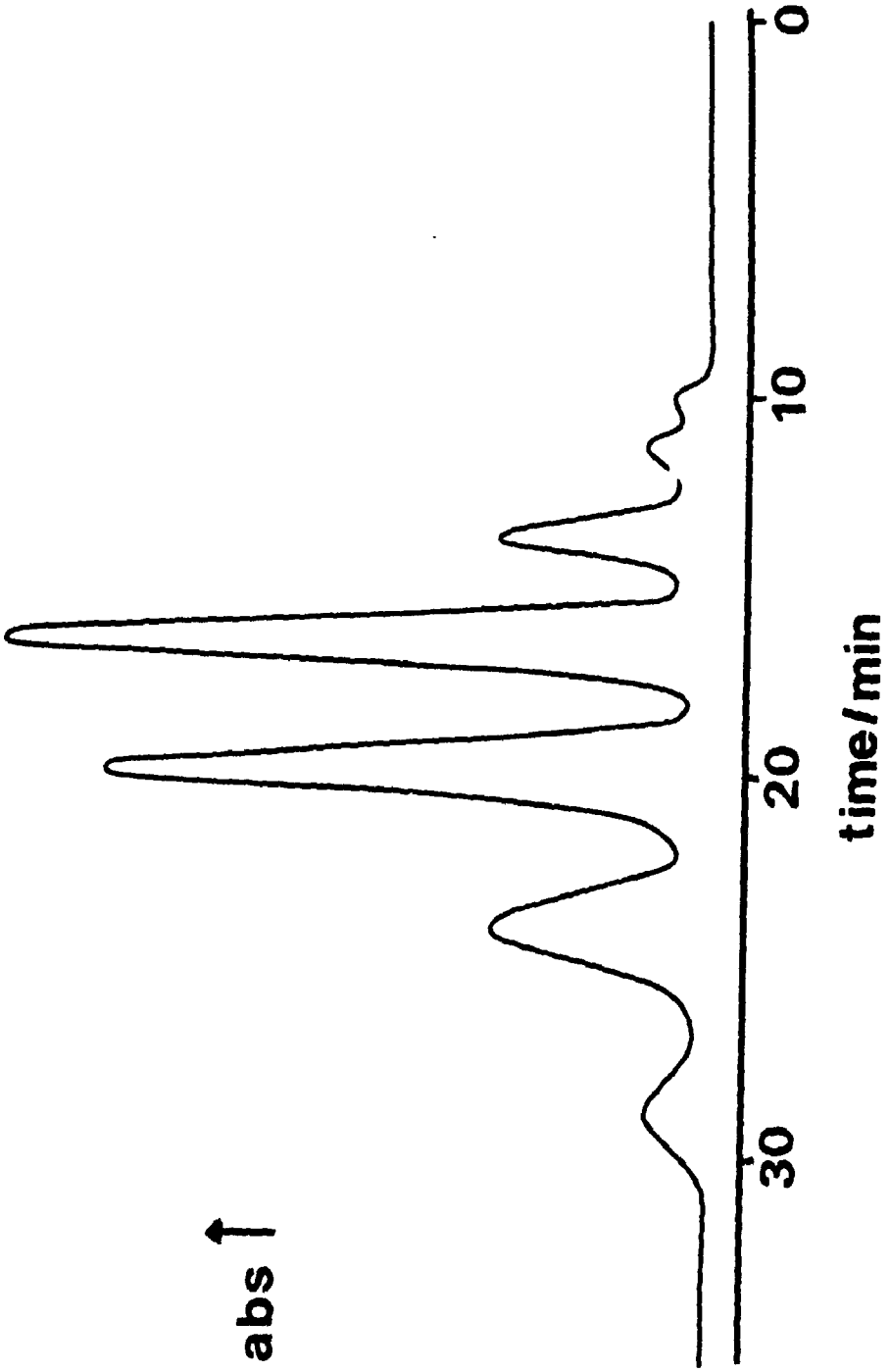
abs
0
10
20
30
time/min

24.2 min and 29.5 min respectively.

5.3 Radial Surfactant Polymers - Variation in R

5.3.1 *cis,cis*-1,3,5-Triacetyl-cyclohexanetriol

Solid *cis,cis*-1,3,5-cyclohexanetriol (triol) (100 mg, 0.59 mmol), purchased from Fluka, was added to 5 mL (70 mmol) of acetyl chloride. The reaction was sealed and left for sixteen hours. Residual acetyl chloride and acetic acid were removed by rotary evaporation followed by storage of the residue for thirty-six hours in a vacuum dessicator. A solid white precipitate, 135 mg (eighty-eight percent yield) developed on cooling to 4 °C. The recrystallized triacetyl triol, petroleum ether, was a white powder with m.p. 79-80 °C. The recrystallized triacetyl triol eluted as one spot (I_2 visualization) on silica gel with R_f = 0.63 when eluted with ethyl acetate. ^1H NMR [$CDCl_3$, 200 MHz, δ(ppm)]: 4.79 (3H, triplet of triplets, CHO_2C), 2.33 (3H, doublet of triplets, ring proton vicinal and trans to the ester), 2.04 (9H, singlet, CH_3), 1.42 (3H, quartet, ring proton vicinal and cis to the ester). MS (CI) shows $(M+H)^+$ m/e = 259, expected m/e = 259.

5.3.2 *cis,cis*-1,3,5-Tristearoyl-cyclohexanetriol

Stearic acid, 2.03 g (7.14 mmol), was dissolved in 20 mL of thionyl chloride and allowed to react for twelve hours. Stearoyl chloride was isolated by rotary evaporation of the residual thionyl

chloride. Triol (220 mg, 1.31 mmol) was added to the stearoyl chloride in 20 mL of dioxane (dried over molecular sieves). The solution was refluxed for one hour by which time the triol had dissolved. The cooled solution was sealed and left to react for several more days. Dioxane was removed by rotary evaporation and the triester product dissolved in 175 mL of ether. The etheral solution was extracted three times with pH 7.9 sodium bicarbonate buffer, then dried with magnesium sulfate ($MgSO_4$) and concentrated by rotary evaporation. The triester product (R_f = 0.88, silica TLC with ether elution) was fractionated on a silica gel column (65 g) eluted with 2.5 % triethyl amine in ether. The yield of stearoyl triester was 178 mg (fourteen percent yield). Stearoyl triester was a white powder, recrystallized from acetone, with m.p. 51 °C. Stearoyl triester eluted as a single spot on RPTLC, R_f = 0.16, with ethanol. ^1H NMR [$CDCl_3$, 200 MHz, δ(ppm)]: 4.79 (3H, triplet of triplets, CHO_2C), 2.26 (9H, triplet, CH_2CO_2; submerged multiplet three ring protons vicinal and trans to the ester), 1.59 (6H, poorly resolved quintet, $O_2CCH_2\underline{CH}_2$), 1.25 (93 H, broad singlet, fifteen methylenes in each of three chains; partially obscured quartet, three ring protons vicinal and cis to the ester). MS gave m/e = 973, expected m/e = 972.9.

5.3.3 11-(Undecanoyl methyl ester) thiol

The precursor to the terminal mercapto undecanoyl methyl ester was the terminal bromo ester. 11-Bromoundecanoic acid (Aldrich), 2.0 g (7.5 mmol), was dissolved and allowed to react in 10 mL thionyl

chloride for twelve hours. 11-Bromoundecanoyl chloride was isolated by rotary evaporation of residual thionyl chloride. Excess methanol, 10 mL (0.247 mol), was added to the acid chloride and allowed to react for four hours. Excess methanol was removed by rotary evaporation leaving the desired 11-bromoundecanoyl methyl ester. The ester eluted on silica gel (R_f = 0.68 with methylene chloride) as one spot, detected by iodine. ^{1}H NMR of this product gave the expected spectrum. Methylenes α and β to the bromine gave a triplet (δ = 3.40 ppm) and a quintet (δ = 1.85 ppm) respectively.

The terminal thiol was formed by reacting the terminal bromo methyl ester (0.743 g, 2.66 mmol) with sodium hydrogen sulfide (NaSH), purchased from Aldrich. The NaSH was added to the substrate oil as a solution in DMSO. The solution was 0.247 g NaSH (4.40 mmol) in 6 mL DMSO. The reaction proceeded, under nitrogen, for twenty minutes, then was extracted with 150 mL 50/50 ether/hexanes and two portions (50mL) of pH 7.0 phosphate buffer. The ether/hexanes layer was dried with $MgSO_4$ and concentrated. The resulting oil (469 mg, seventy-seven percent yield) had the odour characteristic of thiols and gave a positive test for thiols using Ellman's Reagent. The thiol eluted on silica, R_f = 0.59, when developed with methylene chloride. Iodine visualization gave the characteristic doughnut stain expected of thiols.[8] Visualization with an iodine/azide spray reagent also gave the expected stain, a white spot on brown background.[2]

^{1}H NMR [$CDCl_3$, 200 MHz, δ(ppm)]: 3.67 (3H, singlet, CH_3), 2.52 (2H, quartet, $C\underline{H}_2SH$), 2.30 (2H, triplet, O_2CCH_2), 1.62 (4H, overlapping quintets, $O_2CCH_2C\underline{H}_2$ and $C\underline{H}_2CH_2SH$), 1.28 (13H, broad

singlet, six methylenes interior of the chain, partially obscured triplet, SH). Deuterium exchange collapses the coupling of the thiol to the neighbouring methylene yielding a triplet at δ = 2.47 ppm. DMSO, although an oxidizing agent, does not produce disulfide under these conditions. Treatment of the bromo ester with a limiting amount of NaSH in DMSO quantitatively converts bromine to thiol as determined by ^{1}H NMR.

5.3.4 11-(Undecanoyl methyl ester) disulfide

The 11-(undecanoyl methyl ester) thiol (200 mg, 0,86 mmol) was dissolved in 2 mL of chloroform and 80 mg of I_2 (0.31 mmol) was added. The reaction proceeded for one hour then the solution was diluted to 25 mL with chloroform. The chloroform was extracted twice with 12 mL pH 8 borate buffer, once with 10 mL of 10 % aqueous sodium thiosulfate ($Na_2S_2O_3$) and once with 10 mL of water. The silica TLC (methylene chloride) showed two peaks, one the original thiol and a second peak (R_f = 0.25) visualized by iodine stain and iodine/azide spray.

The chloroform extract was concentrated and applied, in methylene chloride, to a silica gel column (25 g). The slow fraction (R_f = 0.25) above was collected and the methylene chloride concentrated to yield 150 mg of the title compound (0.32 mmol, one hundred percent yield) as a fluffy white precipitate. The precipitate, lustrous white flakes, was recrystallized from warm acetone/water, m.p. 54-55 ^{o}C. ^{1}H NMR [$CDCl_3$, 200 MHz, δ(ppm)]: 3.67 (6H, singlet, CH_3), 2.67 (4H, triplet, CH_2SS), 2.30 (4H, triplet, O_2CCH_2), 1.64 (8H, overlapping

quintets, $C\underline{H}_2CH_2SS$ and $O_2CCH_2C\underline{H}_2$), 1.28 (24H, broad singlet, six methylenes interior of each chain.). High resolution MS gave m/e = 462.2828, expected m/e = 462.2838.

The methylene triplet α to the disulfide bond (δ = 2.67 ppm) has a characteristic splitting observed in all disulfide products examined in this work. The conventional 1:2:1 peak intensities expected for a triplet are not displayed by these compounds. Typically one observes a ratio much closer to 1:1.3:1. This may be caused by restricted rotation about the sulfur-sulfur bond.

Both sodium sulfite and sodium thiosulfate have been used in these syntheses to remove unreacted iodine. Control experiments show that neither reduces the disulfide when used as an aqueous wash. Sodium thiosulfate is preferred since it is less basic in aqueous solution.

Oxidizing agents other than iodine were employed in the thiol oxidation. However, none were as convenient to use or provided such high yields. Agents employed were DMSO/TEA,[9] air oxidation under basic conditions,[9] copper sulfate[9] and potassium ferricyanide.[10] Control experiments showed that excess iodine did not cause overoxidation of the disulfide. The 11-(Undecanoyl methyl ester) disulfide could be reduced to the starting thiol (^{1}H NMR) by treatment with tri-n-butyl phosphine.[11]

5.3.5 11C Monomer

11-Bromoundecanoic acid, 2.86 g (10.8 mmol), was dissolved and allowed to react in 20 mL thionyl chloride for eight hours. 11-Bromoundecanoyl chloride was isolated by rotary evaporation of the residual thionyl chloride. Triol (363 mg, 2.16 mmol) was added to the acid chloride in 20 mL of dry dioxane and the mixture refluxed for one hour. A drying tube excluded moisture during the reflux. The mixture was allowed to react several days further at room temperature. The dioxane was removed by rotary evaporation and the triester dissolved in 175 mL of ether. The etheral solution was extracted three times with 75 mL pH 7.9 sodium bicarbonate buffer, then dried with $MgSO_4$ and concentrated by rotary evaporation. The concentrate was fractionated on a silica gel column (65 g); eluted with 2.5 % TEA in ether. Fractions were tested by TLC. 11C monomer has R_f = 0.68 on silica eluted with ether. The 11C monomer, a clear oil, was isolated by rotary evaporation with ethyl acetate as a cosolvent. The yield of 11C monomer was 990 mg (fifty-two percent yield). 11C monomer shows a single spot (R_f = 0.16), iodine stained, on RPTLC with methanol as solvent. Over a period of many days, at room temperature, the 11C monomer oil will crystallize to form a clear solid. 11C monomer was recrystallized from hexanes, m.p. 31-32 °C. High resolution, single crystal X-ray studies of the 11C monomer are in progress.

^1H NMR [$CDCl_3$, 200 MHz, δ(ppm)]: 4.76 (3H, triplet of triplets, CHO_2C), 3.40 (6H, triplet, CH_2Br), 2.26 (9H, triplet, CH_2CO_2 and submerged multiplet, three ring protons vicinal and trans to the ester),

1.85 (6H, quintet, $C\underline{H}_2CH_2Br$), 1.59 (6H, poorly resolved quintet, $O_2CCH_2C\underline{H}_2$), 1.28 (39 H, broad singlet, six methylenes in each of three chains; partially obscured quartet, three ring protons vicinal and cis to the ester). High resolution MS gave m/e = 870.2644, expected m/e = 870.2621. The two isotopes of bromine, ^{79}Br and ^{81}Br, have approximately equal natural abundances. This gives rise to a characteristic molecular ion 'fingerprint'. The molecular ion should yield four peaks at intervals of two mass units with relative intensities of 1:3:3:1. This was observed experimentally.

5.3.6 8C Monomer

The title compound was prepared and isolated according to the procedure for 11C monomer. 8-Bromooctanoic acid (Aldrich), 3.03 g (13.6 mmol) reacted with 446 mg triol (2.65 mmol) yields 797 mg of 8C monomer (forty percent yield). RPTLC showed one spot (iodine visualization) with R_f = 0.42 eluted with methanol. Silica TLC showed one spot (iodine visualization), with R_f = 0.70 when eluted with ether.

^1H NMR [$CDCl_3$, 200 MHz, δ(ppm)]: 4.80 (3H, triplet of triplets, CHO), 3.41 (6H, triplet, CH_2Br), 2.28 (9H, triplet, CH_2CO_2 and submerged multiplet, three ring protons vicinal and trans to the ester), 1.86 (6H, quintet, $C\underline{H}_2CH_2Br$), 1.61 (6H, poorly resolved quintet, $O_2CCH_2C\underline{H}_2$), 1.34 (21 H, broad singlet, three methylenes in each of three chains; partially obscured quartet, three ring protons vicinal and cis to the ester). High resolution MS gave m/e = 744.1251,

expected m/e = 744.1236. The molecular ion had the expected 1:3:3:1 isotonic ratio.

5.3.7 6C Monomer

The title compound was prepared and isolated according to the procedure for 11C monomer. 6-Bromooctanoic acid (Aldrich), 2.64 g (13.5 mmol) reacted with 455 mg triol (2.33 mmol) yields 948 mg of 6C monomer (fifty-two percent yield). RPTLC showed one spot (iodine visualization) with R_f = 0.60 eluted with methanol. Silica TLC showed one spot (iodine visualization), with R_f = 0.68 eluted with ether.

^{1}H NMR [$CDCl_3$, 200 MHz, δ(ppm)]: 4.79 (3H, triplet of triplets, CHO), 3.41 (6H, triplet, CH_2Br), 2.30 (9H, triplet, CH_2CO_2 and submerged multiplet, three ring protons vicinal and trans to the ester), 1.87 (6H, quintet, $C\underline{H}_2CH_2Br$), 1.64 (6H, poorly resolved quintet, $O_2CCH_2C\underline{H}_2$), 1.5-1.3 (9H, overlapping multiplets, one methylene interior each chain; partially obscured quartet, three ring protons vicinal and cis to the ester). High resolution MS gave m/e = 660.0301, expected m/e = 660.0297. The molecular ion had the expected 1:3:3:1 isotopic ratio.

5.3.8 3° SH 11C Monomer

A 6 mL solution of DMSO containing 84 mg of NaSH (1.5 mmol) was added to 226 mg of 11C monomer (0.259 mmol), under nitrogen. The

reaction, stirred, was allowed to proceed for thirty minutes. It was then extracted with 100 mL of 50/50 hexanes/ether and four 20 mL portions of pH 7.4 phosphate buffer. The hexanes/ether extract was dried with $MgSO_4$ and concentrated by rotary evaporation. The yield of 3° SH 11C monomer was 126 mg (sixty-six percent yield). The resulting oil had a characteristic thiol odour and gave a positive test with Ellman's Reagent.

^{1}H NMR [$CDCl_3$, 200 MHz, δ(ppm)]: 4.78 (3H, triplet of triplets, CHO_2C), 2.52 (6H, quartet, $C\underline{H}_2SH$), 2.27 (9H, triplet, CH_2CO_2 and submerged multiplet, three ring protons vicinal and trans to the ester), 1.63 (12H, overlapping quintets, $C\underline{H}_2CH_2CO_2$ and $C\underline{H}_2CH_2SH$), 1.28 (42 h, broad singlet, six methylenes in each of three chains; partially obscured quartet, three ring protons vicinal and cis to the ester; partially obscured triplet, SH).

5.3.9 3° SH 8C Monomer

Preparation and isolation of the 3° SH 8C monomer was analogous to the 3° SH 11C monomer. A 5 mL solution of DMSO with 35 mg of NaSH (0.62 mmol) added to 60 mg (0.080 mmol) of 8C monomer (allowed to react for fifteen minutes) gave 20 mg (0.029 mmol) of the title compound. The yield was low, thirty-six percent, in part because a portion of the product hexanes/ether solution was spilled. The concentrated oil had a characteristic thiol odour and gave a positive test with Ellman's Reagent.

^{1}H NMR [$CDCl_3$, 200 MHz, δ(ppm)]: 4.79 (3H, triplet of triplets,

CHO_2C), 2.52 (6H, quartet, $C\underline{H}_2SH$), 2.27 (9H, triplet, CH_2CO_2 and submerged multiplet, three ring protons vicinal and trans to the ester), 1.60 (12H, overlapping quintets, $C\underline{H}_2CH_2C\underline{H}_2$ and $C\underline{H}_2CH_2SH$), 1.33 (24H, broad singlet, three methylenes in each of three chains; partially obscured quartet, three ring protons vicinal and cis to the ester; partially obscured triplet, SH).

A derivative of the 3° thiol was prepared to confirm its structure. 3° SH 8C monomer reacted with excess methyl methanethiosulfinate[12] to produce a terminal methyl disulfide derivative on each chain. The ^1H NMR triplet at δ = 1.33 ppm (SH), and the quartet at δ = 2.52 ($C\underline{H}_2SH$) disappeared, as expected. In their stead two new peaks appear; a triplet at δ = 2.69 ppm ($C\underline{H}_2SS$) and a singlet at δ = 2.19 ppm ($SSCH_3$). High resolution MS gave m/e = 744.2721, expected m/e = 744.2714.

5.3.10 3° SH 6C Monomer

Preparation and isolation of the 3° SH 6C monomer was analogous to the 3° SH 11C monomer. A 4 mL solution of DMSO with 38 mg of NaSH (0.68 mmol), added to 68 mg (0.10 mmol) of 8C monomer (reacted for twenty minutes), gave 43 mg (0.083 mmol) of the title compound. The yield was eighty-three percent. The concentrated oil had a characteristic thiol odour and gave a positive test with Ellman's Reagent.

^1H NMR [$CDCl_3$, 200 MHz, δ(ppm)]: 4.81 (3H, triplet of triplets, CHO_2C), 2.53 (6H, quartet, $C\underline{H}_2SH$), 2.29 (9H, triplet, CH_2CO_2 and

submerged multiplet, three ring protons vicinal and trans to the ester), 1.62 (12H, overlapping quintets, $C\underline{H}_2CH_2CO_2$ and $C\underline{H}_2CH_2SH$), 1.45 (9H, overlapping multiplets, one interior methylene in each of three chains; partially obscured quartet, three ring protons vicinal and cis to the ester), 1.34 (3H, triplet, SH).

5.3.11 1° SH 11C Monomer

The first degree thiol substituted 11C monomer, in common with the two analogous thiols, cannot be synthesized as a pure compound due to the equivalence of the three target chains. The statistical distribution of products was outlined in the previous chapter.

11C Monomer, 1.23 g (1.4 mmol), was dissolved in 2 mL of stirred DMSO under nitrogen. Over a period of fifteen minutes, 10 mL of DMSO solution containing 0.42 mmol of NaSH, was added dropwise to the stirred 11C monomer solution under nitrogen. The reaction was allowed to proceed an additional twenty-five minutes, then was extracted with 100 mL of 50/50 hexanes/ether and three 20 mL portions of pH 7.4 phosphate buffer. The hexanes/ether solution was dried with $MgSO_4$ and concentrated by rotary evaporation. The yield of 1° SH 11C monomer, and related products, was 659 mg.

Reaction of the 11C monomer with NaSH as the limiting reagent results in a partial conversion of the ^1H NMR triplet at δ = 3.41 ppm (CH_2Br) to a quartet at δ = 2.53 ppm ($C\underline{H}_2SH$). Integration of these two NMR peaks showed approximately ten percent conversion of the terminal bromine to thiol. The ester linkages were unaffected by the

substitution reaction. NaSH was added to the mixture in a stoichiometric amount intended to convert ten percent of the bromines to thiols. Although the reaction appeared to go to completion (^{1}H NMR), the overall yield was rather low. It appears that a significant amount of triester was lost in the aqueous extraction. This is not surprising since, by design, the triesters are surfactants.

High dilution conditions and vigorous stirring are necessary to minimize multiple thiol substitution on individual molecules. Unless these conditions are fulfilled, local concentration gradients result in mutiple substitution beyond that predicted by the binomial distribution. Oxidation under these conditions (experimentally observed) resulted in a shift in the product distribution upon reaction to higher order oligomers.

5.3.12 1° SH 8C Monomer

The preparation of 1° SH 8C monomer was analogous to that of 1° SH 11C monomer. 8C Monomer (401 mg, 0.537 mmol) was dissolved in 2 mL of stirred DMSO under nitrogen. Over a period of five minutes, 10 mL of DMSO solution containing 0.240 mmol of NaSH was added dropwise to the stirred 8C monomer solution under nitrogen. The reaction was allowed to proceed for an additional five minutes before extraction. NaSH was added in sufficient amount to convert fifteen percent of the bromine groups to thiol functions. The ^{1}H NMR triplet at δ = 3.40 ppm (CH_2Br) was partially converted to a quartet at δ =

2.51 ppm ($C\underline{H}_2SH$). The conversion, measured by ^1H NMR, was thirteen percent. The ester linkages were unaffected by the substitution reaction. The yield of 1° SH 8C monomer, and related products, was 171 mg.

5.3.13 1° SH 6C Monomer

The preparation of 1° SH 6C monomer was analogous to that of 1° SH 11C monomer. 6C Monomer (614 mg, 0.926 mmol) was dissolved in 2 mL of stirred DMSO under nitrogen. Over a period of fifteen minutes, 10 mL of DMSO solution containing 0.560 mmol of NaSH was added dropwise to the stirred 6C monomer solution under nitrogen. The reaction was allowed to proceed for thirty minutes before extraction. NaSH was added in sufficient amount to convert twenty percent of the bromines in solution to thiols. The ^1H NMR triplet at δ = 3.38 ppm (CH_2Br) was partially converted to a quartet at δ = 2.50 ppm ($C\underline{H}_2SH$). The conversion, measured by ^1H NMR, was twenty percent. The ester linkages were unaffected by the substitution reaction. The yield of 1° SH 6C monomer, and related products, was 324 mg.

5.3.14 11C Dimer

A 1° SH 11C monomer mixture (425 mg) with ten percent bromine to thiol conversion was oxidized with excess I_2 (61 mg, 0.24 mmol). The reaction, which was allowed to proceed for ninety minutes under nitrogen, took place in 10 mL of chloroform with two drops of added

pyridine. The dark brown reaction mixture quickly precipitated a dark, fluffy pyridine salt. The reaction mixture was extracted with 75 mL of 50/50 hexanes/ether and two 25 mL portions of pH 7.4 phosphate buffer. Residual I_2 was removed by extraction with 20 mL of 5 % $Na_2S_2O_3$. Further extraction with two more 25 mL aliquots of buffer was followed by drying with $MgSO_4$. The oxidized mixture was concentrated by rotary evaporation. The major components of this mixture were 11C monomer, 11C dimer and a lesser amount of larger oligomer. RPTLC of the mixture in ethanol gave R_f = 0.51 for the monomer, 0.29 for the dimer and 0.0 for the larger oligomer. GPC of the oxidized mixture resulted in the large oligomer eluting first, followed by 11C dimer and then 11C monomer. The three compounds, detected by RPTLC, elute as distinct, but closely spaced, bands. Small fractions (less than 2 mL) were therefore necessary to effect separation. RPTLC and GPC are interesting, complementary techniques. Large molecules, such as the 11C dimer considered here, elute very quickly by GPC while they move extremely slowly on RPTLC plates with normal elution. This is the reverse of the order seen with smaller molecules such as 11C monomer. The yield of 11C dimer from the column was 37 mg (0.022 mmol). Based on the product distribution of the original mixture,[13] allowing for oligomer formation, the yield was forty-seven percent yield.

^1H NMR [$CDCl_3$, 200 MHz, δ(ppm)]: 4.79 (6H, triplet of triplets, CHO_2C), 3.40 (8H, triplet, CH_2Br), 2.66 (4H, triplet, CH_2SS), 2.26 (18H, triplet, CH_2CO_2 and submerged multiplet, six ring protons vicinal and trans to the ester), 1.84 (8H, quintet, $C\underline{H}_2CH_2Br$), 1.58 (16H,

multiplet, $O_2CCH_2C\underline{H}_2$ and $C\underline{H}_2CH_2SS$), 1.27 (78 H, broad singlet, six methylenes in each of six chains; partially obscured quartet, six ring protons vicinal and cis to the ester). Neither high resolution MS nor MS(CI) could detect a molecular ion at m/e = 1647.

5.3.15 8C Dimer

The title compound was synthesized and isolated by procedures analogous to those employed to produce 11C dimer. A 1° SH 8C monomer mixture (450 mg) with fourteen percent bromine to thiol conversion was oxidized with excess I_2 (76 mg, 0.30 mmol). The reaction was allowed to proceed for seventy-five minutes before extraction. RPTLC showed 8C monomer, 8C dimer and some larger oligomer. Eluted with methanol, the R_f's for these three components were 0.46, 0.14 and 0.0 respectively. GPC fractionation yielded 45 mg (0.032 mmol) of the 8C dimer. Based on the product distribution of the original mixture,[13] allowing for oligomer formation, the yield was fifty percent.

^1H NMR [$CDCl_3$, 200 MHz, δ(ppm)]: 4.80 (6H, triplet of triplets, CHO_2C), 3.40 (8H, triplet, CH_2Br), 2.66 (4H, triplet, CH_2SS), 2.27 (18H, triplet, CH_2CO_2 and submerged multiplet, six ring protons vicinal and trans to the ester), 1.85 (8H, quintet, $C\underline{H}_2CH_2Br$), 1.60 (16H, multiplet, $O_2CCH_2C\underline{H}_2$ and $C\underline{H}_2CH_2SS$), 1.33 (42 H, broad singlet, three methylenes in each of six chains; partially obscured quartet, six ring protons vicinal and cis to the ester).

Contrary to the results for 11C dimer, a large mass ion was observed for 8C dimer. MS(CI) gave a molecular ion $(M + H)^+$ m/e=

1489, expected m/e = 1395. The isotopic pattern of the observed molecular ion showed approximately the correct 1:4:6:4:1 intensity distribution at two mass unit intervals. This is the intensity distribution expected for molecules containing four bromine substituents. The origin of the extra 94 mass units is unknown. The ^{1}H NMR and chromatograpic behaviour (before and after MS) of this compound support the 8C dimer structure. The unusual headgroup structure of the dimer may result in a gas phase complexation of some type.

5.3.16 6C Dimer

The title compound was synthesized and isolated by procedures analogous to those employed to produce 11C dimer. A 1° SH 6C monomer mixture (283 mg) with twenty percent bromine to thiol conversion was oxidized with excess I_2 (54 mg, 0.21 mmol). The reaction was allowed to proceed for ninety minutes before extraction. RPTLC showed 6C monomer, 6C dimer and some larger oligomer (presumably trimer). Eluted with methanol, the R_f's for these three components were 0.59, 0.43 and 0.29 respectively. GPC fractionation yielded 37 mg (0.030 mmol) of 6C dimer. Based on the product distribution of the original mixture,[13] allowing for oligomer formation, the yield was seventy-eight percent.

^{1}H NMR [$CDCl_3$, 200 MHz, δ(ppm)]: 4.81 (6H, triplet of triplets, CHO_2C), 3.41 (8H, triplet, CH_2Br), 2.67 (4H, triplet, CH_2SS), 2.30 (18H, triplet, CH_2CO_2 and submerged multiplet, six ring protons vicinal

and trans to the ester), 1.87 (8H, quintet, $C\underline{H}_2CH_2Br$), 1.64 (16H, multiplet, $O_2CCH_2C\underline{H}_2$ and $C\underline{H}_2CH_2SS$), 1.45 (18 H, broad singlet, three methylenes in each of six chains; partially obscured quartet, six ring protons vicinal and cis to the ester).

MS(CI) gave a molecular ion $(M + H)^+$ m/e= 1323, expected m/e = 1227. The isotopic pattern of the observed molecular ion showed approximately the correct 1:4:6:4:1 intensity distribution at two mass unit intervals. This is the intensity distribution expected for molecules containing four bromine substituents. The origin of the extra 96 mass units is unknown. The ^1H NMR and chromatograpic behaviour (before and after MS) of this compound support the 6C dimer structure. Oxidation with TEA as the base and Na_2SO_3 extraction gave the identical molecular ion and isotope distribution. The unusual headgroup structure of the dimer may result in a gas phase complexation of some type.

5.3.17 1° SH 11C Dimer

11C Dimer (14 mg, 8.5 μmol) was dissolved in 1 mL of DMSO under nitrogen. NaSH (5.1 μmol) in 50 μL of DMSO was added dropwise to the rapidly stirred dimer solution over the course of several minutes. The reaction, under a blanket of nitrogen, was allowed to proceed for ten minutes before extraction. The DMSO solution was extracted with 50 mL of ether and two portions of 15 mL pH 7.4 phosphate buffer. The ethereal solution was dried with $MgSO_4$ and concentrated by rotary evaporation. NaSH was added in a stoichiometric amount to convert

fifteen percent of the terminal bromines to thiols. ^{1}H NMR showed fourteen percent of the triplet at δ = 3.39 ppm (CH_2Br) was converted to a quartet at δ = 2.50 ppm ($C\underline{H}_2SH$). The ester and disulfide linkages were unaffected by the substitution reaction. The yield of 1° SH 11C dimer, and related products, was 10 mg.

5.3.18 1° SH 8C Dimer

The 1° SH 8C dimer was prepared by the procedure used to synthesize and isolate 1° SH 11C dimer. 8C Dimer (52 mg, 37 μmol) was dissolved in 2 mL of DMSO under nitrogen. NaSH (15 μmol) in 125 μL of DMSO was added dropwise to the rapidly stirred dimer solution over the course of several minutes. The reaction, under nitrogen, was allowed to proceed for twelve minutes before extraction. NaSH was added in a stoichiometric amount to convert ten percent of the terminal bromines to thiols. ^{1}H NMR showed ten percent of the triplet at δ = 3.38 ppm (CH_2Br) was converted to a quartet at δ = 2.50 ppm ($C\underline{H}_2SH$). The ester and disulfide linkages were unaffected by the substitution reaction. The yield of 1° SH 8C dimer, and related products, was 36 mg.

5.3.19 1° SH 6C Dimer

The 1° SH 6C dimer was prepared by the procedure used to synthesize and isolate 1° SH 11C dimer. 6C Dimer (42 mg, 36 μmol) was dissolved in 1 mL of DMSO under nitrogen. NaSH (21 μmol) in 180 μL of DMSO was added dropwise to the rapidly stirred dimer solution over the

course of several minutes. The reaction, under nitrogen, was allowed to proceed for ten minutes before extraction. NaSH was added in a stoichiometric amount to convert fifteen percent of the terminal bromines to thiols. ^{1}H NMR showed sixteen percent of the triplet at δ = 3.39 ppm (CH_2Br) was converted to a quartet at δ = 2.50 ppm ($\underline{CH}_2SH$). The ester and disulfide linkages were unaffected by the substitution reaction. The yield of 1° SH 6C dimer, and related products, was 26 mg.

5.3.20 11C Tetramer

The title compound was prepared by iodine oxidation of a mixture containing a small amount of 3° SH 11C monomer and a large excess of 1°SH 11C monomer. The oxidation and extraction were based on the analogous preparation of 11C dimer. 1° SH 11C Monomer (354 mg, twenty percent thiol conversion) and 3° SH 11C monomer (19 mg, 26 μmol) were oxidized with a slight excess of I_2 (60 mg, 0.23 mmol) in 10 mL of chloroform with two drops of added pyridine. The oxidation was allowed to proceed for two hours before extraction. The reaction mixture was then fractionated by GPC with chloroform elution. RPTLC (70/30 acetonitrile/tetrahydrofuran) showed four spots. The major products were 11C monomer (R_f = 0.51), 11C dimer (R_f = 0.25) and 11C tetramer + oligomer (R_f = 0.0). A small spot at R_f = 0.11 was probably due to 11C trimer. Fractionation of the mixture was performed by GPC. A small amount of higher order oligomer (identified as such by ^{1}H NMR) eluted prior to 11C tetramer. The yield of 11C

tetramer (42 mg, 13 μmol) was fifty percent based on 3° SH 11C monomer.

The ^{1}H NMR spectrum was characterized based on the peaks resonant above 2.0 ppm. ^{1}H NMR [$CDCl_3$, 200 MHz, δ(ppm)]: 4.79 (12H, triplet of triplets, CHO_2C), 3.39 (12H, triplet, CH_2Br), 2.66 (12H, triplet, CH_2SS), 2.25 (36H, triplet, CH_2CO_2 and submerged multiplet, twelve ring protons vicinal and trans to the ester).

5.3.21 6C Tetramer

The title compound was prepared by iodine oxidation of a mixture containing a small amount of 3° SH 6C monomer and a large excess of 1°SH 6C monomer. The preparation is based on that of 11C dimer described above. 1° SH 6C Monomer (454 mg, twenty percent thiol conversion) and 3° SH 6C monomer (22 mg, 42 μmol) were oxidized with excess I_2 (100 mg, 0.39 mmol) in 10 mL of chloroform with two drops of added pyridine. The oxidation was allowed to proceed for approximately two hours before extraction. RPTLC (methanol) showed four spots. The major products were 6C monomer (R_f = 0.64), 6C dimer (R_f = 0.46) and 6C tetramer + oligomer (R_f = 0.0). A small spot at R_f = 0.29 was probably 6C trimer. The mixture was fractionated by GPC. A small amount of higher order oligomer (identified as such by ^{1}H NMR) eluted prior to 6C tetramer. The yield of 6C tetramer (31 mg, 13 μmol) was thirty-three percent based on 3° SH 6C monomer.

The ^{1}H NMR spectrum was characterized based on the peaks resonant above 2.0 ppm. ^{1}H NMR [$CDCl_3$, 200 MHz, δ(ppm)]: 4.79 (12H, triplet

of triplets, CHO_2C), 3.40 (12H, triplet, CH_2Br), 2.65 (12H, triplet, CH_2SS), 2.28 (36H, multiplet, CH_2CO_2 and, twelve ring protons vicinal and trans to the ester).

5.3.22 8C Tetramer

The title compound was prepared by iodine oxidation of a mixture containing a small amount of 3° SH 8C monomer and a large excess of 1°SH 8C monomer. The preparation, but not isolation, was based on that of 11C dimer described above. Pyridine was not used to neutralize the hydrogen iodide produced by the oxidation. 1° SH 8C Monomer (181 mg, twenty-five percent thiol conversion) and 3° SH 8C monomer (13 mg, 21 μmol) were oxidized with excess I_2 (79 mg, 0.31 mmol) in 10 mL of chloroform. The oxidation was allowed to proceed for fifty minutes before extraction. The chloroform solution (diluted to 30 mL) was extracted with two portions of 20 mL pH 7.0 phosphate buffer, 20 mL of 10 % aqueous $Na_2S_2O_3$, and a further 20 mL of pH 7.0 buffer. The chloroform extract was dried with $MgSO_4$, then concentrated by rotary evaporation. The chloroform residue, 174 mg, was fractionated by elution through a preparative C_{18} SEP-PAK cartridge. The sample was applied to the cartridge, attached to a 10 mL syringe, as a methanol/oil mixture. Elution required six 10 mL portions of methanol, two 10 mL portions of ethanol and two 10 mL portions of chloroform. The 8C tetramer eluted in the chloroform fractions. The 8C tetramer has R_f = 0.0 on RPTLC. The yield of 8C tetramer (10 mg, 3.5 μmol) was seventeen percent based on 3° SH 8C

monomer.

The ^{1}H NMR spectrum was characterized based on the peaks resonant above 2.0 ppm. ^{1}H NMR [$CDCl_3$, 200 MHz, δ(ppm)]: 4.81 (12H, triplet of triplets, CHO_2C), 3.41 (12H, triplet, CH_2Br), 2.67 (12H, triplet, CH_2SS), 2.28 (36H, triplet, CH_2CO_2 and submerged multiplet, twelve ring protons vicinal and trans to the ester).

5.3.23 1° NBD 11C Monomer

Thiol bearing surfactants prepared in this work were labelled with a reactive haloacetyl derivative (IANBD) of NBD, Figure 4.1b. A 1° SH 11C monomer sample (53 mg, ten percent thiol conversion) was dissolved in 3 mL of 2/1 dioxane/pH 7.4 phosphate buffer. Excess IANBD (15 mg, 37 μmol) was added and the reaction, under nitrogen allowed to proceed for two hours at which point cysteine (Nutritional Biochemicals), 15 mg, 124 μmol, was added to quench the reaction. After thirty minutes of further reaction, the solution was extracted with 30 mL of ether and three portions of 15 mL of pH 7.4 phosphate buffer. The ethereal extract, a brilliant fluorescent green, was dried with $MgSO_4$ and concentrated by rotary evaporation. Silica TLC (90/10 ether/acetone) showed two dominant orange spots at R_f = 0.64 and 0.40. 1° NBD 11C Monomer, R_f = 0.64, was isolated with a preparative silica gel column (30 g, 95/5 ether/acetone). The title compound elutes as the first colored band. Reverse phase HPLC (2.0 mL/min, acetonitrile) on this product showed one peak (470 nm) with a retention time of 6.3 min. The yield[13] (4 mg, twenty percent) was

incorporate into a bilayer, should reside with their alkyl tails in the bilayer interior. Tracer diffusion coefficients were measured for NBD-citronellol, NBD-solanesol, and NBD-dolichol sequestered in liquid crystal phase (29 °C) DMPC bilayers. NBD labelled phosphatidylethanolamine (NBD-PE) was also measured in order to provide a constant point of reference since, presumably, the diffusion coefficient of NBD-PE reflects the self diffusion of the host lipid.

The results of these measurements are found in Table 6.1. The same results are displayed graphically in Figure 6.1. Surprisingly, all the labelled alcohols diffuse at the same rate. This rate, in fact, is equal to that of the lipid self diffusion as measured by NBD-PE. The means are equal according to the student t test at a ninety-five percent confidence level. The diffusion coefficient of the NBD-PE is 5.0×10^{-12} m^2s^{-1}. Vaz et. al.[1] found NBD-PE diffused at a rate of 5.7×10^{-12} m^2s^{-1} in DMPC multibilayers at 30 °C. Essentially all the incorporated fluorophore is mobile, as evidenced by mobile fractions which approach one. The equivalence of the diffusion coefficient for these probes is very surprising since the largest probe, NBD-dolichol, has a hydrocarbon tail which is an order of magnitude larger than NBD-citronellol, the smallest probe.

The lack of size discrimination observed for the NBD labelled isoprenoids was unexpected. To further explore the size effect in membranes, we measured the diffusion coefficient of the fluorescent polyaromatic hydrocarbons tetracene and rubrene incorporated in DMPC multibilayers. Both these molecules have a significant absorption at 476 nm which makes them amenable to diffusion measurements by FPR. They have, however, only recently been exploited for FPR diffusion

The ^{1}H NMR spectrum was characterized based on the peaks resonant above 2.0 ppm. ^{1}H NMR [$CDCl_3$, 200 MHz, δ(ppm)]: 8.47 (1H, doublet, ring proton α to the nitro), 6.21 (1H, doublet, ring proton β to the nitro), 4.81 (3H, triplet of triplets, CHO_2C), 4.51 (4H, singlet, $NC\underline{H}_2C\underline{H}_2O_2C$), 3.51 (3H, singlet, NCH_3), 3.40 (4H, triplet, CH_2Br), 3.15 (2H, singlet, O_2CCH_2S), 2.53 (2H, triplet, SCH_2), 2.27 (9H, triplet, CH_2CO_2; submerged multiplet, three ring protons vicinal and trans to the ester).

5.3.25 1° NBD 6C Monomer

The 1° NBD 6C monomer was prepared and isolated using the same methods outlined for 1° NBD 11C monomer. A 1° SH 6C monomer sample (18 mg, sixteen percent thiol conversion) was dissolved in 3 mL of 2/1 dioxane/pH 7.4 phosphate buffer. Excess IANBD (15 mg, 37 μmol) was added to the mixture. Following quenching and extraction, the title compound was isolated by silica gel column chromatography (30 g, 90/10 ether/acetone). Silica TLC (90/10 ether/acetone) showed two dominant orange spots at R_f = 0.54 and 0.26. 1° NBD 6C Monomer, R_f = 0.54, was isolated with a preparative silica gel column (30 g, 90/10 ether/acetone). The title compound elutes as the first colored band. Reverse phase HPLC (2.0 mL/min, 75/25 acetonitrile/water) on this product showed one peak (470 nm) with a retention time of 5.8 min. The yield[13] (2 mg, ten percent) was determined spectroscopically by the absorbance of the NBD chromophore.

The ^{1}H NMR spectrum was characterized based on the peaks resonant

above 2.0 ppm. ^{1}H NMR [$CDCl_3$, 200 MHz, δ(ppm)]: 8.46 (1H, doublet, ring proton α to the nitro), 6.21 (1H, doublet, ring proton β to the nitro), 4.80 (3H, triplet of triplets, CHO_2C), 4.50 (4H, singlet, $NC\underline{H}_2C\underline{H}_2O_2C$), 3.49 (3H, singlet, NCH_3), 3.41 (4H, triplet, CH_2Br), 3.11 (2H, singlet, O_2CCH_2S), 2.52 (2H, triplet, SCH_2), 2.31 (9H, triplet, CH_2CO_2; submerged multiplet, three ring protons vicinal and trans to the ester).

5.3.26 3° NBD 11C Monomer

3° SH 11C Monomer (7 mg, 9 μmol) was allowed to react with excess IANBD (15 mg, 37 μmol) in 1.5 mL of dry dimethylformamide (DMF) which (BDH, spectroscopic grade) was saturated with nitrogen and contained 28 μmol of TEA. After thirty-five minutes, the reaction mixture was extracted with 75 mL of ether and three 30 mL aliquots of pH 7.4 buffer. The ethereal solution was dried with $MgSO_4$ and concentrated by rotary evaporation. Mono- and di-labelled monomer was evident by both silica TLC and reverse phase HPLC analyses. The triply labelled material was isolated by column chromatography (50 g s''ica, 50/50 ether/ethyl acetate). The title compound had R_f = 0.29 on silica TLC with the ether/ethyl acetate solvent. Reverse phase HPLC showed one peak (470 nm) (2.0 mL/min, acetonitrile) at 6.0 min for the pure 3° NBD 11C monomer. RPTLC (methanol) of the pure triply labelled monomer showed one orange spot R_f = 0.41. The yield (by weight) was approximately 2 mg (1 μmol). Based on starting material, the percentage yield was approximately ten percent.

The ^{1}H NMR spectrum was characterized based on the peaks resonant above 2.0 ppm. ^{1}H NMR [$CDCl_3$, 200 MHz, δ(ppm)]: 8.43 (3H, doublet, ring proton α to the nitro), 6.17 (1H, doublet, ring proton β to the nitro), 4.76 (3H, triplet of triplets, CHO_2C), 4.47 (12H, singlet, $NC\underline{H}_2C\underline{H}_2O_2C$), 3.48 (9H, singlet, NCH_3), 3.10 (6H, singlet, O_2CCH_2S), 2.49 (6H, triplet, SCH_2), 2.31 (9H, triplet, CH_2CO_2; submerged multiplet, three ring protons vicinal and trans to the ester).

5.3.27 1° NBD 8C Dimer

1° SH 8C Dimer (18 mg, fifteen percent thiol conversion) was dissolved in a 1 mL solution of 1 % TEA in DMF. Excess IANBD (15 mg, 37 μmol) was added and the reaction, under nitrogen, allowed to proceed for ninety minutes. The reaction mixture was extracted with 35 mL of ether and four 15 mL aliquots of pH 7.4 phosphate buffer. The ethereal extract was dried with $MgSO_4$ and concentrated by rotary evaporation. Silica TLC (ether solvent) of the extract showed two bright orange spots (IANBD and the title compound) and several dim orange spots. The 1° NBD 8C dimer had R_f = 0.48 on silica, with ether as the solvent, while IANBD had R_f = 0.28 under the same conditions. The reaction mixture was fractionated on a silica gel column (30 g, ether eluent) and the mono-labelled dimer isolated. The pure compound eluted as one spot on silica TLC (above) and on RPTLC (methanol eluent) with R_f = 0.21. The yield of 1° NBD 8C dimer was not measured, however, it was very small.

The ^{1}H NMR spectrum was characterized based on the peaks resonant

above 2.0 ppm. ^{1}H NMR [$CDCl_3$, 200 MHz, δ(ppm)]: 8.46 (1H, doublet, ring proton α to the nitro), 6.20 (1H, doublet, ring proton β to the nitro), 4.79 (6H, triplet of triplets, CHO_2C), 4.48 (4H, singlet, $NC\underline{H}_2C\underline{H}_2O_2C$), 3.48 (3H, singlet, NCH_3), 3.39 (6H, triplet, CH_2Br), 3.10 (2H, singlet, O_2CCH_2S), 2.65 (4H, triplet, CH_2SS), 2.50 (2H, triplet, SCH_2), 2.26 (18H, triplet, CH_2CO_2; submerged multiplet, six ring protons vicinal and trans to the ester). A small triplet δ = 3.17 ppm was present in the spectrum. Control experiments show it originated from a small amount of terminal iodine contamination of the labelled dimer. Presumably I^- generated by the labelling reaction displaced some of the terminal bromine in the alkyl chains.

5.3.28 1° NBD 6C Dimer

1° SH 6C Dimer (12 mg, fifteen percent thiol conversion) was dissolved in a 1 mL solution of 1 % TEA in DMF. Excess IANBD (12 mg, 29 μmol) was added and the reaction, under nitrogen, was allowed to proceed for ninety minutes. The reaction mixture was extracted and dried in a manner analogous to the 1° NBD 8C dimer preparation. Silica TLC (ether solvent) of the extract showed two bright orange spots (IANBD and the title compound) closely spaced together. Cysteine (20 mg, 165 μmol) was added to the mixture as a solution in 10 mL of 50/50 dioxane/pH 7.4 buffer to facilitate extraction of the residual IANBD. Further extraction with 35 mL of ether and three aliquots of 15 mL pH 7.4 buffer removed the residual IANBD as a water soluble cysteine adduct. The extract was fractionated on a silica gel

column (30 g, ether eluent) and the mono-labelled dimer isolated. A very small amount of the doubly labelled dimer was present as a contaminant. The pure compound eluted as one spot on silica TLC (above) and on RPTLC (methanol eluent) with R_f = 0.48. The yield[13] of 1° NBD 6C dimer (0.7 mg, one percent) was determined spectroscopically by the absorbance of the NBD chromophore.

The ^{1}H NMR spectrum was characterized based on the peaks resonant above 2.0 ppm. ^{1}H NMR [$CDCl_3$, 200 MHz, δ(ppm)]: 8.46 (1H, doublet, ring proton α to the nitro), 6.20 (1H, doublet, ring proton β to the nitro), 4.79 (6H, triplet of triplets, CHO_2C), 4.48 (4H, singlet, $NC\underline{H}_2C\underline{H}_2O_2C$), 3.48 (3H, singlet, NCH_3), 3.40 (6H, triplet, CH_2Br), 3.10 (2H, singlet, O_2CCH_2S), 2.65 (4H, triplet, CH_2SS), 2.51 (2H, triplet, SCH_2), 2.29 (18H, multiplet, CH_2CO_2; six ring protons vicinal and trans to the ester). As was the case for 1° NBD 8C dimer, a small triplet δ = 3.17 ppm (CH_2I) is present in the spectrum.

5.3.29 1° NBD 11C Dimer

First degree thiol substituted 11C dimer was allowed to react with IANBD using the procedures outlined above for the preparation of 1° NBD 8C dimer. While chromatographically it appeared labelled dimer was formed, the yield was extremely meagre and the product could not be isolated and identified spectroscopically. The yield for this reaction, from the results outlined above, is known to be meagre. The larger size of the 11C dimer may be related to our difficulty in synthesizing this compound. FPR measurements were not performed using

this probe because it could not be positively identified.

5.3.30 1° NBD 11C Tetramer, 1° NBD 6C Tetramer

The first degree thiol substituted mixtures of both the 11C and 6C tetramers were synthesized using the principles outlined for synthesis of the corresponding thiol dimers. The IANBD labelling reaction, despite a great number of trials, did not produce labelled tetramers of these compounds. The reason for the failure of this reaction is uncertain. It may be due to a conformational effect of the very large tetramers or it may simply be due to the inherently poor yields of the IANBD reaction (see above) in organic solution.

REFERENCES

(1) Petersen, N. O. *Spectrosc. Int. J.* **1983**, *2*, 408.

(2) Ashworth, M. R. *The Determination of Sulphur-Containing Groups*; Academic: New York, 1977; Vol. 3, pp 174, 176.

(3) Glaser, C. B.; Maeda, H.; Meinhofer, J. *J. Chromatog.* **1970**, *50*, 151.

(4) Molecular Probes Inc., Eugene, OR, personal communication, 1990.

(5) Balcom, B. J.; Petersen, N. O. *J. Org. Chem.* **1989**, *54*, 1922.

(6) Haugland, R. P. *Handbook of Fluorescent Probes*; Molecular Probes: Eugene, OR, 1989.

(7) Monroe, B. M. In *Singlet Oxygen*; Frimer, A. A. Ed.; CRC Press: Boca Raton, FL, 1985; Vol. 1, pp 177, 224.

(8) Iodine stains thiols in an unusual manner. Iodine which initially sublimes onto the thiol is reduced to colorless iodide ion. The spot on the TLC plate with the most thiol will be the last place on the plate to stain brown. Once all the thiol has been oxidized, the conventional iodine stain appears. Frequently the periphery of the thiol TLC spot will have stained while the centre, where the thiol concentration is still significant, remains colorless. Thus the TLC spot has the appearance of a doughnut; A brown ring surrounding a colorless centre.

(9) Cappozzi, G.; Modena, G. In *The Chemistry of the Thiol Group*; Patai, S., Ed.; Wiley: New York, 1974; Part 2, pp 785, 839.

(10) Thyagarajan, B. S. *Chem. Rev.* **1958**, *58*, 439.

(11) Humphrey, R. E.; Potter, J. L. *Anal. Chem.* **1965**, *37*, 164.

(12) Smith, D. J.; Maggio, E. T.; Kenyon, G. L. *Biochemistry* **1975**, *14*, 766.

(13) Based on equations given as Reference 34, Chapter Four of this work.

(14) The yield calculation is based on a binomial distribution of thiols on the monomer or dimer.

CHAPTER SIX

DIFFUSION MEASUREMENTS

6.1 Overview

Lateral diffusion measurements were made in DMPC model membranes using the fluorescently labelled molecules described in Chapter Four. Additional diffusion measurements, with a subset of these probes, were undertaken in viscous isotropic solution to understand their behavior in more clearly defined model systems. Diffusion of the intrinsically fluorescent hydrocarbons tetracene and rubrene was examined in both model membranes and isotropic solution to aid in understanding the dynamics of the membrane interior.

The diffusion measurements in this chapter are divided into three sections. In the first section we consider the effect of probe chain length on the rate of diffusion in model membranes. In the second we examine the effect of probe chain length on the diffusion coefficient in viscous solution. The third section considers the effect on the diffusion coefficient of altering the headgroup area of the probe.

6.2 Hydrodynamic Interactions in the Membrane Interior, DMPC Bilayers

6.2.1 Measurements in the Liquid Crystal State

The NBD labelled isoprenoid alcohols comprise an homologous series of labelled hydrocarbon polymers which, since they will

incorporate into a bilayer, should reside with their alkyl tails in the bilayer interior. Tracer diffusion coefficients were measured for NBD-citronellol, NBD-solanesol, and NBD-dolichol sequestered in liquid crystal phase (29 °C) DMPC bilayers. NBD labelled phosphatidylethanolamine (NBD-PE) was also measured in order to provide a constant point of reference since, presumably, the diffusion coefficient of NBD-PE reflects the self diffusion of the host lipid.

The results of these measurements are found in Table 6.1. The same results are displayed graphically in Figure 6.1. Surprisingly, all the labelled alcohols diffuse at the same rate. This rate, in fact, is equal to that of the lipid self diffusion as measured by NBD-PE. The means are equal according to the student t test at a ninety-five percent confidence level. The diffusion coefficient of the NBD-PE is 5.0×10^{-12} m^2s^{-1}. Vaz et. al.[1] found NBD-PE diffused at a rate of 5.7×10^{-12} m^2s^{-1} in DMPC multibilayers at 30 °C. Essentially all the incorporated fluorophore is mobile, as evidenced by mobile fractions which approach one. The equivalence of the diffusion coefficient for these probes is very surprising since the largest probe, NBD-dolichol, has a hydrocarbon tail which is an order of magnitude larger than NBD-citronellol, the smallest probe.

The lack of size discrimination observed for the NBD labelled isoprenoids was unexpected. To further explore the size effect in membranes, we measured the diffusion coefficient of the fluorescent polyaromatic hydrocarbons tetracene and rubrene incorporated in DMPC multibilayers. Both these molecules have a significant absorption at 476 nm which makes them amenable to diffusion measurements by FPR. They have, however, only recently been exploited for FPR diffusion

Table 6.1: Probe Diffusion in DMPC Multibilayers

Probe	lipid/label	D (10^{13} m^{-2} s)[a]	Xm[b]	N[c]
		Liquid Crystal Phase 29 °C		
NBD-PE[d]	1200[e]	50 ± 2	0.97	38
NBD-citronellol	1500	48 ± 3	1.01[f]	24
NBD-solanesol	2000	53 ± 2	0.97	24
NBD-dolichol[d]	2000	46 ± 2	0.98	39
Tetracene	1200	110 ± 9	0.86	15
Rubrene	3300	58 ± 3	0.89	20
		Gel Phase 19 °C		
NBD-PE	1500	0.32 ± 0.01	0.66	20
NBD-citronellol	1500	1.00 ± 0.05	0.83	18
NBD-solanesol[d]	2000	0.14 ± 0.02	0.40	22
NBD-dolichol	2000	0.08 ± 0.01	0.70	5
Tetracene[g]	1200	-	-	-
Rubrene[g]	3300	-	-	-

[a] Diffusion coefficient, standard error of the mean.

[b] Mobile fraction.

[c] Number of measurements.

[d] Aggregate of two sample preparations.

[e] Second preparation has lipid/label = 1500.

[f] Mobile fractions larger than 1.0 are physically impossible. This is the fitted value.

[g] Diffusion measurements proved impossible due to extreme monitor beam photobleaching.

Figure 6.1: Tracer diffusion coefficients of NBD labelled isoprenoid alcohols, and PE, rubrene and tetracene in the liquid crystal phase. The labelled isoprenoid alcohols are NBD-citronellol, NBD-solanesol, and NBD-dolichol. The measurements were made on liquid crystal phase DMPC multibilayers at 29 °C. Error bars represent standard errors of the mean.

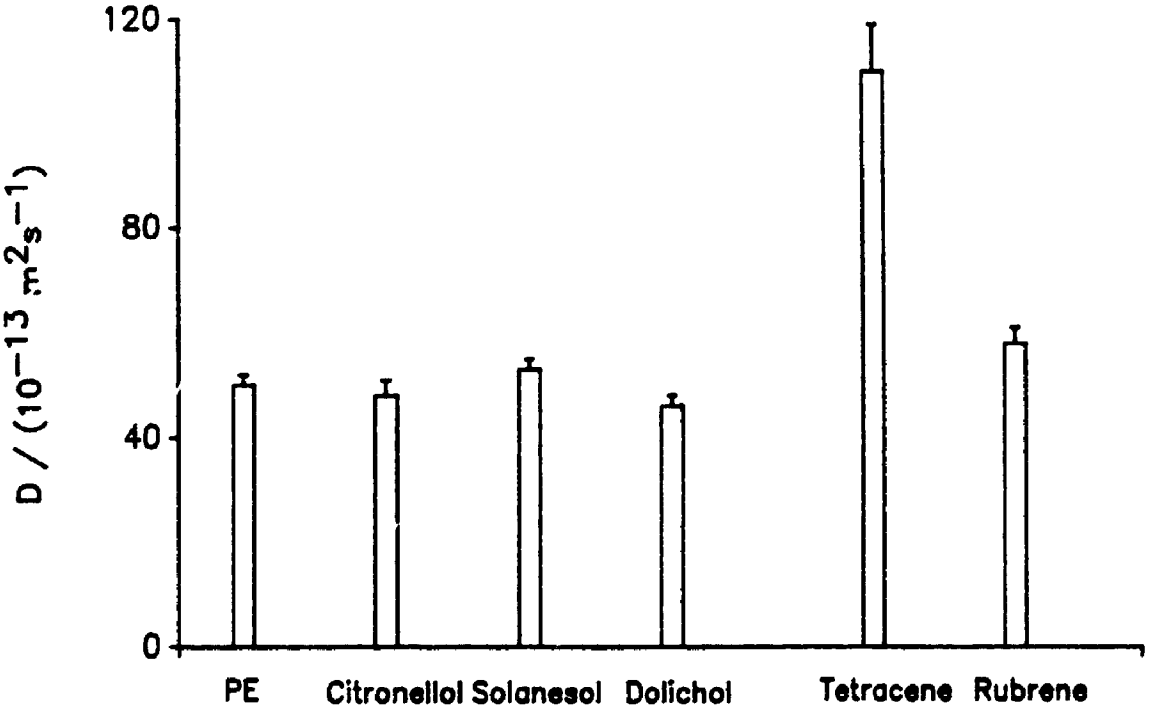
120
80
40
0
D / (10^{-13} m^2s^{-1})
PE
Citronellol
Solanesol
Dolichol
Tetracene
Rubrene

measurements.[2,3] These molecules were not employed as labelling agents, but as intrinsically fluorescent non-polar probes. Their lack of polarity suggests they should reside in the hydrocarbon interior of the bilayer. Results of our diffusion measurements with rubrene and tetracene are shown in Table 6.1 and Figure 6.1. Rubrene, which is approximately twice as large as tetracene, moves substantially slower. Both move faster than NBD-PE as evidenced by the student t test at a ninety-five percent confidence level. The mobile fractions for both these probes are less than one, due to a small amount of monitor beam photobleaching. The molecular structures of rubrene and tetracene are shown in Figure 6.2.

Diffusion coefficients of the labelled isoprenoid alcohol probes were also measured as a function of unlabelled alcohol concentration in the membrane preparation. The isoprenoid alcohols are incorporated into the dry lipid film prior to swelling and formation of vesicles. In the case of added citronellol and solanesol, trace amounts of the corresponding labelled alcohols diffuse at rates faster than found in the absence of unlabelled alcohol. It appears that the two smaller alcohols may have a 'fluidizing' effect on the membrane at low alcohol concentrations. This effect is observed because of disordering in the host matrix caused by the additive. Disrupting the packing of the host lipid will result in faster probe diffusion. Added dolichol, in contrast, appears to have little effect on the membrane; NBD-dolichol and NBD-PE diffuse at rates slightly slower than found in the absence of free dolichol. Other experimental techniques, however, have indicated dolichol has a 'fluidizing' effect on the membrane.[4,5] Schroeder et. al.[5], however, have found that the fluidizing effect of

Figure 6.2: Fluorescent polyaromatic hydrocarbons rubrene and tetracene. Both tetracene (a) and rubrene (b) are well suited to FPR diffusion measurements.

a

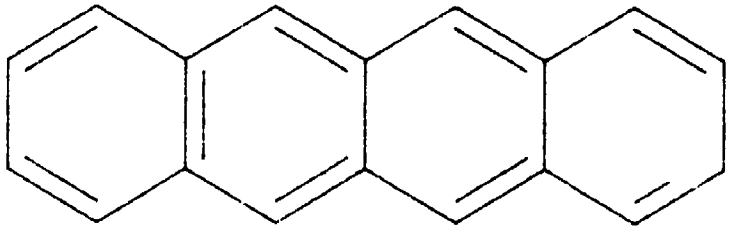

b

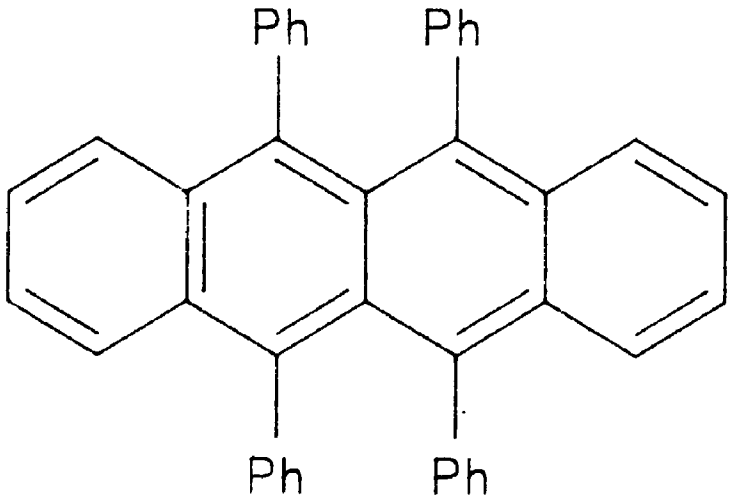

dolichol does not extend to the surface of the bilayer. Ubiquinone, a polyisoprenoid quinone with a tail group similar to the isoprenoid alcohols, is known to alter the fluidity of model membranes.[6] Altering the fluidity of the membrane, by whatever means, should change the rate of probe diffusion in the membrane.[7]

Previous investigators have postulated that dolichol will aggregate at high concentrations in the bilayer.[4,8] If labelled dolichol were able to join in these aggregates, one might expect the diffusion coefficient to decrease. Our diffusion results provide no evidence of this behavior. The results of our work on the free alcohol dependence of the diffusion coefficient are found in Table 6.2 and Figure 6.3.

6.2.2 Measurements in the Gel State

The liquid crystal to gel phase transition in a phospholipid bilayer is characterized by a melting of the ordered, rigid hydrocarbon chains.[9,10] In the liquid crystal phase the hydrocarbon chains are disordered and the interior viscosity decreases with increasing temperature.[11] FPR diffusion measurements were undertaken in the gel phase (19 $^{\circ}$C) of DMPC membranes. The rigid interiors would suggest that a probe's hydrocarbon tail length should have a significant effect on lateral diffusion in this phase. Diffusion measurements were undertaken utilizing the NBD labelled probes mentioned previously, as well as tetracene and rubrene. Not surprisingly, diffusion in the gel phase of the membrane does depend on the size of the probe. NBD-citronellol, in accord with its smaller

Table 6.2: Concentration Effects Unlabelled Alcohol DMPC Multibilayers 29 °C

Alcohol	alcohol/lipid	D (10^{13} m^{-2} s)[a]	Xm[b]	N[c]
Citronellol[d]	0.002	66 ± 4	0.98	20
	0.004	62 ± 4	1.00	19
	0.025	58 ± 5	0.97	20
	0.050	55 ± 3	0.99	20
	0.020	66 ± 5	1.00	14
	0.000	48 ± 3	1.01[e]	24
Solanesol[f]	0.033	63 ± 4	0.98	17
	0.003	70 ± 6	0.98	17
	0.000	53 ± 2	0.97	24
Dolichol[g]	0.003	42 ± 3	0.98	19
	0.017	49 ± 2	0.97	17
	0.017[h]	42 ± 2	0.97	20
	0.000[i]	46 ± 2	0.98	39

[a] Diffusion coefficient, standard error of the mean.

[b] Mobile fraction.

[c] Number of measurements.

[d] Probe NBD-citronellol. Lipid/NBD-citronellol = 1500.

[e] Mobile fractions larger than 1.0 are physically impossible. This is the fitted value.

[f] Probe NBD-solanesol. Lipid/NBD-solanesol = 2000.

[g] Probe NBD-dolichol. Lipid/NBD-dolichol = 2000.

[h] Probe NBD-PE. Lipid/NBD-PE = 1200.

[i] Aggregate of two sample preparations.

Figure 6.3: Lateral diffusion coefficients of labelled isoprenoid alcohols in model membranes as a function of unlabelled alcohol concentration. The measurements were performed on liquid crystal phase DMPC multibilayers at 29 °C. The unlabelled alcohols correspond to the labelled probe used. NBD-citronellol (o), NBD-solanesol (●), and NBD-dolichol (Δ). Diffusion of NBD-PE (▲) was measured in the presence of free dolichol. Error bars represent standard errors of the mean.

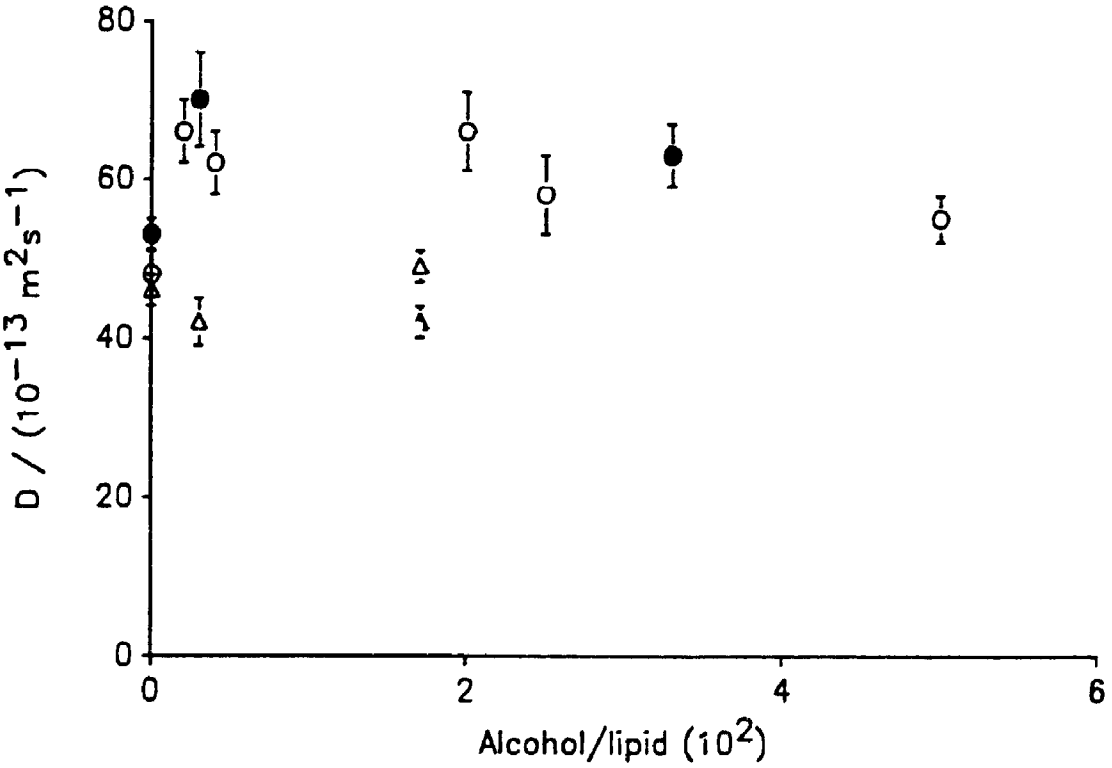
80
60
40
20
0
D / (10^{-13} $m^2 s^{-1}$)
0
2
4
6
Alcohol/lipid (10^2)

size, diffuses faster than the labelled lipid (NBD-PE) in the gel phase. NBD-PE diffuses at a rate of 3.2×10^{-14} m^2s^{-1} in the gel phase. The student t test, ninety-five percent confidence interval, shows that all three labelled alcohols diffuse at rates different from that of NBD-PE and each other. The diffusion coefficients measured in the gel state, Table 6.1 and Figure 6.4, were lower by factors of approximately fifty for NBD-citronellol and five hundred for NBD-dolichol versus their diffusion rates in liquid crystal membranes. Observation of diffusion coefficients which depend on size, in the expected manner, strongly suggest that we are measuring motion of the labelled probes and not an artifact.

Our diffusion results in the gel phase are characterized by mobile fractions of less than one. This probably relates to the mechanism of diffusion in the gel phase. This mechanism is uncertain, but has been related to probe movement along cracks or fissures in the bilayer assembly.[12] Probes which are not accessible to these defect structures will not appear mobile on the time scale of the experiment. Uncertainty in the mechanism, however, does not prevent the general observation that molecules with longer hydrocarbon tails should move slower due to the rigidification of the hydrocarbon interior. This is what we observe experimentally. Our value for the gel phase diffusion coefficient of NBD-PE (3.2×10^{-14} m^2s^{-1}) is in qualitative agreement with the results of Derzko and Jacobson.[12]

Curiously, the diffusion coefficient of the polyaromatic hydrocarbons rubrene and tetracene could not be measured below the main phase transition. Monitor photobleaching was so extreme for these probes that it proved impossible to focus the laser on the surface of

Figure 6.4: Tracer diffusion coefficients of NBD labelled isoprenoid alcohols, and PE in the gel phase. The labelled isoprenoid alcohols are NBD-citronellol, NBD-solanesol, and NBD-dolichol. The measurements were made on gel phase DMPC multibilayers at 19 °C. Error bars represent standard errors of the mean.

Figure 6.5: Lateral diffusion coefficients of trace amounts of NBD labelled isoprenoid alcchols in paraffin oil as a function of temperature. The probes employed were NBD-citronellol (o) and NBD-solanesol (Δ). The diffusion coefficients have units of 10^{-12} m^2s^{-1}. Error bars represent standard errors of the mean.

the bilayer. Alteration of the microscope's plane of focus produced a brief flare of fluorescence which was extinguished in less than one second.

This is a potentially significant observation that has two possible explanations. The first is that tetracene and rubrene aggregate in the gel phase bilayer. Dimerization of tetracene is known to render it nonfluorescent (476 nm irradiation) and is believed to be an important mode of photobleaching.[3,13] The high local concentration of tetracene or rubrene in these postulated aggregates would surely speed the dimerization and thereby increase the photobleaching rate. This presumes that rubrene has a similar, self-catalyzed, mode of decay.

The second, more interesting, possibility is that the flat board-like structure of these molecules might result in their sequestering in the gel phase with a conformation amenable to efficient excitation by the incident laser beam. Increasing the efficiency of excitation will surely increase the rate of photobleaching as well. The intriguing idea has been raised that if the second explanation is true, it may be possible to map fluid and gel regions of a real cell or complicated vesicle by irradiation with a very low power laser beam. Those regions in the bilayer with a favorable probe orientation (gel phase) should emit more fluorescence than the corresponding liquid crystal regions. Further studies are contemplated to examine the origin of this effect and to exploit the tetracene and rubrene probes should case two above prevail.

Trissl[14] has reported that rubrene will not incorporate into a

black lipid membrane. As in our experiment, fluorescence was used as a means of detection. It seems likely that, in fact, rubrene did incorporate but was bleached to such an extent that minimal fluorescence was observed. Our experiments clearly show that rubrene will incorporate into DMPC bilayers.

6.3 Three-Dimensional Diffusion - Chain Length Effect

While the size dependent diffusion of the NBD labelled isoprenoid alcohols in the gel phase is reassuring, the non-dependence of the diffusion coefficient in the liquid crystal phase is disquieting. In an effort to better understand the diffusive behavior of the NBD labelled isoprenoid alcohols in general, a series of studies in three-dimensional viscous solution was undertaken. We performed these experiments to answer a simple question: Can the diffusion of various NBD labelled alcohols be distinguished by FPR in simple solvent systems which are analogous to the membrane interior?

The theory behind the FPR technique, discussed in Chapter Three, assumes that recovery of the observed fluorescent signal occurs due to lateral diffusive motion. One might ask how the FPR technique can presume to measure isotropic diffusion coefficients when the recovery is clearly not solely due to lateral diffusion. Motion of fluorophores along the direction of the optical axis will contribute to the recovery signal. The question is, to what extent will this corrupt the diffusion measurement. A detailed analysis of this contribution to the signal has not yet been published. A common assumption, however, is that the observed sample region approximates

a three-dimensional Gaussian function.[15] The excitation profile in this case is given by Equation 6.1.

$$I(r,z) = I_o \exp\left(-2\, r^2 / w_r^2 \right) \exp\left(-2\, z^2 / w_z^2 \right) \qquad (6.1)$$

In Equation 6.1, z is the distance along the optical axis from the focal plane and w_z is the 'width' of the profile, defined as per Chapter Three, in the z direction. If $w_z > w_r$, as is usually the case,[15] the contribution of motion in the z domain to the observed recovery will be small. Calculations by Qian and Elson,[16] however, suggest that, for our experimental geometry, the measured diffusion coefficient will be underestimated in three-dimensional solution.

6.3.1 Measurements in Paraffin Oil

Diffusion measurements were undertaken for the labelled alcohols citronellol and solanesol in paraffin oil. Paraffin oil was chosen as the solvent since it is a hydrocarbon chain medium with a viscosity (65 cP at 25 °C) within the range estimated for the bilayer interior. The data shown in Table 6.3 and Figure 6.5 illustrate that tracer diffusion coefficients of NBD-citronellol and NBD-solanesol are distinguishable in this model system. As expected, NBD-citronellol moves faster than NBD-solanesol. More extensive measurements were not pursued in this system due to binding of the NBD labelled alcohols to the inner surface of the glass capillary. The fluorescence intensity, judged by eye, originating from the glass surface was larger than the intensity observed in the center of the capillary. Diffusion

Table 6.3: Probe Diffusion in Paraffin Oil

Probe	T (K^{-1})	D (10^{13} m^{-2} s)[a]	Xm[b]	N[c]
NBD-citronellol[d]	304	55 ± 4	1.00	8
	299	58 ± 4	0.99	10
	297	54 ± 2	0.98	10
	293	42 ± 3	0.98	10
	291	35 ± 2	0.98	9
	300	49 ± 3	0.97	17
	310	80 ± 9	0.96	8
	293	38 ± 2	0.98	9
NBD-solanesol[e]	296	17 ± 2	0.96	10
	304	28 ± 1	0.89	15
	297	18 ± 1	0.85	10
	291	15 ± 1	0.87	7

[a] Diffusion coefficient, standard error of the mean.

[b] Mobile fraction.

[c] Number of measurements.

[d] [NBD-citronellol] = 1.4×10^{-5} mol L^{-1}.

[e] [NBD-solanesol] = 5.7×10^{-5} mol L^{-1}, first two data points.
[NBD-solanesol] = 1.4×10^{-5} mol L^{-1}, second two data points.

Figure 6.5: Lateral diffusion coefficients of trace amounts of NBD labelled isoprenoid alcchols in paraffin oil as a function of temperature. The probes employed were NBD-citronellol (o) and NBD-solanesol (Δ). The diffusion coefficients have units of 10^{-12} m^2s^{-1}. Error bars represent standard errors of the mean.

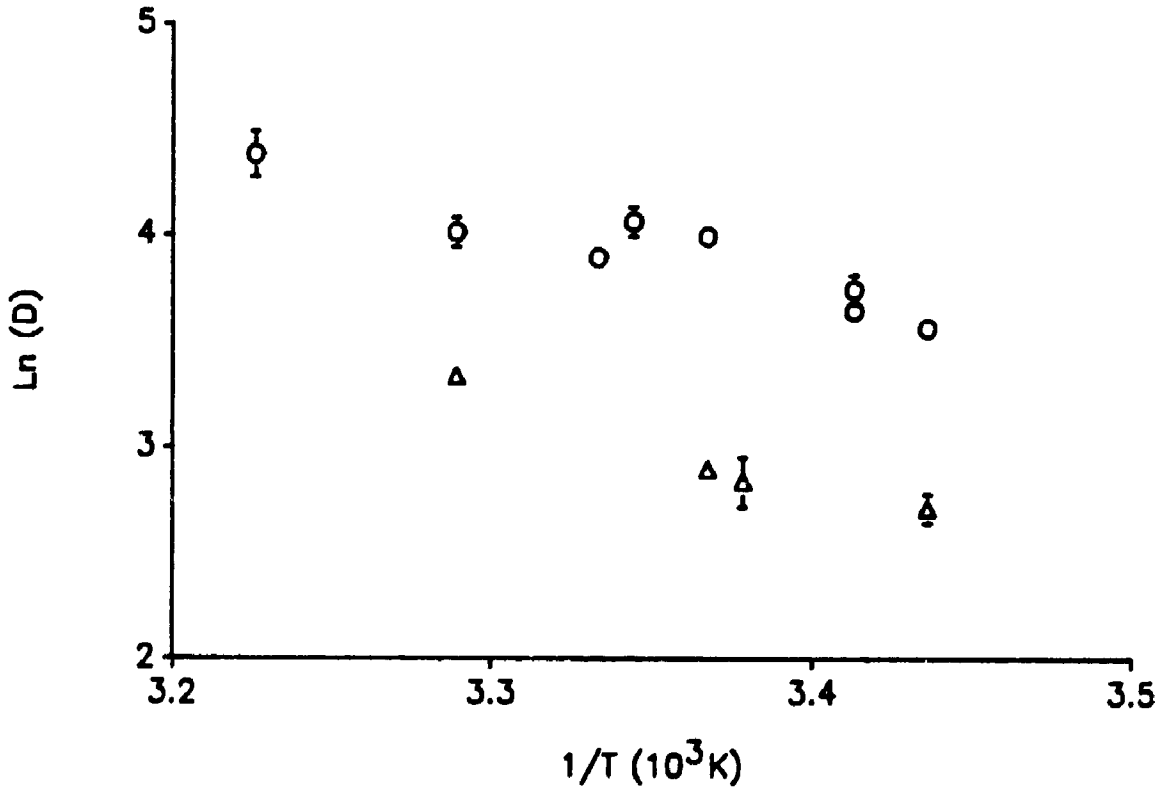
5
4
3
2
3.2
3.3
3.4
3.5
1/T (10³K)
D (Å)

coefficients of the labelled alcohols measured at the glass surface were approximately fourfold slower than diffusion coefficients measured in the center of the capillary tube. Presumably, surface aggregation occurs because of the polarity of the NBD moiety and/or its ester link. The non-polar paraffin oil will have difficulty solubilizing probes that have significant polarity.

6.3.2 Measurements in Glycerol/Water

More extensive diffusion measurements were undertaken in glycerol/water solution. Tracer diffusion coefficients, as a function of temperature in 80/20 glycerol/water, are given in Table 6.4 (Figure 6.6) for NBD-citronellol and NBD-solanesol. Once again the probes are clearly distinguishable. Figure 6.7 shows a plot of the product ($D * \mu / T$) versus temperature, for each probe. The viscosity of the glycerol/water medium, as a function of temperature, is known from the literature.[17] The slope of zero for each probe, over the narrow temperature range examined, suggests the Stokes-Einstein Equation (Equation 6.2) is obeyed and the small glycerol and water molecules appear as a continuum to the diffusing chains.

$$D = \frac{2\,k\,1}{6\,\pi\,\mu\,d} \qquad (6.2)$$

In Equation 6.2, k is Boltzman's constant, T is the Kelvin temperature, μ is the viscosity, and d is the particle diameter. D, of course, is the diffusion coefficient. If the Stokes-Einstein Equation holds, the radius of the diffusing particle is better

Table 6.4: Probe Diffusion in 80/20 Glycerol/Water

T (K^{-1})	μ (cP^{-1})	D (10^{13} m^{-2} s)[a]	Xm[b]	N[c]
		NBD-citronellol[d]		
300	39	41 ± 5	0.99	9
297	46	33 ± 2	0.97	9
295	52	29 ± 2	0.98	10
291	67	23 ± 1	0.99	10
		NBD-solanesol[e]		
301	37	25 ± 3	0.94	10
298	44	18 ± 1	0.94	10
295	54	16 ± 1	0.94	10
291	67	14 ± 1	0.94	10

[a] Diffusion coefficient, standard error of the mean.

[b] Mobile fraction.

[c] Number of measurements.

[d] [NBD-citronellol] = 9.3×10^{-6} mol L^{-1}.

[e] [NBD-solanesol] = 7.0×10^{-6} mol L^{-1}.

Figure 6.6: Lateral diffusion coefficients of trace amounts of NBD labelled isoprenoid alcohols in 80/20 glycerol/water as a function of temperature. The probes employed were NBD-citronellol (o) and NBD-solanesol (Δ). The diffusion coefficients have units of 10^{-13} m^2s^{-1}. Error bars represent standard errors of the mean.

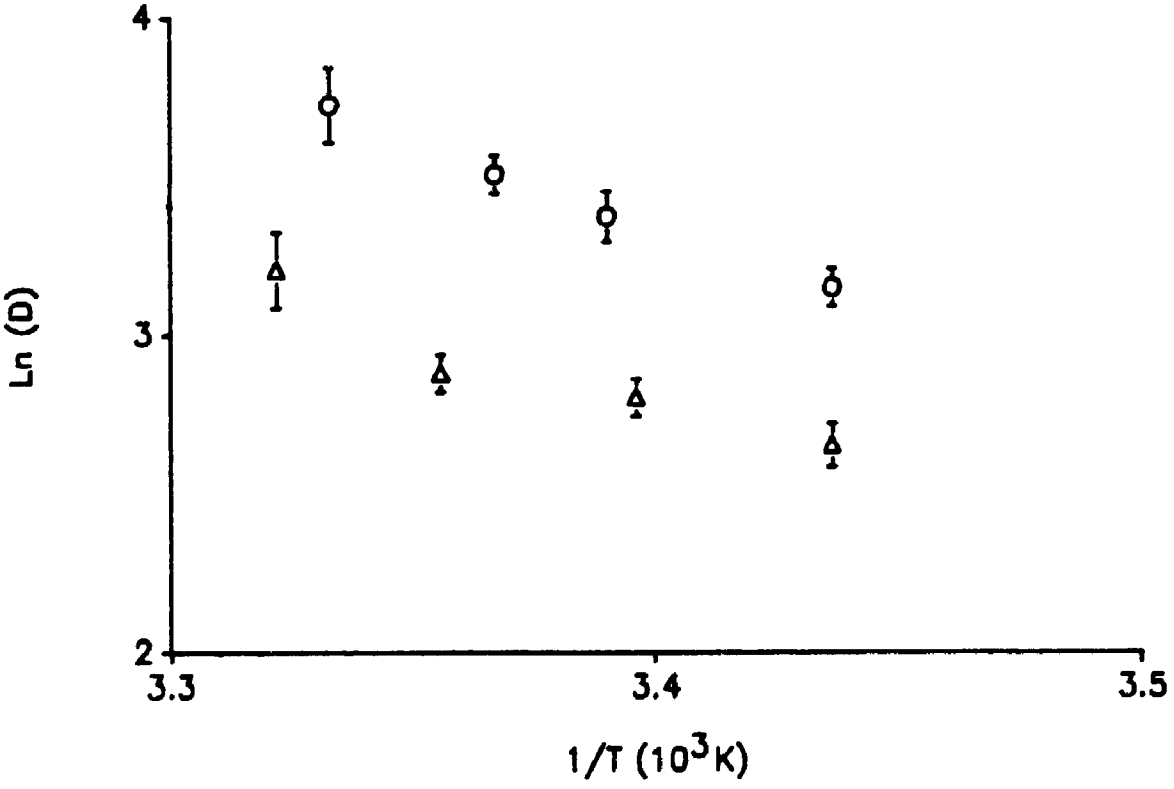
4
3
2
3.3
3.4
3.5
1/T (10³K)
ln (Ω)

Figure 6.7: Examination of Stokes-Einstein behavior in 80/20 glycerol/water. Plots of $D^* \mu / T$ versus T should yield straight lines with a slope of zero if Stokes-Einstein behavior is observed. The probes employed were NBD-citronellol (o) and NBD-solanesol (Δ). Error bars represent standard errors of the mean.

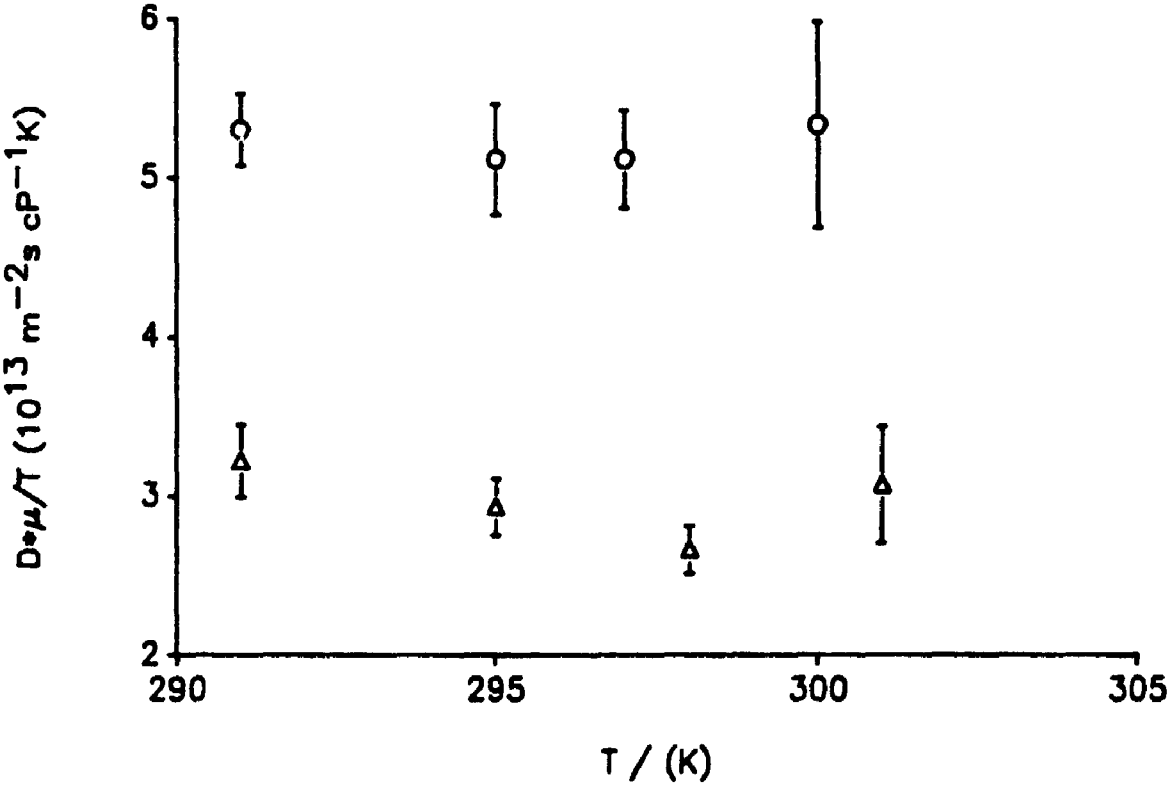
6
5
4
3
2
290
295
300
305
T / (K)
D*μ/T (10^13 m^-2 s cP^-1 K)

represented as the radius of an equivalent hydrodynamic sphere.[18] This equivalent radius is related to the radius of gyration of the chain molecules.

The labelled alcohols were quite soluble in glycerol/water mixtures and no surface aggregation was observed. Glycerol/water solvent mixtures may be used to sample a wide range of viscosities postulated for the interior of the bilayer, however, their viscosity is very sensitive to water content and glycerol is quite hygroscopic. Our methodology for sample preparation requires heating the glycerol solutions and exposure to the atmosphere for not less than ten minutes. Reproducible results, under these conditions, proved very elusive in samples with less than twenty percent added water due to the hygroscopic nature of glycerol. Glycerol/water is a poor approximation, other than in bulk viscosity, to the interior of the membrane. Experiments were therefore undertaken in a third model system.

6.3.3 Measurements in Poly(propylene glycol)

The final model system investigated, poly(propylene glycol) ethers (PPG), displayed the advantages of the previous two systems without their disadvantages. The PPG ethers are linear chain media commercially available in a variety of average chain lengths. The variable chain length results in a series of solvents with different viscosities at room temperature. The NBD labelled isoprenoid alcohols dissolved freely in these polymers with no surface binding. The polymers are not hygroscopic and our diffusion measurements are very

reproducible. The results of our diffusion measurements in the PPG polymers, including rubrene and tetracene, are shown in Table 6.5 and in an abridged form in Figure 6.8. The approximate viscosity range of the bilayer interior is shown by the boxed region of Figure 6.8.

Once again there is a measurable difference between diffusion coefficients of the various labelled alcohols. Contrary to the results in glycerol/water mixtures, the PPG solvents did not reflect Stokes-Einstein behavior. Plots (Figure 6.9) of ($D * \mu / T$) versus μ yield straight lines of positive slope. Stokes-Einstein behavior would result in a slope of zero for each probe. The observed slopes are dependent on the size of the diffusing molecule and vary by a factor of approximately five. Diffusion measurements of tetracene and rubrene in these polymers are difficult to perform due to the ease of monitor beam photobleaching. Rubrene, however, diffuses more slowly than tetracene as outlined in Table 6.5.

Diffusion coefficients in polymer systems are frequently interpreted in terms of reptation theory introduced by de Gennes in 1971.[19] The solvent and probe molecules in our system, however, are of insufficient length to display the highly entangled behavior required for reptation.[20] The critical exponent for the length dependence of the diffusion coefficient varies between -0.40 and -0.75, dependent on solvent, rather than -0.50 predicted for diffusion with a reptation mechanism. The complicated behavior of the diffusion coefficient in this chain media is not at present amenable to theoretical treatment. Within a particular solvent, however, it appears the critical feature is the hydrodynamic length of the diffusing probe. Figure 6.10 shows a comparison of the diffusion coefficient of NBD labelled poly(ethylene

Notes to Table 6.5

[a] Diffusion coefficient, standard error of the mean.

[b] Mobile fraction.

[c] Number of measurements.

[d] Probe concentration = 3.5×10^{-6} mol L^{-1}.

[e] [tetracene] = 9.6×10^{-5} mol L^{-1}.

[f] [tetracene] = 5.7×10^{-5} mol L^{-1}.

[g] [rubrene] = 6.8×10^{-5} mol L^{-1}.

[h] [rubrene] = 4.7×10^{-5} mol L^{-1}.

Table 6.5: Probe Diffusion in Poly(propylene glycol) at 25 °C

Solvent (mol/g)	μ (cP^{-1})	D (10^{13} m^{-2} s)[a]	Xm[b]	N[c]
		NBD-methanol[d]		
425	80	85 ± 10	0.99	10
1000	150	64 ± 8	1.00	18
2000	300	63 ± 7	0.98	9
3000	600	53 ± 5	0.98	10
4000	930	59 ± 5	0.98	8
		NBD-citronellol[d]		
425	80	70 ± 7	0.99	19
1000	150	44 ± 3	1.00	18
2000	300	38 ± 2	0.97	17
3000	600	36 ± 2	0.98	16
4000	930	39 ± 3	0.98	10
		NBD-solanesol[d]		
425	80	41 ± 2	0.97	10
1000	150	34 ± 2	0.96	10
2000	300	20 ± 1	0.95	10
3000	600	16 ± 1	0.95	10
4000	930	14 ± 1	0.93	10

(continued)

Table 6.5 (continued)

Solvent (mol/g)	μ (cP^{-1})	D (10^{13} m^{-2} s)[a]	Xm[b]	N[c]
		NBD-dolichol[d]		
425	80	33 ± 4	0.99	10
1000	150	24 ± 2	0.95	9
2000	300	14 ± 1	0.93	10
3000	600	12 ± 1	0.92	10
4000	930	11 ± 1	0.93	10
		Tetracene		
2000	300	53 -	0.94	1
4000	930	54 ± 2	0.93	4
		Rubrene		
2000	300	26 ± 2	0.81	10
4000	930	22 ± 2	0.78	7

Figure 6.8: Lateral diffusion coefficients of trace amounts of NBD labelled isoprenoid alcohols in neat PPG polymer solutions as a function of polymer size. The larger PPG polymers are more viscous. The probes employed were NBD-citronellol (o), NBD-solanesol (●), and NBD-dolichol (Δ). The approximate viscosity range of the bilayer interior is shown by the boxed region. Error bars represent standard errors of the mean.

a

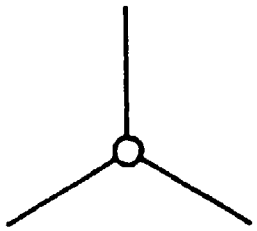

b

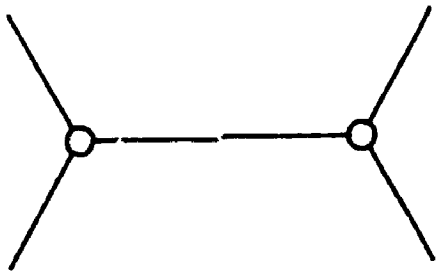

c

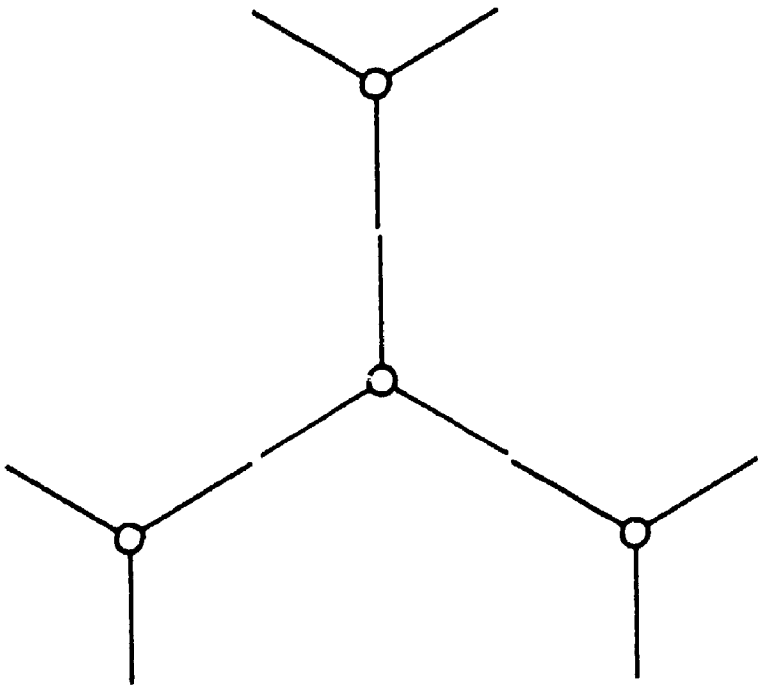

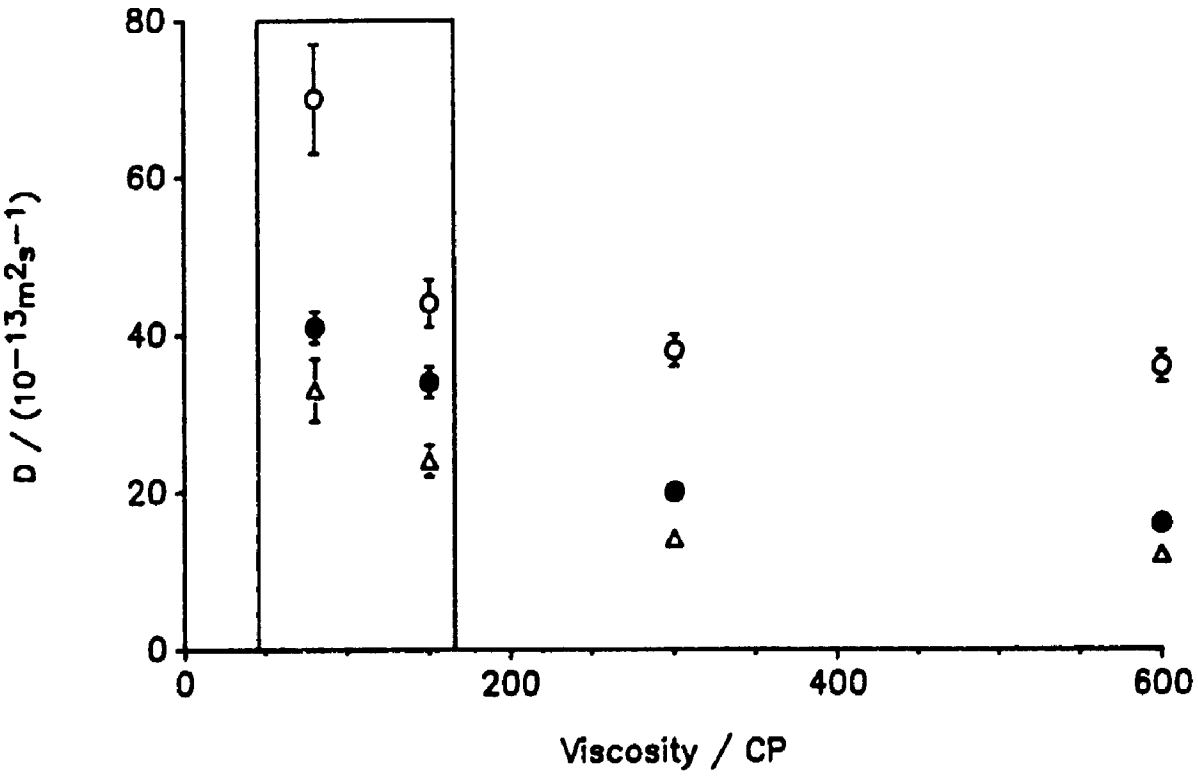
80
60
40
20
0
0
200
400
600
D / ($10^{-13}m^2s^{-1}$)
Viscosity / CP

Figure 6.9: Examination of Stokes-Einstein behavior in PPG polymers. Plots of $D * \mu / T$ versus μ should yield straight lines with a slope of zero if Stokes-Einstein behavior is observed. The probes employed were, NBD-methanol (o), NBD-citronellol (●), NBD-solanesol (Δ), and NBD-dolichol (▲). Error bars represent standard errors of the mean.

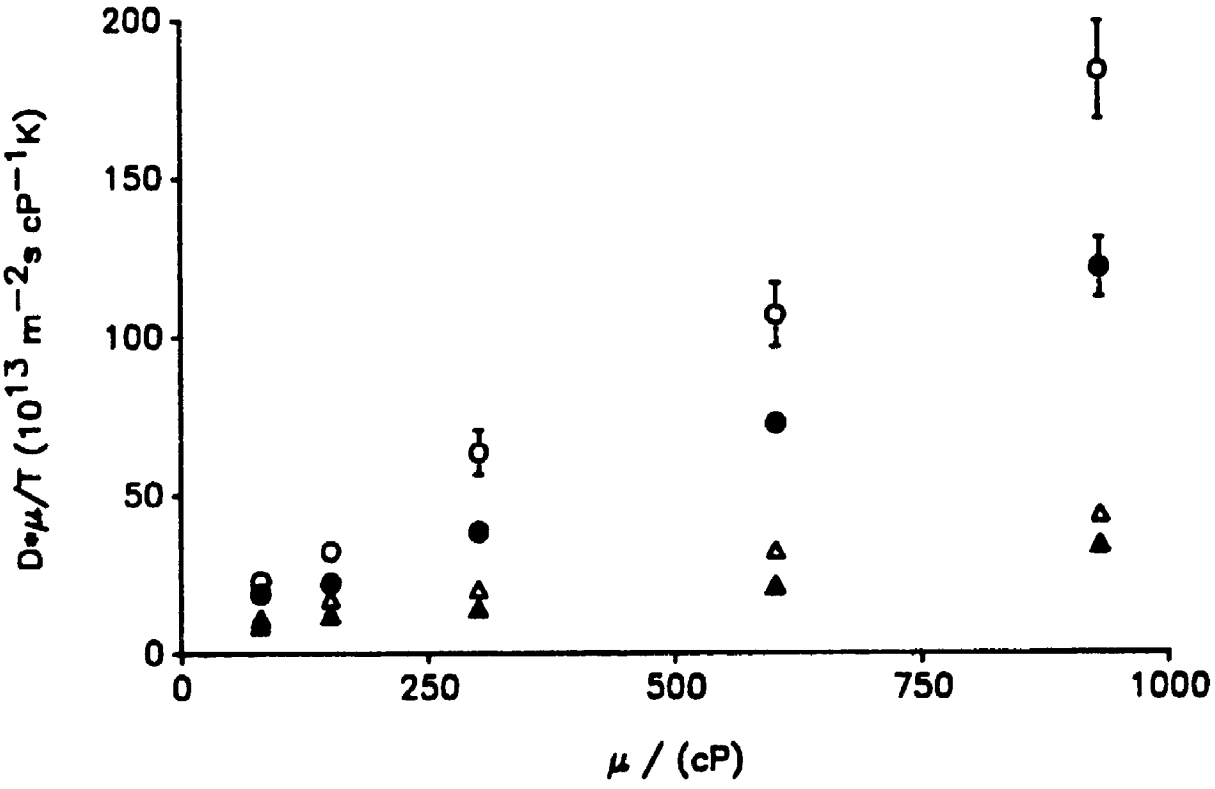
200
150
100
50
0
0
250
500
750
1000
D•μ/T (10^13 m^-2 s cP^-1 K)
μ / (cP)

Figure 6.10: Comparison of the diffusion coefficients of (o) NBD-solanesol and (Δ) NBD labelled poly(ethylene glycol) methyl ether in PPG polymer. The average molecular weight of the unlabelled glycol is 750 g/mol. The two labelled probes have approximately the same length. Error bars represent standard errors of the mean.

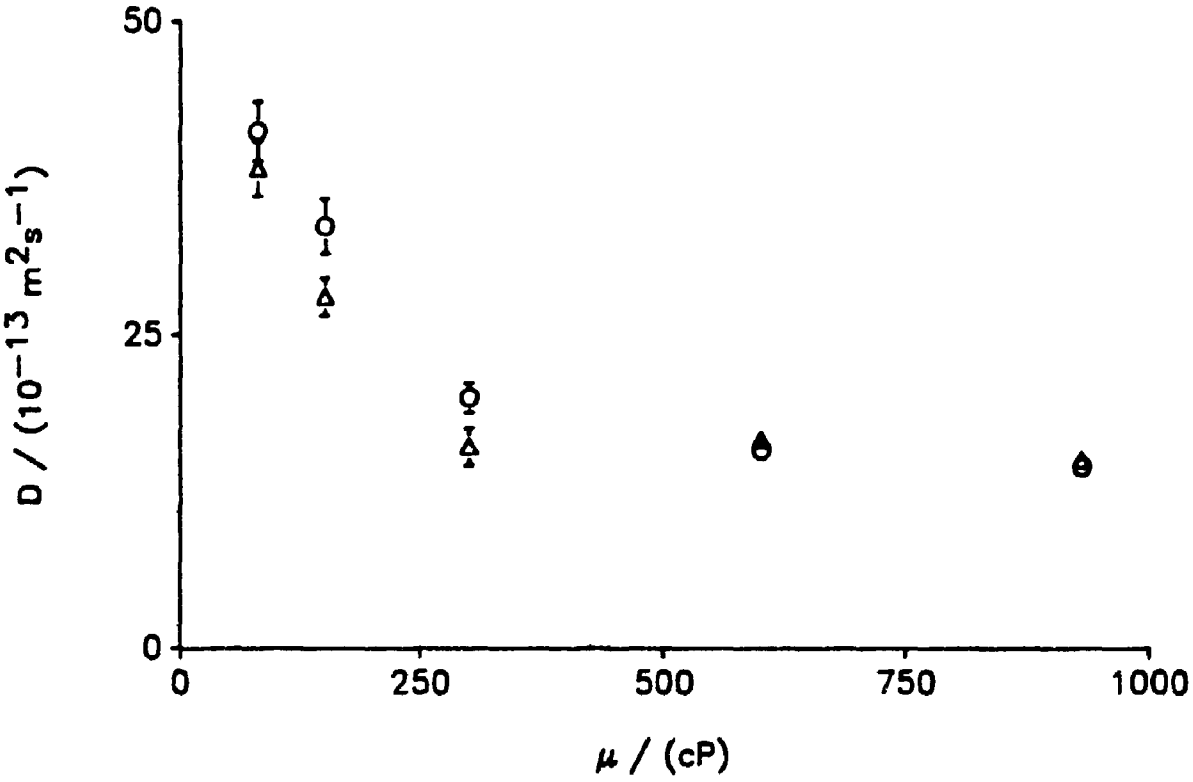
50
25
0
0
250
500
750
1000
D / (10^{-13} $m^2 s^{-1}$)
μ / (cP)

glycol) methyl ether of average molecular weight 750 g/mol and NBD labelled solanesol.[21] The labelled polyether probe and labelled solanesol have approximately the same length. They display nearly identical diffusion coefficients over the range of solvents investigated. Few investigators have considered FPR as a means of measuring lateral diffusion coefficients in polymer melts.[22,23] The ease of the experiment and current interest in polymer diffusion, suggests this may be a fruitful area of future endeavor.

6.4 Variation in Probe Headgroup Area, DMPC Bilayers

6.4.1 Measurements in the Liquid Crystal State

Lateral diffusion coefficients of labelled monomers and dimers, based on the triester structure outlined in Chapter Four, were measured in DMPC membranes. These measurements were performed, at a tracer level, in both liquid crystal (29 °C) and gel (19 °C) phase membranes. Unfortunately, synthetic difficulties precluded measurements on the 1° NBD 11C dimer and the corresponding labelled tetramers.

The results of our measurements, in the liquid crystal phase, for labelled monomers with alkyl chains of six, eight, and eleven carbons are displayed in Table 6.6 and Figure 6.11. Included for comparison purposes are the diffusion measurements for NBD-PE in DMPC bilayers. Once again we observe mobile fractions of approximately one. There appears to be little dependence of the diffusion coefficient on hydrocarbon length or degree of labelling.

Similar results, Table 6.6 and Figure 6.11, are observed for the

Table 6.6: Probe Diffusion in DMPC Multibilayers

Probe	lipid/label	D (10^{13} m^{-2} s)[a]	Xm[b]	N[c]
		Liquid Crystal Phase 29 °C		
1° NBD 6C monomer	1500	50 ± 5	1.01[d]	20
1° NBD 8C monomer	1500	65 ± 5	0.96	21
1° NBD 11C monomer	1500	47 ± 4	0.97	17
3° NBD 11C monomer	1000[e]	46 ± 4	0.98	17
1° NBD 6C dimer	2000	52 ± 4	0.98	21
1° NBD 8C dimer	1500	61 ± 5	1.00	21
NBD-PE[f]	1200	50 ± 2	0.97	38
		Gel Phase 19 °C		
1° NBD 6C monomer	1500	0.18 ± 0.04	0.64	12
1° NBD 8C monomer	1500	0.11 ± 0.02	0.52	10
1° NBD 11C monomer	1500	0.14 ± 0.01	0.42	2
3° NBD 11C monomer	1000[e]	-[g]	-	5
1° NBD 6C dimer	2000	0.35 ± 0.21	0.50	5
1° NBD 8C dimer	1500	0.38 ± 0.08	0.41	6
NBD-PE	1500	0.32 ± 0.01	0.66	20

[a] Diffusion coefficient, standard error of the mean.

[b] Mobile fraction.

[c] Number of measurements.

[d] Mobile fractions larger than 1.0 are physically impossible. This is the fitted value.

[e] Lipid/probe = 3000.

[f] Aggregate of two preparations. One has lipid/label = 1500.

[g] Diffusion measurements proved impossible due to negligible recovery.

Figure 6.11: Tracer diffusion coefficients of NBD labelled triester monomers and dimers, and PE in the liquid crystal phase. The labelled monomers are 1° NBD 6C monomer (6M), 1° NBD 8C monomer (8M), 1° NBD 11C monomer (11M), and 3° NBD 11C monomer (11M3). The labelled dimers are 1° NBD 6C dimer (6D) and 1° NBD 8C dimer (8D). PE of course refers to the NBD labelled analogue. The measurements were made on liquid crystal phase DMPC multibilayers at 29 °C. Error bars represent standard errors of the mean.

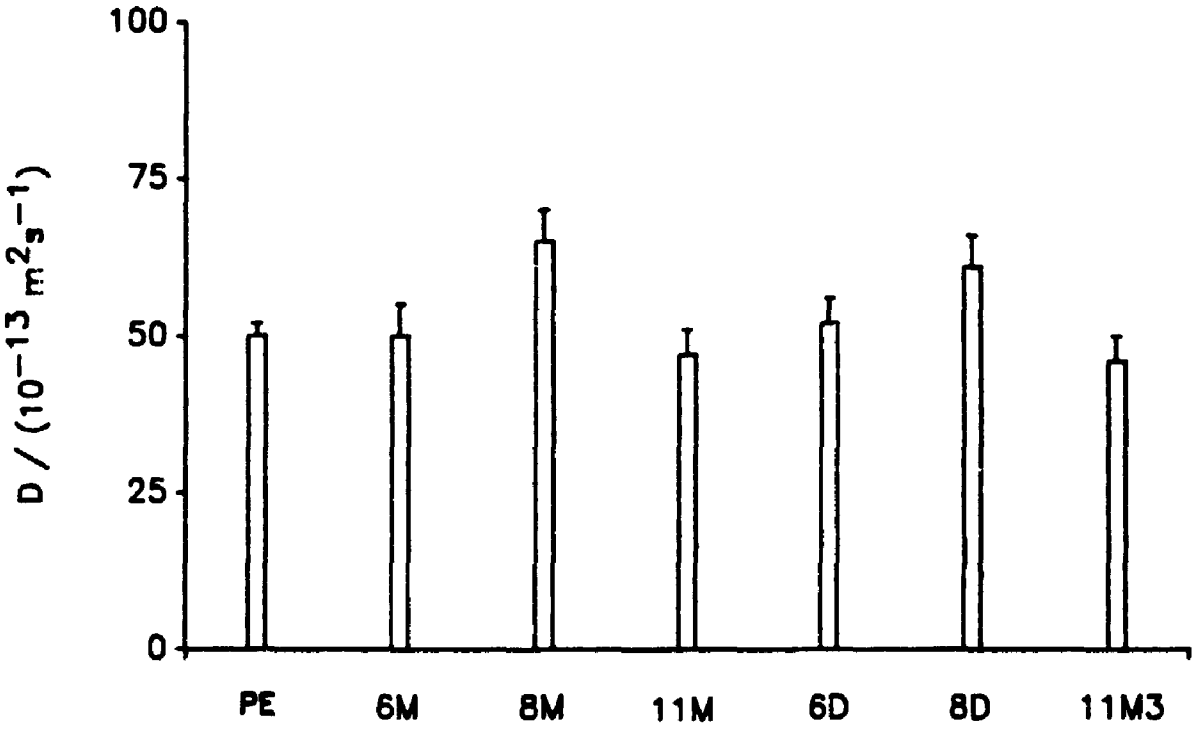
100
75
50
25
0
D / (10^{-13} m^2s^{-1})
PE
6M
8M
11M
6D
8D
11M3

labelled dimers. All the probes except 1° NBD 8C monomer and 1° NBD 8C dimer have the same diffusion coefficient as NBD-PE. The comparison of means was made with the student t test at a ninety-five percent confidence level. Both the eight carbon triester monomer and dimer diffuse somewhat faster than NBD-PE. It seems unlikely this is more than an artifact since both 11C monomer derivatives diffuse at the same rate as NBD-PE.

6.4.2 Measurements in the Gel State

Diffusion measurements (Table 6.6) were performed on DMPC bilayers below the main phase transition temperature for the labelled triester monomers and dimers mentioned previously. The results are displayed graphically in Figure 6.12. As expected, one observes greatly decreased diffusion coefficients and mobile fractions which are substantially less than one. In the case of the triply labelled 3° NBD 11C monomer, there is essentially no recovery and, therefore, no measurable diffusion coefficient. Evidently, the presence of three bulky NBD labels in the frozen matrix effectively immobilizes this probe.

The three singly labelled monomers diffuse at similar rates and are significantly slower than NBD-PE under identical conditions. The labelled dimers, however, diffuse at the same rate as NBD-PE as judged by the student t test at a ninety-five percent confidence level. The error in the measurement of 1° NBD 6C dimer is quite large. Diffusion of the dimer species faster than the corresponding monomer is contrary to expectation.

fixed frame of reference.

The observed recovery of the fluorescence in a spot photobleaching experiment is due to the flux observed through the microscope optics. This is the flux with respect to the laboratory, or area, fixed frame of reference. To measure a true diffusion coefficient, the second term of Equation 7.1 must be zero, or insignificant, with respect to the first term. As discussed above, the multibilayers themselves do not move during the course of an experiment. Therefore, gross displacement of the vesicle structure does not cause the observed recovery. Alternate systems, investigated before the 'lipid sandwich' method was developed, invariably suffered from flow of the multibilayer assemblies.

The absence of gross displacement of the multibilayer, however, does not ensure that the second term of Equation 7.1 is insignificant. One must still examine the contribution to the observed recovery of convective flow of the host lipid in the multibilayer. Theoretical treatments of flow and diffusive recovery of the fluorescent signal after photobleaching suggest a functional form for the recovery which differs for diffusion and flow.[1] The statistical nature of the experiment, however, means that in a practical sense, it is impossible to discriminate between the two. The conditions of mechanical and thermal equilibrium, however, still apply. Convective flow will occur only in the presence of an active stimuli such as a pressure or temperature gradient. To the best of our knowledge, convective lipid flow has not been observed in model membrane systems. Convective flow has been postulated to occur in eukaryotic cell membranes with an unknown driving force.[2]

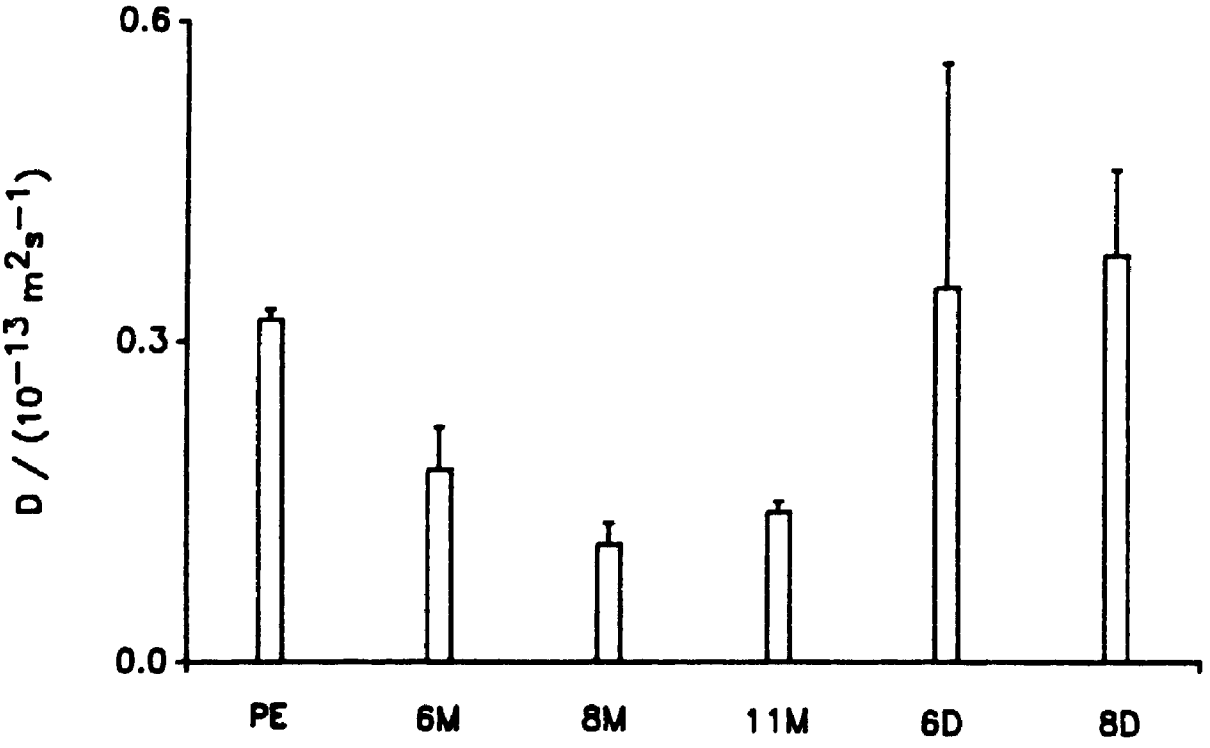
0.6
0.3
0.0
D / (10^{-13} m^2s^{-1})
PE
6M
8M
11M
6D
8D

Diffusion measurements of labelled monomers and dimers were not pursued in model viscous isotropic solutions. These measurements were not undertaken because the isotropic solution does not mimic the liquid crystal ordering of our probes in the membrane. Examination of a headgroup effect presumably requires this ordering. Isotropic solution studies to investigate the hydrocarbon chain length effect, as discussed earlier, are valid since the head group and its interaction with neighboring lipids are not of primary concern for these probes.

REFERENCES

(1) Vaz, W. L.; Clegg, R. M.; Hallmann, D. *Biochemistry* **1985**, *24*, 781.

(2) Bjarneson, D. W.; Petersen, N. O. *J. Am. Chem. Soc.* **1990**, *112*, 988.

(3) Bjarneson, D. W. The University of Western Ontario, unpublished results, 1990.

(4) Valtersson, C.; Van Duyn, G.; Verkleij, A. J.; Chojnacki, T.; de Kruijff, B.; Dallner, G. *J. Biol. Chem.* **1985**, *260*, 2742.

(5) Schroeder, F.; Gorka, C.; Williamson, L. S.; Wood, W. G. *Biochim. Biophys. Acta* **1987**, *902*, 385.

(6) Spisni, A.; Masotti, L.; Lenaz, G.; Bertoli, E.; Pedulli, F.; Zannoni, C. *Arch. Biochem. Biophys.* **1978**, *190*, 454.

(7) Lenaz, G. Castelli, G. P. In *Structure and Properties of Cell Membranes*; Benga, G. Ed.; CRC Press: Boca Raton, FL, 1985; Vol. 1, pp 93, 136.

(8) McCloskey, M. A.; Troy, F. A. *Biochemistry* **1980**, *19*, 206.

(9) Nagle, J. F. *Ann. Rev. Phys. Chem.* **1980**, *31*, 157.

(10) Nagle, J. F. *Faraday Discuss. Chem. Soc.* **1986**, *81*, 151.

(11) Silver, B. L. *The Physical Chemistry of Membranes*; Solomon: New York, 1985; pp 75, 109.

(12) Derzko, Z.; Jacobson, K. *Biochemistry* **1980**, *19*, 6050.

(13) Wei, K. S.; Livingston, R. *Photochem. Photobiol.* **1967**, *6*, 229.

(14) Trissl, H. W. *Biochim. Biophys. Acta* **1974**, *367*, 326.

(15) Petersen, N. O.; Felder, S.; Elson, E. L. In *Handbook of Experimental Immunology*; Weir, D. M., Ed.; Blackwell: Edinburgh, 1986; Vol. 1, pp 24.1, 24.23.

(16) Qian, H.; Elson, E. L. In *Digitized Video Microscopy*; Liss, 1990; In Press.

(17) *Landolt-Bornstein Zahlenwerte und Funktionen*; Springer-Verlag: Berlin, 1969; Vol. 2(5a), p 371.

(18) Tanford, C. *Physical Chemistry of Macromolecules*; Wiley: New York, 1961; p 344.

(19) de Gennes, P. G. *J. Chem. Phys.* **1971**, *55*, 572.

(20) Klein, J. *Philos. Mag. A* **1981**, *43*, 771.

(21) Giroux, C. B.Sc. Thesis, The University of Western Ontario, London, Ont. 1989.

(22) Smith, B. A. *Macromolecules* **1982**, *15*, 469.

(23) Smith, B. A.; Samulski, E. T.; Yu, L. P.; Winnik, M. A. *Macromolecules* **1985**, *18*, 1901.

CHAPTER SEVEN

DISCUSSION

7.1 Validity of the Measurements

Fluorescence Photobleaching Recovery Measurements of diffusion are subject to large statistical errors. The meagre light intensities and small observation areas give rise to a significant uncertainty in the measured light intensity, resulting in a poorly measured diffusion coefficient. The unexpected results for the labelled isoprenoid alcohols and the triester dimers mean that a consideration of the random and systematic errors of our measurements takes on an added importance.

A great deal of time and effort was expended in developing the 'lipid sandwich' technique for preparing vesicles, as described in Chapter Three. Our intention was to reproducibly generate phospholipid bilayers incorporating the probe of interest. This goal was achieved with NBD-PE and NBD-citronellol serving as the trial probes. Diffusion coefficients measured from separate multibilayer preparations generally differed by less than the standard deviation associated with a series of measurements on one preparation. In the liquid crystal phase membranes, the typical population standard deviation of the diffusion coefficient was thirty percent of the mean. This is a large relative error which necessitates a large number of experiments to accurately measure the diffusion coefficient. The population standard deviation associated with measurements in three-dimensional solution was typically twenty percent, or less, of

the mean. Presumably the bilayer results are less precise due to a small natural variation in the vesicles.

The 'lipid sandwich' technique has the advantage that the swollen multibilayers develop from the lipid film forming the top layer of the assembly. Diffusion measurements are performed with this structure inverted so there are no obstructions between the multibilayers chosen for diffusion measurements and the top coverslip. In addition, this arrangement permits the multibilayers to sit, in mechanical equilibrium, on the glass coverslip forming the bottom of the sandwich structure. Situating the wax-sealed sandwich structure in a water-filled, temperature controlled, copper disk ensures that the system is also in thermal equilibrium.

Multibilayers resting on the bottom coverslip of this structure do not move over the time course of the experiment. A typical measurement with three bleach/recovery sequences requires approximately thirty seconds in the liquid crystal phase. Frequent checks were made using the microscope eyepiece and associated cross hairs to ensure that the multibilayers do not move or change shape.

Concern with the mechanical stability of the multibilayer assembly relates to the measured diffusion coefficient through Equation 7.1.

$$n_1 = J_1^a + c_1 v^a \qquad (7.1)$$

In Equation 7.1, n_1 is the flux of material relative to the laboratory frame of reference, while J_1^a is the flux due to diffusion and $c_1 v^a$ describes the convective flow of the system with respect to the area

fixed frame of reference.

The observed recovery of the fluorescence in a spot photobleaching experiment is due to the flux observed through the microscope optics. This is the flux with respect to the laboratory, or area, fixed frame of reference. To measure a true diffusion coefficient, the second term of Equation 7.1 must be zero, or insignificant, with respect to the first term. As discussed above, the multibilayers themselves do not move during the course of an experiment. Therefore, gross displacement of the vesicle structure does not cause the observed recovery. Alternate systems, investigated before the 'lipid sandwich' method was developed, invariably suffered from flow of the multibilayer assemblies.

The absence of gross displacement of the multibilayer, however, does not ensure that the second term of Equation 7.1 is insignificant. One must still examine the contribution to the observed recovery of convective flow of the host lipid in the multibilayer. Theoretical treatments of flow and diffusive recovery of the fluorescent signal after photobleaching suggest a functional form for the recovery which differs for diffusion and flow.[1] The statistical nature of the experiment, however, means that in a practical sense, it is impossible to discriminate between the two. The conditions of mechanical and thermal equilibrium, however, still apply. Convective flow will occur only in the presence of an active stimuli such as a pressure or temperature gradient. To the best of our knowledge, convective lipid flow has not been observed in model membrane systems. Convective flow has been postulated to occur in eukaryotic cell membranes with an unknown driving force.[2]

The observation of a constant diffusion coefficient in the liquid crystal phase, for all the NBD labelled species, suggests we could be measuring an artifact and not true diffusion coefficients. Such an artifact could be caused by reversible photobleaching. If the recovery of the fluorescence signal is not due to diffusive motion, but instead occurs due to reversible photobleaching, then the recovery would reflect the kinetics of the reverse reaction. Scalettar et. al.[3] have recently proposed that reversible photobleaching can occur due to depletion of the ground state by intersystem crossing to the triplet state. This is a short-lived effect and is unlikely to occur on the millisecond time scale of our diffusion measurements. Bleaching an entire vesicle showed there was negligible recovery due to reversible photobleaching. This is a control experiment described in Chapter Three.

If flow does not cause the observed recovery, and if photobleaching is irreversible, then perhaps we are measuring the same diffusing entity in all our membrane experiments. This entity need not be the labelled molecule of interest. This could occur since it is fluorescence we observe, presumably due to NBD, not necessarily the labelled species. Phospholipid multibilayers prepared in the absence of NBD label are not fluorescent. Therefore an impurity, if present, does not originate in the bilayer preparation. Another possible source of contamination could be free NBD from chemically impure samples. For this reason great care was taken in the synthesis, purification, and stability analysis of all our labelled compounds. If an impurity is present, it is unlikely to be significant compared to the true labelled compound. Diffusion coefficients measured in the

gel state show distinctly different size dependencies for all our labelled compounds. Had our measurements reflected the motion of a common impurity in our preparations, one would expect to observe an invariant diffusion coefficient in our gel phase experiments.

Microscopic observation of our multibilayers reveals no anomalous structure in the presence of fluorophore. Altering the plane of focus of the microscope under laser illumination reveals that the fluorescence originates only from the lamella of the bilayer structure. Focusing the laser beam on the interior or exterior of a unilamellar vesicle reveals minimal fluorescence. The small amount of signal detected by eye is very diffuse and originates primarily from out of focus membranes. Changing the plane of focus to the dorsal or ventral surfaces of the membrane reveals a bright spot of fluorescence. This is true in both the liquid crystal and gel phase membranes. It indicates that the fluorophore is not water soluble, and therefore aqueous diffusion is not responsible for the observed recovery. This observation, however, must be tempered by the knowledge that NBD fluorescence is quenched by water.

Examination of the structure of our labelled probes reveals they are, in any case, too hydrophobic to reside as individual entities in the aqueous medium surrounding the vesicle. The synthesis of all our labelled compounds involved aqueous extraction. Minimal color was observed in the aqueous phase for extractions of the nearly pure materials. This indicates they are not water soluble. Control experiments indicate that the pure, unlabelled triesters have little tendency to form micelles or reverse micelles in aqueous solution. The significant losses observed in the syntheses of triester based

species probably depends on the presence of organic solvents such as DMSO in the aqueous phase. The labels themselves, NBD-acid and IANBD, are not water soluble although (vide infra) they have significant polarity.

Thus it appears that the result of our FPR measurements on cell membranes is a true measure of lateral diffusion coefficients. This idea is supported by the close agreement found between our measurement of the rate of diffusion of NBD-PE in DMPC multibilayers and a measurement on the same system by Vaz et. al.[4] We measure the diffusion coefficient to be 5.0×10^{-12} m^2s^{-1} at 29 °C while Vaz et. al. measure 5.7×10^{-12} m^2s^{-1} at 30 °C.

7.2 Hydrodynamic Interactions in the Membrane Interior

The preceding discussion reveals that the invariance of our measured diffusion coefficients with molecular size and shape, in the liquid crystal phase, does not result from systematic error in the performance of our experiments. If one accepts this conclusion, then the consistency of the results suggests a common mechanism for both labelled phospholipids and our series of labelled isoprenoid alcohols.

The common feature in the isoprenoid alcohol series, other than the fundamental isoprene unit, is the NBD label. Fluorescence quenching studies have shown shown that NBD in the terminal position of flexible phospholipid acyl chains, has sufficient polarity to loop back toward the aqueous interface.[5,6] NBD attached to the terminus of rigid steroids such as cholesterol will not loop back to the surface.[5,6]

Indirect evidence for the polarity of NBD comes from observations

made earlier in this thesis. The chromatographic behavior of the NBD labelled isoprenoid alcohols and triesters depended to a large extent, with silica gel, on the NBD label. For example, the R_f for NBD labelled citronellol, solanesol, and dolichol is essentially the same for all three molecules. Separations on silica gel are primarily based on polar interactions with the silica surface.[7] Diffusion measurements in paraffin oil, a totally hydrocarbon medium, were marred by surface aggregation. This aggregation was presumed to occur due to the polarity of the NBD moiety or its ester linkage.

If the NBD label is sufficiently polar to reside somewhere near the vicinity of the bilayer/water interface it appears likely that the rate of lateral diffusion of the labelled isoprenoid alcohols is limited by the free area fluctuations at the surface. NBD need not reside at the interface to experience this effect. The alkyl chains of the host phospholipid are quite ordered near the aqueous surface but are more random in their motion near the interior of the membrane.[8,9] If NBD resides in the vicinity of the ordered portion of the alkyl chains, its motion will be limited by their lateral motion according to the Free Area Theory. If the bulk of the probe chain resides in the interior of the membrane, and the interior is quite fluid, one might anticipate little or no dependence of the diffusion coefficient on probe chain length.

Companion diffusion measurements with non-polar fluorophores support this interpretation. Tetracene and rubrene have no tendency to reside near the aqueous surface because they are non-polar. They diffuse faster than NBD-PE and the labelled isoprenoid alcohols. Free Area Theory suggests that diffusion faster than the host lipid is

not possible. Violation of this basic tenet of the theory suggests that the rate of diffusive motion for tetracene and rubrene is not controlled by the surface behavior of the bilayer assembly. Rather, they must move in the hydrocarbon interior of the membrane although, presumably, there will be some coupling to the rate of host lipid diffusion.

Diffusion measurements of the labelled alcohols in the gel phase also support this mechanism. As discussed previously, the hydrocarbon chains in the gel phase are packed in a crystalline state. The alkyl chains of the labelled alcohols should have an effect on the diffusion coefficient if the membrane interior becomes more restrictive to lateral motion. This effect is observed experimentally.

Not only do the labelled isoprenoid alcohols span an order of magnitude in length but they vary by approximately a factor of four in mass. Clearly this variation in mass is unimportant, as is the variation in size. Molecular dynamics studies of impurity diffusion in two-dimensional hard disk systems suggest that there should be a mass dependence of the diffusion coefficient.[10] We do not observe this behavior. Presumably this occurs because the restricting feature of NBD labelled alcohol diffusion is the NBD headgroup itself, and the alkyl chains are unimportant. This view, promulgated earlier in the chapter, essentially views the labelled alcohols as a ball and chain system. The ball restricts the long range motion while the chain is permitted a great deal of dynamic freedom. Increasing the length of chain in this analogy does not alter the long range motion but does increase the overall dimensions of the molecule. This analogy is not exact since the cross-sectional area of the NBD label is not vastly

different from that of the isoprene chains.

A continuum mechanics interpretation of the non-dependence of the diffusion coefficient on size would hold that the membrane has a high Reynolds number and so viscous, not inertial, effects on the diffusion coefficient are of paramount importance. Our model of the system would suggest that the hydrodynamic restriction on motion is the NBD label itself.

The experiments in three-dimensional solutions were intended to explore what might have been expected to occur if the NBD labelled alcohols diffused in the disordered region of the membrane interior. Our experiments indicate that had this been true, diffusion of the labelled alcohols should have been distinguishable, based on their length, in the liquid crystal phase. The model systems are not a true rendering of the membrane interior, since unquestionably the membrane interior must retain some residual order perpendicular to the aqueous interface. The PPG matrices, however, are random media with all manner of interacting chains.

Diffusion coefficients measured in three-dimensional solution, although they approximate the viscosity of the membrane interior, are not directly comparable to those measured in the membrane. Direct comparisons are not appropriate because, as mentioned above, the alkyl chains of the membrane possess some residual order while the polymers do not. Comparing viscosities based on assigning a three-dimensional tensor viscosity to the thin anisotropic membrane sheet is fraught with difficulty due to the restrictive geometry of the membrane. Systematic error in the three-dimensional diffusion coefficient, due to relaxation of the concentration gradient in the z dimension,[11] also

precludes direct comparison of diffusion coefficients in the two media.

Recently Rajarathnam et. al.[12] measured the rate of lateral diffusion of headgroup labelled ubiquinone in model membranes and mitochondrial membranes. Ubiquinone is an integral component of the electron transfer chain that mediates the transfer of electrons in the mitochondrial membrane.[13] It possesses a quinone headgroup and a linear chain made up of ten unsaturated isoprene units. Their diffusion measurements with relatively large probe concentrations using a variant of the basic FPR technique, confirmed our results with the structurally similar isoprenoid alcohols. They found that the labelled ubiquinone diffused, in both types of membranes, at the same rate as NBD-PE. They suggest, as do we, that the NBD label is sufficiently polar to penetrate to some degree into the region of the more rigid phospholipid acyl chains. Figure 7.1 illustrates the NBD location suggested by our experiments. Based on this mechanism for lateral diffusion of the labelled isoprenoid alcohols, one could predict that the apparent activation energy for these probes should be equal to the four to eight kcal per mole observed for NBD-PE.

Steady state fluorescence quenching experiments were performed in an effort to confirm the location of the NBD moiety associated with our labelled alcohols sequestered in bilayers. Small unilamellar vesicles, formed from DMPC with lipid/label ratios of approximately 500/1 were used for these experiments. The set of labels investigated comprised three NBD labelled molecules (NBD-PE, NBD-cholesterol, NBD-PC), for which the probe location in the membrane is known and two, NBD-citronellol and NBD-solanesol, which have an uncertain probe

Figure 7.1: Cross-section of a membrane bilayer illustrating the proposed location of the NBD probe (dark circle) for our labelled isoprenoid alcohols. This location is inferred by a variety of diffusion measurements and steady state fluorescence quenching experiments.

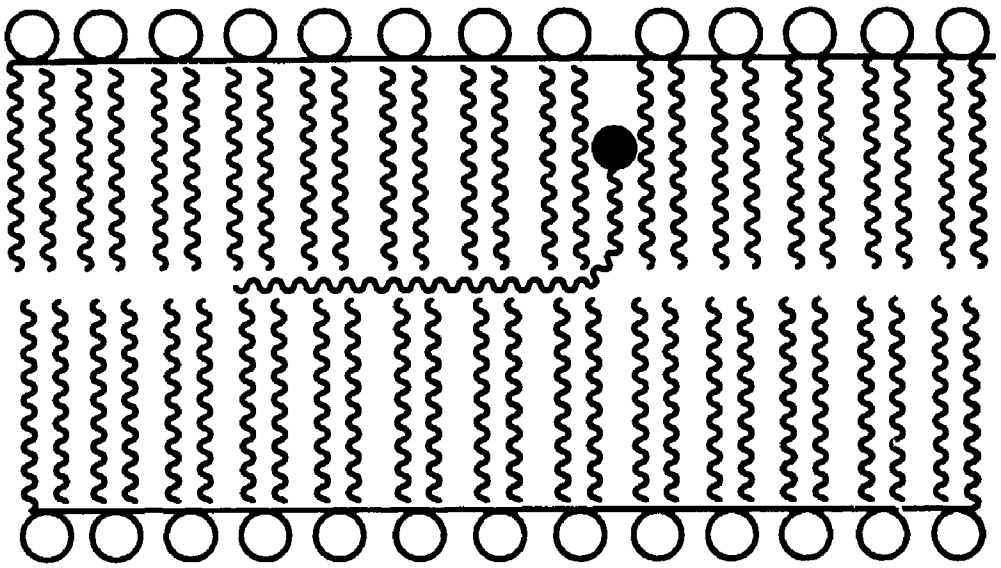

location. NBD-PE is known to localize the NBD label near the aqueous interface,[5,6] while NBD-cholesterol, due to the rigid steroid ring structure, submerges the NBD label in the membrane interior.[5,6] The NBD label in NBD-PC has been shown to loop back toward the aqueous interface.[5,6] The quenching agent, Co^{2+}, is known to quench NBD fluorescence with a collision quenching mechanism.[14]

An important distinction should be drawn at this point between the two sets of molecules described above. The first group are known surfactants to which a fluorescent probe has been added. Whatever the orientational tendency of the second group, their hydrophilic contribution to the orienting force is provided solely by the NBD label and its associated ester linkage.

The results of the steady state quenching experiments are shown in Figure 7.2 as a Stern-Volmer plot. The slope of such plots cannot be interpreted as true quenching rate constants since the system is anisotropic and the quencher and fluorophore are physically separated. Non-linear behavior of the Stern-Volmer plot in this context has been interpreted as an indication that quencher bound to the surface of the vesicle is the effective quenching species, and surface saturation has occurred.[8] Chattopadyay and London[6] interpret the slope as an indication of the degree of exposure of the NBD group to the aqueous quencher. Fluorophores sequestered in the interior of the membrane will be quenched less effectively than those at the surface.

The results displayed in Figure 7.2 demonstrate the NBD probe does not reside at the bilayer surface. Weak quenching with the surface bound cobalt indicates only that the NBD label is not within the critical quenching distance of the cobalt ion. The measurement

Figure 7.2: Stern-Volmer plot of fluorescence quenching of NBD labelled molecules in DMPC bilayers by aqueous Co^{2+}. The labelled probes are NBD-PE (●), NBD-PC (o), NBD-cholesterol (Δ), NBD-citronellol (□), and NBD-solanesol (▲).

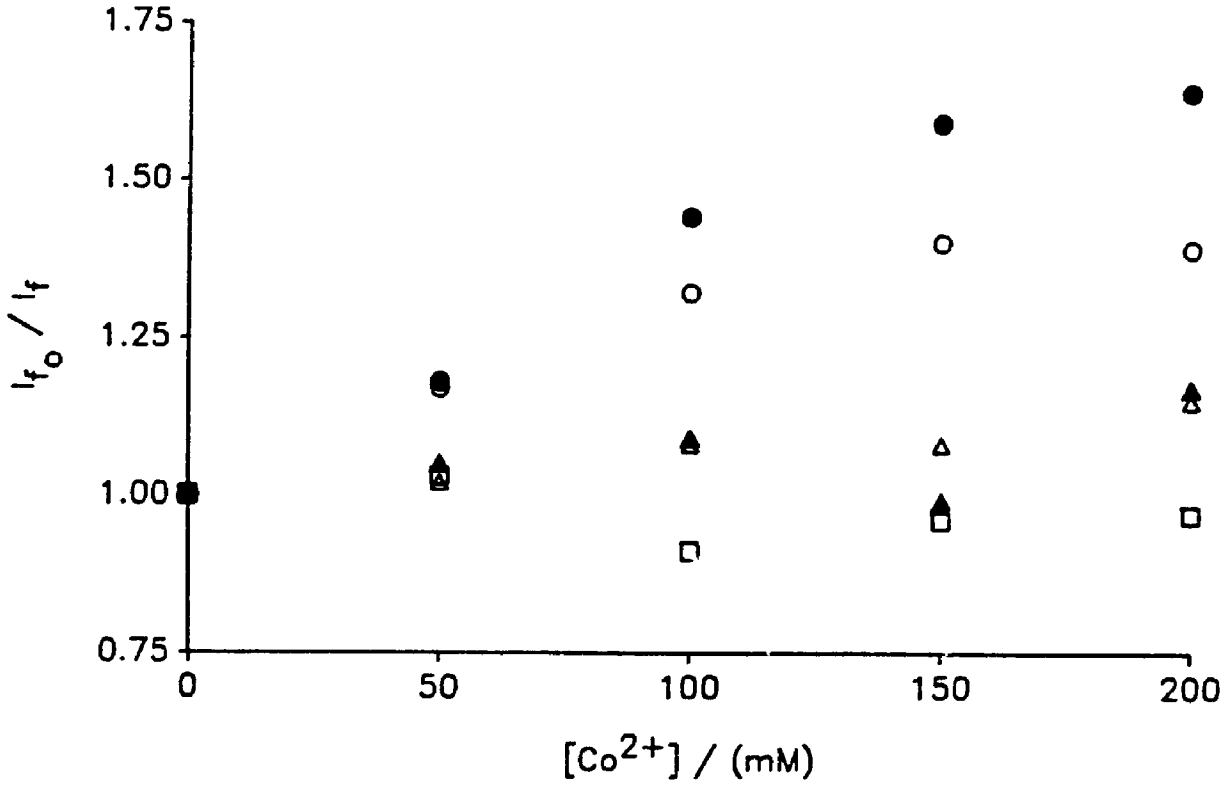
1.75
1.50
1.25
1.00
0.75
I_{f_o} / I_f
0
50
100
150
200
$[Co^{2+}]$ / (mM)

does not indicate how deep the probe resides in the membrane. A more precise interpretation of these results is clouded by uncertainty about possible binding of the Co^{2+} to the bilayer surface and by possible differential lifetime effects of the various NBD species.[6]

Nitroxyl spin labels are efficient contact quenchers of NBD fluorescence. Spin labels attached to phospholipids at various points along the hydrocarbon chain have been used to identify NBD at several different depths in model membrane system.[5] This 'parallax' measurement, although conceptually simple, proved difficult in our hands. Reproducibility was elusive although initial results indicated the NBD labelled isoprenoid alcohols were poorly quenched by nitroxyl spin labels attached to the five and ten carbon positions in the phospholipid acyl chains.

Steady state fluorescence anisotropy measurements in small unilamellar vesicles were performed to examine the short time scale 'mobility' of the various NBD labelled species. Our results, Table 7.1, show that the NBD labelled alcohols reorient to a lesser extent than the controls during the fluorescence lifetime of the probe. This probably occurs because the structural feature orienting these molecules is the label itself. Therefore it will reorient less during its lifetime.

Table 7.1: Fluorescence Anisotropy Measurements in DMPC Bilayers

Probe	lipid/label	r[a]
	Liquid Crystal Phase 31 °C	
NBD-PE	576	0.165
NBD-PC	392	0.129
NBD-cholesterol	569	0.118
NBD-citronellol	440	0.218
NBD-solanesol	373	0.183

[a] The anisotropy was calculated according to the equation

$$r = (I_{vv} - G\, I_{vh}) / (I_{vv} + 2\, G\, I_{vh})$$

I refers to the fluorescence intensity detected by the fluorimeter. Subscripts vv and vh refer to the polarization of the excitation and emission optics. G is an instrumental correction factor.

7.3 Variation in Headgroup Size

Diffusion measurements of the labelled monomers and dimers described in the previous chapter show no effect of the headgroup size on the diffusion coefficient in liquid crystal phase membranes. This result is both intriguing and confusing. The surfactant nature of our triesters, discussed in Appendix Three, requires fewer companion measurements since the diffusive motion may be considered in terms of oriented molecular motion.

The three labelled monomers appear to diffuse at rates independent of their hydrocarbon length. This is expected based on analogous experiments performed on labelled NBD-PE of different chain lengths.[4] The differences in chain length for the 6C, 8C, and 11C monomers are trivial compared to the differences encountered with the labelled alcohols.

The NBD probe is of significant size compared to the triester monomers. In order to investigate possible putative effects of the probe on the motion of the triester unit, FPR measurements were performed with the triply labelled 11C monomer. No difference in diffusion coefficient was observed in the liquid crystal phase. Therefore, one may conclude that, although the probe may loop back to the surface, this does not alter its diffusive motion. Support for the looping behavior in our other mono-labelled triesters comes from a qualitative lack of significant fluorescence quenching by intramolecular bromine. Bromine is known to be an efficient fluorescence quencher.[15] Had the NBD label localized in the membrane interior, the intramolecular quenching by two resident bromines would

have been extreme.

Monolayer studies (Appendix Three) have shown that the triesters will incorporate in the bilayer with a 'closed', all axial, conformation. The projected area of the closed conformation is approximately that of the host phospholipid. Therefore agreement with Free Area Theory is to be expected. The apparent activation energy for diffusion is also predicted to be four to eight kcal per mole as observed for NBD-PE.

In the gel state, all three mono-labelled probes move at the same rate which is slower than NBD-PE, despite the similar projected area in the liquid crystal phase. Presumably, the inherently different nature of these surfactants accounts for the difference. Molecular interpretations of this discrepancy are impossible at present.

No discrepancy in diffusion coefficient amongst the labelled monomers and NBD-PE in the liquid crystal phase was expected. Diffusion of the labelled dimer species also at the same rate, or slightly faster, in the liquid crystal phase was surprising. Two possible explanations account for this behavior. (1) The dimer may diffuse through discrete movements of the individual monomer units, making up the dimer, by pivoting on the disulfide linkage. The dimer, under this mechanism, will not move as a discrete unit. Presumably, however, the motion of the individual monomers will be highly correlated. Since the FPR diffusion measurement is made over an area ($\approx$ 1 μm^2) much larger than the monomer dimensions, this correlation may not be observable as an alteration of the diffusion coefficient. (2) The Free Area Theory may be a poor approximation to the lateral

diffusion of test molecules slightly larger than the host lipid. Certainly the sharp drop in the diffusion coefficient with size, larger than phospholipids, is unrealistic. Clifford and Dickinson[16] have suggested, based on computer simulation, that lateral diffusion based on molecular jumps into free area voids is not the mechanism of two-dimensional lateral diffusion at moderate to high densities.

It seems likely that both explanations outlined above contain a modicum of truth. At this point our inability to label the triester tetramers is particularly galling. These molecules would be the ideal means to discriminate between the explanations. Four monomers covalently linked would be more highly correlated in their motion and large scale diffusion by discrete monomeric jumps would be less likely to masquerade as true monomer diffusion.

The precision in our data does not permit detailed commentary on the effect of changing the dimeric point of attachment. Presumably the deeper the disulfide bond in the bilayer, the more freedom the dimer unit will possess to move by correlated jumps of the individual monomers. One would not expect, however, the dimer to move faster than the host phospholipid as suggested by the diffusion measurements for the 8C dimer. Once more inability to label the 11C dimer clouds our consideration of this point.

Results from the laboratory of Harden McConnell at Stanford University support, with qualification, the first mechanism outlined above. McConnell and coworkers[17-19] have measured the lateral diffusion coefficient of lipids bound to labelled antibodies in phospholipid bilayers and supported monolayers. The macromolecular antibody will bind, due to its flexible Y shape, two haptenated lipids

widely separated on the vesicle or monolayer surface. For this system one expects large scale diffusive motion of the individual monomeric phospholipids to be correlated with the corresponding monomer only over large distances. Unlike our dimers, the antibody linked lipids will diffuse as individual units on a molecular scale. Diffusion measurements on the supported monolayers reveal that the bound phospholipids diffuse at half the rate of unbound labelled lipids.[18,19] This result has been interpreted in terms of a frictional coefficient for the aggregate which is twice that of the isolated lipids. Similar experiments with vesicles, however, have revealed no difference in the diffusion of the antibody bound species and free lipid.[17]

It is difficult to reconcile these two results. Our experiments, however, resemble the second case where no difference is observed. Differences in lateral density may account for the different behavior in the vesicle and supported monolayer systems.

In the gel state both labelled dimer probes diffuse faster then the corresponding monomers. Their rates of motion are equal to that of NBD-PE. It is difficult to interpret these results in terms of a molecular mechanism. Diffusion measurements which systematically differ, although not in the manner expected, between labelled monomer, dimer and PE, help confirm the integrity of the measurement.

7.4 Summation

We have demonstrated that valid diffusion measurements may be performed with a series of NBD labelled polymers in DMPC model

membranes. Surprisingly, all the labelled probes diffuse at rates equal to that of the host lipid's self-diffusion. The non-polar fluorophores, tetracene and rubrene, diffus. at rates faster than lipid self-diffusion in the same model system. Systematic differences are observed between the NBD labelled species in the condensed, gel state of the DMPC bilayers.

These results indicate that hydrodynamic interactions in the interior of the bilayer have an insignificant effect on the rate of probe diffusion in the liquid crystal phase. In the gel phase, however, the condensed state of the hydrocarbon chains significantly retards the rate of probe diffusion. The rate in the gel state also depends on the chain length of the diffusing molecule. The liquid crystal results may be interpreted in terms of the Free Area Theory. Fluorescence quenching results indicate, however, that the polar headgroup of our NBD labelled alcohols is not located at the water/bilayer interface. Diffusion measurements for our labelled triester dimers indicate that a sharp drop in rate with increasing diffusant radius, predicted by Equation 2.11, may be physically unrealistic.

Figure A1.1: DCC reaction with NBD-acid. This scheme shows the formation of the O-acylisourea intermediate (1), the undesirable N-acylurea (2) and the synthetically useful anhydride (3). The N-acylurea forms via an O → N acyl migration.

(19) Subramian, S.; Seul, M.; McConnell, H. M. *Proc. Natl. Acad. Sci.* **1986**, *83*, 1169.

CHAPTER EIGHT

CONCLUSION

We have successfully undertaken a systematic examination of the size dependence of lateral diffusion coefficients in model phospholipid membranes. This study, of necessity, involved a multi-disciplinary strategy. Key to this strategy was the synthesis of an homologous series of probe molecules with defined structural differences in two discrete dimensions. The first series of probe molecules differed systematically in length while the second series differed in radius. The fundamental synthetic goal was achieved although the entire series proved difficult to assemble. Lateral diffusion coefficients of the labelled probes, in trace amounts, were measured in DMPC multibilayers.

Fluorescence Photobleaching Recovery diffusion measurements in liquid crystal phase bilayers revealed a surprising lack of dependence on the depth of the probe penetration in the bilayer. Insignificant effects were observed, even for probes which were an order of magnitude longer than the smallest probe used. The labelled isoprenoid alcohols citronellol, solanesol, and dolichol diffuse at the rate of lipid self-diffusion which is 5×10^{-12} $m^2 s^{-1}$. Companion experiments with model polymer systems, non-polar fluorescent aromatics and measurements of gel phase diffusion indicate the diffusive behavior of our NBD labelled isoprenoid alcohols may be described by Free Area Theory in the liquid crystal phase. The polarity of the NBD label itself seems to be sufficient to localize it in proximity to the bilayer/water interface. Fluorescence quenching experiments, however,

indicate it is not at the interface. Lateral diffusion of the labelled probes is nevertheless controlled by the lateral density of the host phospholipids.

Related Fluorescence Photobleaching Recovery diffusion measurements in DMPC multibilayers examined the effect of altering the radii of the diffusing probe molecules. Labelled surfactant dimers, with a novel triester structure, diffuse at rates comparable to that of the host lipid. This suggests that the dependence of D on probe radii is not as severe as the inverse exponential dependence predicted by Free Area Theory.[1] Our inability, however, to measure diffusion coefficients of probes with radii larger than the labelled dimers precludes development of a new diffusion model.

Both series of probes indicate the lateral diffusion coefficient has less dependence on molecular size and shape than one might anticipate. This permits us to make a few generalizations about the lateral diffusion coefficient of biological molecules in model membranes. Unlabelled polyisoprenoid alcohols will probably diffuse at the rate of lipid self-diffusion. Surfactant biological molecules such as vitamin A, α-tocopherol, vitamin K_1, and ubiquinol will also diffuse at this rate. This presumes the molecules will orient, to some extent, in a bilayer. A large number of related molecules, one may also predict, will diffuse at this rate. The key structural feature, controlling the rate of diffusion, appears to be orientation, not the details of molecular architecture. Thus in biophysical calculations involving long range diffusive transport of non-protein biomolecules, the lipid self-diffusion coefficient is likely an excellent estimate of the molecules' rate of motion.

Future studies suggested by these results include the following. (1) An attempt should be made, once again, to determine the depth of the NBD label attached to our isoprenoid alcohols in phospholipid bilayers. (2) It would be worthwhile to attempt labelling the triester dimers and tetramers with an acetamide analog of IANBD. This probe, under development by Molecular Probes,[2] may help improve the yield of the labelling reaction sufficiently to isolate the labelled material. (3) It would be illuminating as well to crosslink, and label, the triester monomers, dimers, and tetramers nearer the triester headgroup. Such probes will result in more correlated motion of the constituent monomers and will help answer the questions raised in Chapter 7.3 about interpreting our dimer diffusion results. The synthesis of said molecules, however, will be more difficult than the syntheses described here.

Our synthetic strategy reaped significant benefits from an Organic Chemistry point of view. The solvent dependence of the DCC coupling reaction (Appendix One) was shown to result from hydrogen bonding to the solvent molecules and not carboxylic acid dimer formation as previously postulated.[3] We observed, and quantified, an intramolecular singlet oxygen 'ene' reaction (Appendix Two) with our labelled isoprenoid alcohols. This is an intriguing system with potential for further theoretical and experimental examination. Finally, and perhaps most significantly, the surfactant triesters based on *cis,cis*-1,3,5-cyclohexanetriol are a novel, radially symmetric surfactant with very interesting surface behavior. The terminal thiol analogs should form a two-dimensional, hexagonal, molecular net when oxidized in the form of a monolayer. Future

studies will examine the surface behavior of these molecules as a function of hydrocarbon chain length and extent of polymerization.

REFERENCES

(1) Vaz, W. L.; Goodsaid-Zalduondo, F.; Jacobson, K. *FEBS Lett.* **1984**, *174*, 199.

(2) Molecular Probes, Eugene, OR, personal communication.

(3) DeTar, D. F.; Silverstein, R. *J. Am. Chem. Soc.* **1966**, *88*, 1013.

APPENDIX ONE

SOLVENT DEPENDENCE OF CARBOXYLIC ACID CONDENSATIONS WITH DICYCLOHEXYLCARBODIIMIDE[1]

A1.1 Introduction

Dicyclohexylcarbodiimide (DCC) has, over the past twenty-five years, proven to be an exceptionally useful reagent.[2-4] The carbodiimide coupling reaction we have investigated is widely used in the fields of synthetic organic chemistry,[4-8] enzymology[3,13-17] peptide synthesis,[4,9-12] and polymer chemistry.[4,18-22]

The reaction mechanism (Figure A1.1) was proposed by Khorana[2] in 1958. Results of subsequent investigators, based mostly on product data, have supported this proposal. Although the O-acylisourea (1) intermediate has not been isolated, (an O-acylisourea has been observed in solution[23] and in a peptide synthesis[24]) studies on model intramolecular O-acylisoureas have supported its existence.[25]

The major imperfection in the reaction is a significant side reaction which yields, via an intramolecular O → N acyl migration, the undesirable N-acylurea (2) product. Additives such as N-hydroxysuccinimide, which trap the O-acylisourea, have ameliorated the problem of this rearrangement in certain cases. From a synthetic point of view, however, one still wishes the anhydride to effectively compete with this rearrangement. Figure A1.1 shows that the efficiency of anhydride production is dependent on acid concentration.

Our original intent was to derivatize rare, biologically significant, isoprenoid alcohols using DCC and N-methyl-N-(7-nitrobenz-2-oxa-1,3,-diazol-4-yl)-6-aminohexanoic acid (NBD-acid), a fluorescent

Figure A1.1: DCC reaction with NBD-acid. This scheme shows the formation of the O-acylisourea intermediate (1), the undesirable N-acylurea (2) and the synthetically useful anhydride (3). The N-acylurea forms via an O → N acyl migration.

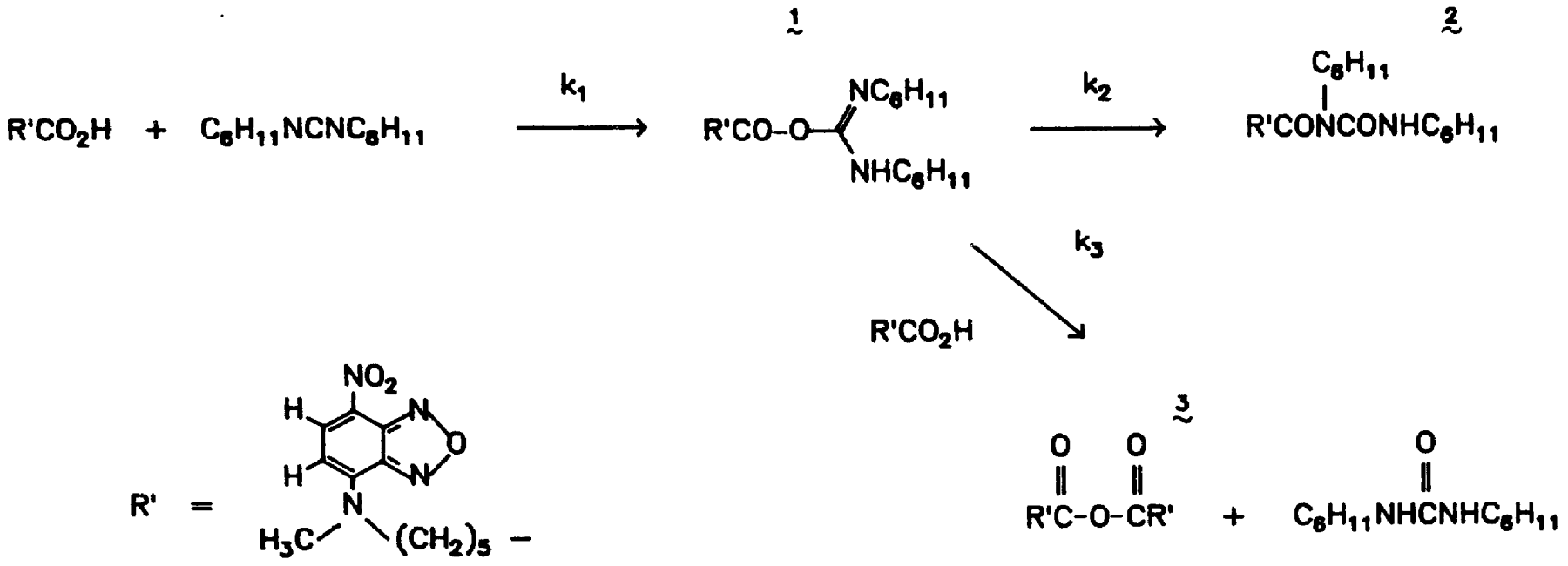
1
2
3
k1
k2
k3
R'CO2H + C6H11NCNC6H11
R'CO-O
NC6H11
NHC6H11
C6H11
R'CONCONHC6H11
R'CO2H
R' =
NO2
H
H
N
O
N
N
H3C
(CH2)5
O O
R'C-O-CR'
+
O
C6H11NHCNHC6H11

carboxylic acid ($R'CO_2H$, Figure A1.1). Proceeding through the anhydride and utilizing a 4-pyrrolidinopyridine catalyst,[8] we hoped to produce these delicate esters in high yield and purity. Unfortunately, NBD-acid proved to have limited solubility in most of the organic solvents suggested in the literature.

Initial experiments indicated a striking dependence of the reaction efficiency on both the acid concentration and the nature of the solvent. Through a systematic evaluation of the solvent dependence we hoped to learn more about the fundamental nature of the reaction, thereby permitting a rational choice of the best solvent for synthetic purposes.

Environmental effects on the DCC condensation reaction have taken on an added importance with the increasing use of DCC, and other carbodiimides, to modify or inhibit the function of carboxylic acid residues in proteins[15-17] and polymer resins.[20-22] The final product in most cases is uncertain and may be sensitive to the location of the carboxylic acid residue.

Using reverse phase HPLC and a programmable sample injector/dilutor, we observed the redistribution of the NBD probe amongst the acid, N-acylurea, and anhydride as a function of time and solvent. The intense absorption of the NBD moiety[26] (λ_{max}= 476 nm, ε_{max}= 3.44 x $10^4 mol^{-1} L\ cm^{-1}$) makes it a convenient tag to follow the course of the reaction.

A1.2 Results

Figure A1.2 shows an example of the disappearance of NBD-acid (A), with concommitant appearance of both anhydride (AA) and N-acylurea (NA), as the reaction proceeds. Concentrations are determined by the UV/VIS absorption of NBD present in each species.

The rate of acid decay is analyzed in terms of the mechanism outlined in Figure A1.1. If one presumes formation of O-acylisourea (AD^*) is the rate limiting step and DCC (D) is present in large excess, the result is -

$$\frac{d[A]}{dt} = - k_1[A][D] - k_3[A][AD^*] \qquad (A1.1)$$

With a steady state concentration of AD^*, one integrates to yield -

$$\ln [A] = \ln \Gamma^{1/2} + \ln [A]_0 - k_1[D]t \qquad (A1.2)$$

In this equation the variable Γ is -

$$\Gamma = (k_2 + 2k_3[A]) / (k_2 + 2k_3[A]_0) \qquad (A1.3)$$

From Equation (A1.2) it is possible to determine k_1, the second order rate constant, by plotting the natural log of acid concentration versus time. A summary of these results is found in Table A1.1 for all solvents at a variety of initial concentrations. Good pseudo first order kinetics ($r^2 > 0.98$) are found for all solvents. Using independently determined values of the ratio k_3/k_2 (vide infra), one may calculate the value of the $\ln \Gamma^{1/2}$ term. This term has no effect on the observed slope and intercept of the experimental ln [A] versus

Figure A1.2: Time course of a sample reaction in acetonitrile. Concentrations are o - [NBD-acid], □ - [N-acylurea] and Δ - [Anhydride]. The sum of [NBD-acid], [N-acylurea] and twice [Anhydride] is a constant, independent of time. The factor of two allows for the two NBD-acid molecules which form each anhydride molecule. Initial conditions $[\text{NBD-acid}]_0 = 2.89 \times 10^{-3}$ M, $[\text{DCC}]_0 = 5.26 \times 10^{-2}$ M.

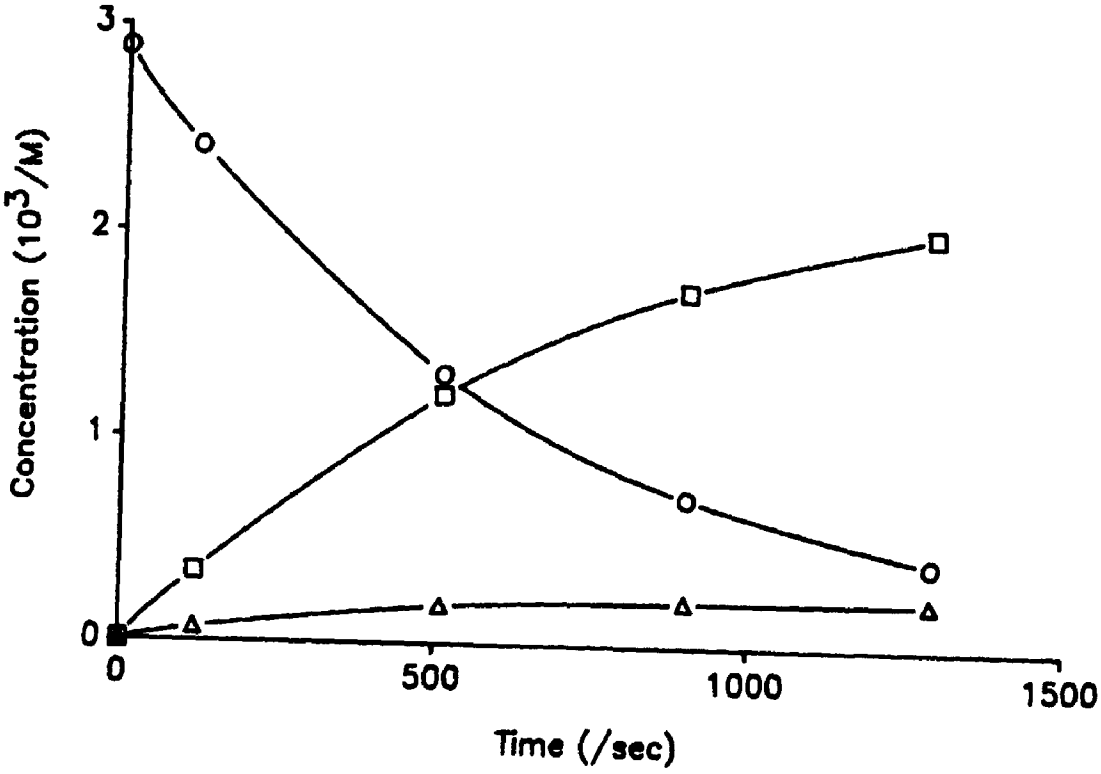
3
2
1
0
Concentration (10^3/M)
0
500
1000
1500
Time (/sec)

Notes to Table A1.1

[a] Solvents arranged in order of NBD-acid solubility.

[b] Average values. Methylene Chloride 41, Nitrobenzene 23, Nitropropane 15, Acetonitrile 2.8, Acetone 0.97, Tetrahydrofuran 0.45.

[c] Average values. Methylene Chloride 6.8×10^2, Nitrobenzene 3.2×10^2, Nitropropane 2.3×10^2, Acetonitrile 73, Acetone 19, Tetrahydrofuran 9.3.

[d] Anhydride yield too meagre to allow determination of (k_3/k_2).

[e] Average of six experiments, $[\text{NBD-acid}]_0$ identical.

[f] Average of five experiments, $[\text{NBD-acid}]_0$ identical.

[g] Average of two experiments, $[\text{NBD-acid}]_0$ identical.

Table A1.1: Rate Constants as a Function of Solvent and Concentration

Solvent[a]	$[NBD\text{-}Acid]_0$ (10^4 M^{-1})	k_1 (10^2 M s)[b]	k_3/k_2 (M)[c]
Methylene Chloride			
	0.59	34.5	—[d]
	1.18	41.8	691
	1.62	38.0	624
	1.77[e]	42.4	697
	2.30	37.5	590
	2.35	42.0	758
Nitrobenzene			
	6.6	22.0	324
	13.2	22.4	306
	19.8	24.4	324
	26.4	23.6	320
Nitropropane			
	2.36	15.1	223
	4.73	15.1	234
	7.09	14.0	236
	9.45	14.4	235
Acetonitrile			
	14.4	2.64	65.7
	17.4[f]	2.83	72.4
	28.9	2.71	73.9
	43.4	2.97	73.1
	57.8	2.95	77.8

(continued)

Table A1.1 (continued)

Solvent[a]	$[NBD\text{-}Acid]_0$ (10^4 M^{-1})	k_1 (10^2 M s)[b]	k_3/k_2 (M)[c]
Acetone			
	4.8	0.75	—[d]
	11.3	1.03	15.9
	11.5	0.52	—[d]
	23.0	0.95	17.0
	33.8	1.20	15.9
	37.6[e]	0.74	18.2
	45.0	1.21	17.8
	46.0[g]	1.00	21.2
	47.2[g]	0.94	18.7
	69.0	0.91	19.6
	92.0	0.89	20.0
Tetrahydrofuran			
	27.7	0.45	9.3

time plots for decays of three half lives.

Since the reaction pathway branches after the rate limiting step, it is impossible to measure independently the rate constants k_3 and k_2. However, by following the growth of anhydride (AA) relative to N-acylurea (NA) one may determine their ratio since

$$\frac{d[AA]}{d[NA]} = (k_3/k_2)[A] \qquad (A1.4)$$

Because the NBD absorbance is conserved (Figure A1.2) one knows -

$$[A] = [A]_0 - 2[AA] - [NA] \qquad (A1.5)$$

Substituting Equation (A1.5) into Equation (A1.4) yields, after applying an integrating factor -

$$[AA] = \frac{\left(2\,(k_3/k_2)\,[A_0] + 1\right)\left(\exp\left(-2\,(k_3/k_2)\,[NA]\right) - 1\right)}{-4(k_3/k_2)} - [NA]/2 \qquad (A1.6)$$

Expanding the exponential and regrouping by powers of (k_3/k_2) gives

$$[AA] = (k_3/k_2)\left([A_0][NA]^2/2\right) + (k_3/k_2)^2\left([NA]^3/3 - [A_0][NA]^2\right) + \ldots \qquad (A1.7)$$

The k_3/k_2 ratio (Table A1.1) is determined by a fit to this equation using a single variable, nonlinear, least squares algorithm[27] keeping up to the seventh power of k_3/k_2. The power series expansion accurately reproduces the experimental curve of anhydride versus N-acylurea (Figure A1.3) when the appropriate value of k_3/k_2 is

Figure A1.3: Growth of anhydride concentration relative to N-acylurea concentration for the sample reaction in Figure A1.2. These concentrations are implicit functions of time. The slope of the experimental curve is governed by Equation (A1.4). As the reaction progresses, less available NBD-acid means the pathway producing anhydride becomes progressively less competitive. The solid line is the best fit result to Equation (A1.7).

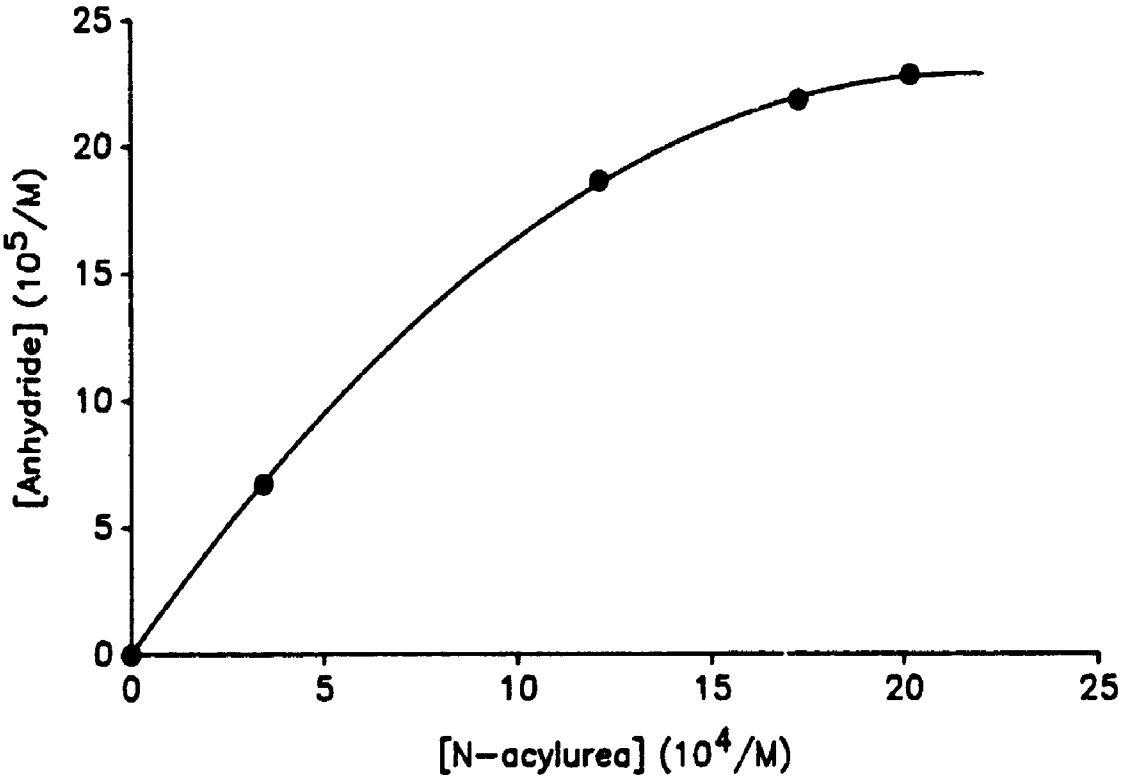
25
20
15
10
5
0
[Anhydride] (10^5/M)
0
5
10
15
20
25
[N–acylurea] (10^4/M)

determined.

The major source of error in this study appears to be the day to day handling and preparation of samples. Values of k_1 and k_3/k_2 determined from a common set of solutions on the same day generally showed relative uncertainties of less than five percent. When a larger number of experiments were attempted over several days, relative uncertainties increased to somewhat over ten percent. Hence, error bars which reflect relative errors of ten percent were assigned to the kinetic results in all solvents.

Additives had minimal effects on the reaction. Equimolar amounts (with respect to acid) of either water, triethyl amine or pyridine were added at a number of initial acid concentrations with no deviation from the kinetics observed in their absence. A large excess, relative to acid, of triethyl amine or pyridine was required to slow the reaction to any measurable extent.

Control experiments exclude the possibility that the NBD moiety is affecting the kinetics of the reaction. Addition of NBD-amine, up to equimolar acid, did not change the rate or extent of acid decay in a series of reactions in methylene chloride.

A1.3 Discussion

Few investigations have considered the effect of solvent on the DCC coupling reaction. DeTar and Silverstein[28] examined the DCC and acetic acid reaction in acetonitrile and carbon tetrachloride. They postulated the reaction in carbon tetrachloride was faster due to reactive acetic acid dimers in this solvent. Less reactive monomers,

they believed, predominated in acetonitrile. Similarly the higher k_3/k_2 ratio, and therefore larger anhydride yield, was attributed to a "cellular effect" of the dimer in carbon tetrachloride. That is, the local concentration of acid in the vicinity of the O-acylisourea is higher because of the residual acid molecule from the just disrupted dimer. Despite a dissenting report from Mironova et. al.,[29] these results have been widely quoted.

DeTar and Silverstein[28] chose to analyze their experimental information with a kinetic scheme which required fitting to many rate constants at once. We simplify the analysis by making the k_1 step pseudo first order with respect to acid and working at acid concentrations which minimize dimer concentration (vide infra). This permits us to use analytic rate equations (Equations (A1.2) and (A1.7)) which require fits to only one variable, k_1 and k_3/k_2 respectively.

The results in Table A1.1 show that, even with minimal dimer concentration, large range of k_1 and k_3/k_2 values are possible. We therefore attempted to correlate the rate constants with a variety of empirical and semi-empirical solvent scales[30,31] and found, except with parameters which measured the solvent's hydrogen bond accepter ability,[30,32] poor or no correlation. The hydrogen bond accepter ability refers to the ease with which a Lewis base solvent accepts a hydrogen bond from a donor Lewis acid. One common measure of this is the wavenumber difference between the OD stretching vibration of deuterated methanol (MeOD) in a test solvent and a reference solvent or MeOD in the gas phase. As shown in Figure A1.4 the correlation of ln (k_1) versus B, the Shorter[33] hydrogen bonding parameter, is very

Figure A1.4: Correlation of ln (k_1) with Shorter's B parameter. Solvents are numbered as follows: (1) methylene chloride; (2) nitrobenzene; (3) nitropropane; (4) acetonitrile; (5) acetone and (6) tetrahydrofuran. The B value for nitropropane is approximated by the literature value for nitromethane. The best fit result is indicated by the solid line. The error bars, relative uncertainties of ten percent, are smaller than the data symbols.

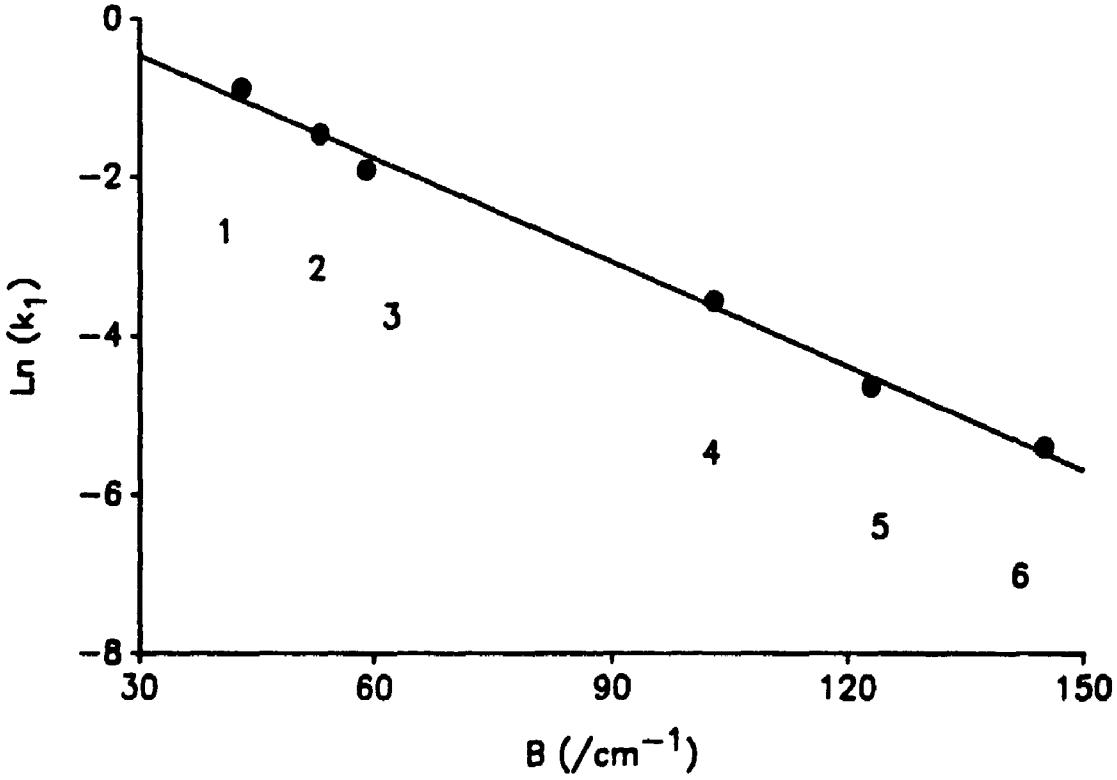
0
-2
-4
-6
-8
Ln (k_1)
1
2
3
4
5
6
30
60
90
120
150
B (/cm^{-1})

good (r^2 = 0.99).

Correlation of ln (k_1) with IR absorbance shifts relates changes in reactivity to changes in the acidic OH bond. One might argue, however, such changes are not solely due to the hydrogen bond 'basicity' of the solvents. To clarify this point we plotted the natural logarithms of the k_1 rate constants versus the Taft et. al.[32,34,35] hydrogen bond accepter basicity (Figure A1.5). Unlike most other solvent property scales which are based on changes of some indicator with solvent, the parameter β is arrived at by averaging multiple normalized solvent effects on a variety of properties involving many diverse types of indicators.

The correlation, except for nitrobenzene, is excellent (r^2 = 0.96). The β value for nitrobenzene, however, is based solely on the UV/VIS absorbance of one indicator[36] and therefore is not as reliable as averaging many experimental cases. Since nitrobenzene clearly falls on the regression line for Shorter's B value, we believe the value given by Taft et. al.[34] may be in error. The results of our kinetic experiments (Figure A1.5) suggest a β value of approximately 0.15, not 0.39 as reported.[36]

Based on equilibrium constants for carboxylic acids in nitrobenzene,[37] acetone,[38] and acetonitrile,[28] plus the fact that monomer-dimer equilibrium constants change little in the hierarchy of linear aliphatic carboxylic acids,[37,39] one may calculate that in the concentration ranges studied, little of the acid will exist as dimer (Table A1.2). An equilibrium constant for carboxylic acids in methylene chloride is not available in the literature. Consistent kinetic results, however, suggest that even in methylene chloride an

Figure A1.5: Correlation of ln (k_1) with Taft's β parameter. Solvent numbering as in Figure A1.4. Nitrobenzene from two sources gave identical values for k_1. The nitropropane β value is approximated by the literature value for nitromethane. The solid line is the best fit result excluding nitrobenzene. The error bars, relative uncertainties of ten percent, are smaller than the data symbols.

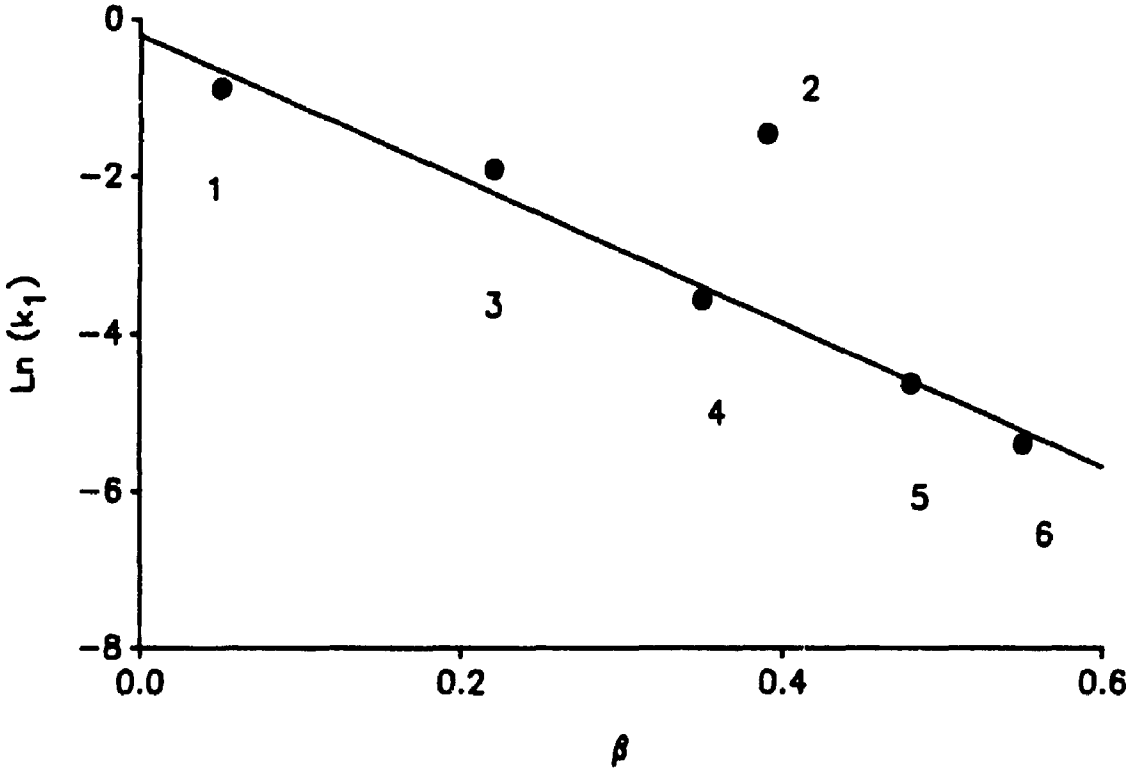
0
-2
-4
-6
-8
Ln (k_1)
0.0
0.2
0.4
0.6
β
1
2
3
4
5
6

insignificant portion of the acid will be in dimer form. Equilibrium constants for carboxylic acids in a related solvent more favourable to dimer, carbon tetrachloride,[40,41] suggest that at most twenty-five percent of the acid in our concentration range is dimerized.

Since acid dimerization is likely to be a function of solvent basicity one might argue that the linearity of the ln (k_1) versus basicity plots merely reflects the extent, however limited, of dimerization in the different solvents. Kinetic arguments, however, show that the initial rate of acid decay in such a system should not be simply proportional to the starting acid concentration.

The equilibrium between monomer and dimer is governed by the equilibrium constant K_{eq}. If one presumes the "cellular effect" is operational then the rate of acid decay will be -

$$\frac{d[A]}{dt} = -2\, k_d\, K_{eq}\, [A]^2 \qquad \text{(A1.8)}$$

In Equation (A1.8) k_d is the bimolecular rate constant for reaction of NBD-acid dimer and DCC.

If the "cellular effect" is not operational but dimer is the active species in the second stage of reaction, then Equation (A1.8) contains a second term which has a fourth power dependence on monomer concentration. Thus, for either mechanism, the initial rate of acid decay should depend on the initial NBD-acid concentration, thereby reflecting the different relative amounts of dimer in solution (Table A1.2). This is contrary to our experimental evidence. We observe a simple first order dependence on acid,[42] and rate constants independent of concentration, in all solvents at all concentrations.

Table A1.2: Dimer Mole Fractions

Solvent	K_{eq}^{a}(M)	$[NBD\text{-}Acid]_0$ (10^4 M^{-1})	Mole Fraction Dimer[a,b]
Acetone	3[c]	4.84	0.003
		92.0	0.05
Acetonitrile	0.5[d]	57.8	0.006
		17.4	0.002
Nitrobenzene	5.8[e]	26.4	0.03
		6.60	0.007

[a] These numbers should be considered estimates only.

[b] Mole fraction estimate calculated as [monomers in form of dimer] / [total monomers].

[c] Ref. 38

[d] Ref. 28

[e] Ref. 37

The k_3/k_2 ratio (Table A1.1) determined from Equation (A1.7) shows a dependence, similar to k_1, on solvent basicity. In fact, if one plots k_1 versus the ratio k_3/k_2 for all solvents (Figure A1.6), a straight line with intercept zero is obtained.

The linear relationship between k_1 and k_3/k_2 is best explained by postulating that k_3 and k_1 depend in similar ways on solvent basicity while k_2 is independent of solvent. Since addition of acid to DCC resembles addition to the O-acylisourea species, *a priori* one might expect similar solvent dependencies of the rate constants k_1 and k_3. If the dominant effect of solvent on k_1 and k_3 is the change in strength of the acid to solvent hydrogen bond, a precise consideration of their mechanisms is unnecessary. It suffices to say they are similar and that breaking the hydrogen bond is involved in the rate limiting step for each. Its contribution, therefore, to their free energies of activation will be identical and k_1 and k_3 will be a constant multiple in all solvents. This contention is supported by the observation that NBD-acid solubility correlates qualitatively with the solvent basicity indicating specific binding of the acid to a basic solvent. The lack of solvent dependence of k_2 is reasonable since this represents an intramolecular rearrangement.

The alternative explanation of Figure A1.6, that k_2 and k_1 are dependent in inverse ways on the solvent while k_3 is independent of it, is unreasonable because the zero intercept of Figure A1.6 would suggest that k_2 must become infinitely fast in a strongly binding solvent. This is not likely to be true for an intramolecular rearrangement. Finally, we consider it unlikely that both k_2 and k_3 are solvent dependent in mutually compensating manners so as to

Figure A1.6 Correlation of k_1 with (k_3/k_2). Solvent numbering as in Figure A1.4. The solid line gives the best fit result. Error bars reflect relative uncertainties of ten percent. Solvents (5) and (6) (unlabelled) have error bars smaller than the data symbols used.

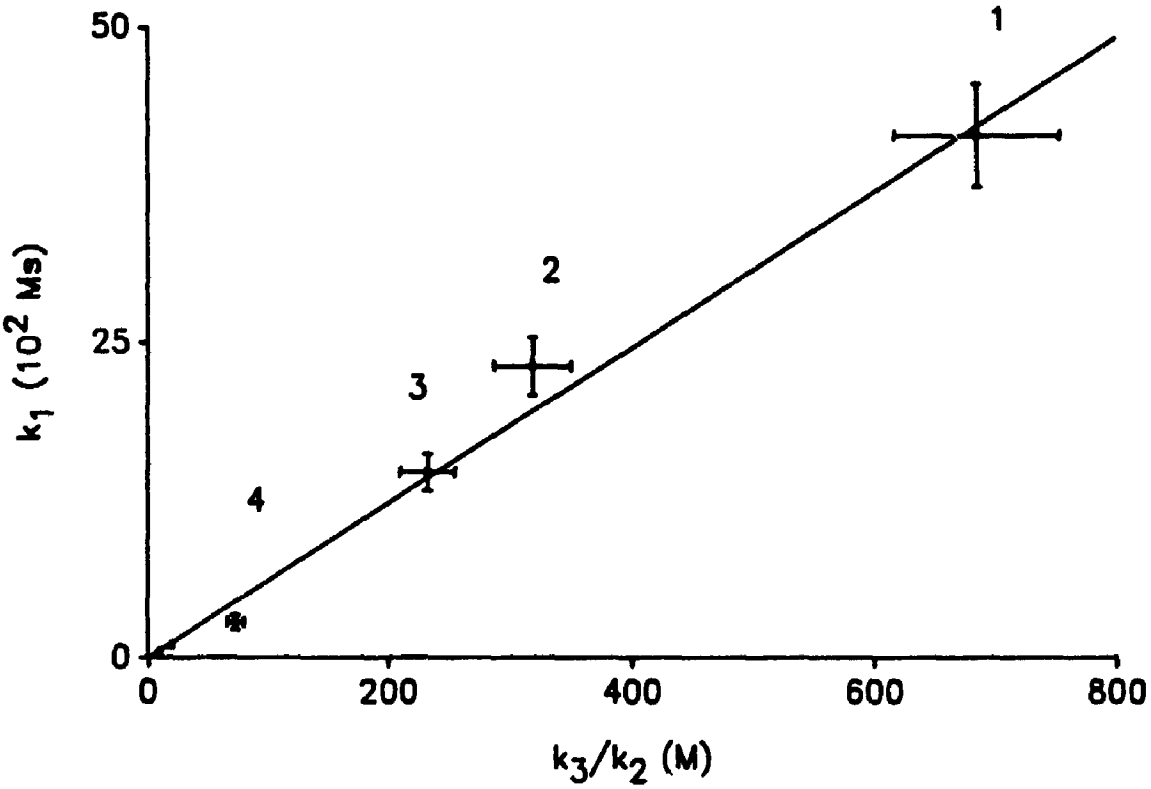
50
25
0
0
200
400
600
800
k_1 (10^2 Ms)
k_3/k_2 (M)
1
2
3
4

maintain the linear relationship. The variety of solvent properties is too great to expect such a coincidence.

Our conclusions are consistent with those of Mironova et. al.[29] who argued that a specific interaction between solvent and acid controlled the kinetics. They did not, however, determine the nature of this interaction nor did they attempt to treat it quantitatively.

The rate constant k_1 is known to increase with acid strength.[43] By analogy, k_3 should also increase with acid strength. In our system one decreases the effective acid strength versus DCC by binding to solvent. While Hegarty et. al.[44] have found, in aqueous solution, a pH dependence of the k_2 rate constant for model O-acylisoureas, such does not appear to be the case here.

A1.4 Conclusion

The second order rate constants k_1 and k_3 are related to the solvent basicity. Desolvation of the acid, for steps k_1 and k_3, is the energetic restriction which results in a free energy of activation dependent on the strength of the hydrogen bond between solvent and acid. The rate constant k_2 for intramolecular N → O acyl transfer is solvent independent.

The cellular effect of DeTar and Silverstein[28] is not the basis for enhanced anhydride yields in solvents such as methylene chloride and carbon tetrachioride. While extensive acid dimerization may complicate the kinetics in a higher concentration range, changes in the ratio k_3/k_2 do not require dimerization. The extent of acid dimerization and values of k_3/k_2 appear to be independent

manifestations of the solvent's hydrogen bonding ability. While this may be a subtle distinction it is fundamental to the nature of this reaction.

Synthetic work requires a compromise between acid solubility and retardation of the k_1 and k_3 rate constants. Solvents in which the acid is the most soluble are those with the slowest k_1 and k_3 rate constants. This relation between solubility and rate constants suggests a useful rule of thumb. For a given DCC and acid concentration, other things being equal, the reaction will be faster and the anhydride yield better in the solvent for which the acid is least soluble.

A1.5 Experimental

HPLC / Reaction Conditions

The HPLC system comprised two Waters 510 pumps controlled by a Waters Automated Gradient Controller. The reaction was followed at 480 nm and 210 nm with a Waters 490 multiwavelength detector. Peak areas at 480 nm were quantified with a Waters 740 integrator. A Gilson 231 programmable sample injector and dilutor were interfaced to the Waters system.

For HPLC analyses we used a Waters C_{18} reverse phase radial compression column. Elution required a 70/30 mixture of acetonitrile and water with a flow rate of 2.0 mL/min. These conditions gave retention times of 1.3 minutes for NBD-acid, 4.3 minutes for anhydride, and 5.6 minutes for N-acylurea. Integrated NBD intensity remained constant with time, only the distribution changed.

Concentrations were calculated by multiplying the normalized intensity for each species by the initial concentration of NBD-acid present. Allowance was made for the two NBD species present in each anhydride molecule.

The dilutor/injector was programmed to initiate the reaction by mixing suitable aliquots of pure solvent and solutions of DCC and NBD-acid. In all cases DCC concentration was maintained in ten fold excess. The dilutor/injector automatically sampled the reaction mixture at appropriate intervals and injected these samples onto the column. Reactions took place in a 2 mL screw top vial sealed with a septum and were quenched upon injection by dilution and separation on the column. No hydrolysis or other reaction of the products occurs while on the column. Mixtures were stirred during reaction with a small stir bar. Temperatures were controlled to within ±1 ^{o}C of 30 ^{o}C.

Chemicals

NBD-acid was prepared by reacting N-methyl-6-aminohexanoic acid and 4-chloro-7-nitrobenz-2-oxa-1,3-diazole (NBD-Cl) as previously described.[45]

The NBD-acid analogue N-(nitrobenz-2-oxa-1,3-diazol-4-yl)-5-pentyl amine (NBD-amine) was prepared by the direct reaction of NBD-Cl and pentyl amine in methanol.[46] The resulting solution was washed with acidic and basic buffers then extracted with ethyl acetate to isolate NBD-amine.

The rearranged N-acylurea product was isolated by column chromatography. The N-acylurea eluted from silica gel with a 75/25 mixture of methylene chloride and ethyl acetate. Recrystallized from

hot ethanol/water mixture, its m.p. was 148-150 °C (uncorrected) on a Gallenkamp melting point apparatus. Identity of this product was confirmed by ^{1}H, ^{13}C NMR and high resolution mass spectroscopy.

The anhydride product was not isolated. However, in the presence of a catalyst and 1-undecanol (esterification conditions), one observes quantitative conversion of the presumed anhydride to the ester product. This product was isolated by column chromatography (previous conditions) and recrystallized from hot petroleum ether. Its m.p. was 63-64 °C (uncorrected) as measured on a Gallenkamp melting point apparatus. It was identified by ^{1}H, ^{13}C NMR and high resolution mass spectroscopy. This confirms the identity of the carboxylic acid anhydride.

Solvents methylere chloride, tetrahydrofuran, and nitrobenzene (Baker), nitropropane (Kodak), acetone and acetonitrile (BDH) were distilled or vacuum distilled and stored over molecular sieves in sealed vessels.

DCC and pentyl amine were purchased from Kodak. NBD-Cl was purchased from Sigma.

REFERENCES

(1) Published in slightly altered form. Balcom, B. J.; Petersen, N. O. *J. Org. Chem.* **1989**, *53*, 1922.

(2) Khorana, H. G. *Chem. Rev.* **1953**, *53*, 145.

(3) Kurzer, F.; Douraghi-Zadeh, K. *Chem. Rev.* **1967**, *67*, 107.

(4) Williams, A.; Ibrahim, I. T. *Chem. Rev.* **1981**, *81*, 589.

(5) Smith, M.; Moffatt, J. G.; Khorana, H. G. *J. Am. Chem. Soc.* **1958**, *80*, 6204.

(6) Neises, B.; Stegleich, W. *Org. Synth.* **1985**, *63*, 183.

(7) Rebek, J.; Feitler, D. *J. Am. Chem. Soc.* **1973**, *95*, 4052.

(8) Hassner, A.; Alexanian, V. *Tetrahedron Lett.* **1978**, *46*, 4475.

(9) Sheehan, J. C.; Hess, G. P. *J. Am. Chem. Soc.* **1955**, *77*, 1067.

(10) Gross, E.; Meinhofer, J. *The Peptides Vol 1*; Academic: New York, 1979; pp 241, 261.

(11) Gross, E.; Meinhofer, J. *The Peptides Vol. 2*; Academic: New York, 1980; pp 123, 135.

(12) Bodansky, M. *Principles of Pe, tide Synthesis*; Springer-Verlag: New York, 1984; pp 9, 58.

(13) George, A. L.; Borders, C. L. *Biochim. Biophys. Acta* **1979**, *87*, 59.

(14) Beechey, R. M.; Roberton, A. M.; Holloway, C. T.; Knight, I. T. *Biochemistry* **1967**, *6*, 3867.

(15) Partis, M. D.; Bertoli, E.; Griffiths, D. E. *J. Gen. Microbiol.* **1980**, *116*, 233.

(16) Georga, F. R. *Biochemistry* **1985**, *24*, 6783.

(17) Argaman, A.; Shoshan-Barmatz, V. *J. Biol. Chem.* **1988**, *263*, 13, 6315.

(18) Schollenberger, C. S.; Stewart, F. D. *J. Elastoplast.* **1971**, *3*, 28.

(19) Brown, D. W.; Lowry, R. E.; Smith, L. E. *Macromolecules* **1981**, *14*, 659.

(20) Scott, L. T.; Rebek, J.; Ovsyanko, L.; Sims, C. L. *J. Am. Chem. Soc.* **1977**, *99*, 625.

(21) Papaspyrides, C.; Birley, A. W. *Polymer*, **1978**, *19*, 1474.

(22) Lum, R. M. *J. Polym. Sci., Polym. Chem. Ed.* **1979**, *17*, 3017.

(23) Ibrahim, I. T.; Williams, A. *Chem. Commun.* **1980**, 25.

(24) Arendt, A.; Kolodziejczyk, A. M. *Tetrahendron Lett.* **1978**, *40*, 3867.

(25) Doleschall, G.; Lempert, K. *Tetrahedron Lett.* **1963**, *18*, 1195.

(26) Measured in ethanol.

(27) Press, W. H.; Flannery, B. P.; Teukolsky, S. A.; Vetterling, W. T. *Numerical Recipes*; Cambridge: New York, 1986; pp 523, 528.

(28) DeTar, D. F.; Silverstein, R. *J. Am. Chem. Soc.* **1966**, *88*, 1013.

(29) Mironova, D. F.; Dvorko, G. F.; Skuratovskaya, T. N. *Ukr. Khim. Zh.* **1969**, *35*, 7, 726.

(30) Barton, A. F. *CRC Handbook of Solubility Parameters and other Cohesion Parameters*; CRC Press: Boca Raton, Fla., 1983; pp 139, 199.

(31) Griffiths, T. R.; Pugh, D. C. *Coord. Chem. Rev.* **1979**, *29*, 129.

(32) Kamlet, M. J.; Abboud, J. M.; Abraham, M. H.; Taft, R. W. *J. Org. Chem.* **1983**, *48*, 2877.

(33) Burden A. G.; Collier, G.; Shorter, J. *J. Chem. Soc. Perkin 2* **1976**, 1627.

(34) Taft, R. W.; Abboud, J. M.; Kamlet, M. J.; Abraham, M. H. *J. Solution Chem.* **1985**, *14*, 3, 153.

(35) Kamlet, M. J.; Abboud, J. M.; Taft, R. W. *Prog. Phys. Org. Chem.* **1981**, *13*, 485.

(36) Ref. 35, Table 22.

(37) Rublo, F. C.; Rodriguez, V. B.; Alameda, E. J. *Ind. Eng. Chem. Fundam.* **1986**, *25*, 142.

(38) Muller, N.; Rose, P. I. *J. Phys. Chem.* **1972**, *69*, 2564.

(39) Tikonov, V. P.; Fuchs, G. I.; Kuznetsova, N. A. *Kolloidn. Zh.* **1974**, *36*, 998.

(40) Barrow, G. M.; Yerger, E. A. *J. Am. Chem. Soc.* **1954**, *76*, 5248.

(41) Reeves, L. W.; Schneider, W. G. *Trans. Farady Soc.* **1958**, *54*, 314.

(42) The reaction is also first order with respect to DCC. In methylene chloride the order is 1.17 std. dev. 0.11, in acetone 1.10 std. dev. 0.05.

(43) Mironova, D. F.; Dvorko, G. F. *Ukr. Khim. Zh.* **1975**, *41*, 8, 840.

(44) Hegarty, A. F.; McCormack, M. T.; Brady, K.; Ferguson, G.; Roberts, P. J. *J. Chem. Soc. Perkin 2* **1980**, 867.

(45) Petersen, N. O. *Spectros. Int. J.* **1983**, *2*, 408.

(46) Gosh, P. B.; Whitehouse, M. W. *Biochem. J.* **1968**, *108*, 155.

APPENDIX TWO

SELF SENSITIZED SINGLET OXYGEN 'ENE' REACTION

A1.1 Introduction

The linear hydrophobic polymers, based on polyisoprenoid alcohols, used in our diffusion measurements displayed an unexpected instability when conjugated with the fluorescent label NBD-acid. The need for a well-defined, coherent series of probes prompted us to investigate the origin of this instability in some detail.

A2.2 Experimental

The simplest isoprenoid alcohol, citronellol, was esterified with NBD-acid according to the procedure outlined in Chapter Five. NBD-undecanol was similarily prepared. These two probes were chosen as model systems due to the simplicity of their alkyl chains and their relative abundance. The decomposition reaction was monitored by silica TLC (75/25 methylene chloride/ethyl acetate) and reverse phase HPLC (2.0 mL/min 70/30 acetonitrile/water). The decomposition product retained the orange color characteristic of the NBD label. This made visualization on TLC plates and observation (480 nm) by HPLC particularly easy. NBD-undecanol and NBD-citronellol had R_f values on silica of 0.85 and 0.87 respectively. The decomposition product of NBD-citronellol had an R_f on silica of 0.75. NBD-citronellol eluted on reverse phase HPLC with a retention time of 14.3 min. The decomposition product of NBD-citronellol eluted with a retention time

of 4.8 min.

A2.3 Results

Control experiments with methylene chloride solutions of NBD-citronellol and NBD-undecanol, analyzed by silica TLC, quickly revealed four critical features of the decomposition reaction. (1) NBD-citronellol decomposes whereas NBD-undecanol is stable. (2) The NBD-citronellol decomposition requires oxygen. (3) The decomposition does not occur without direct sunlight or irradiation by an intense lamp. Cutoff filters (400 nm) do not hinder the reaction. (4) The decomposition product is more polar than the original ester.

This evidence suggests a photochemical reaction involving the NBD chromophore, oxygen, and the isoprene double bond. The singlet oxygen 'ene' fulfills these criteria and is likely responsible for the product degradation.[1] Ground state triplet oxygen is known to undergo triplet-triplet annihilation with varied dye sensitizers to produce the very reactive $^1O_2$ species.[2] The isoprene moiety is vulnerable to the 'ene' reaction because of the trisubstituted double bond.[3] In fact, citronellol is oxidized, intermolecularly, to rose oxide on an industrial scale by the singlet oxygen 'ene' reaction.[4] In 1975 it was estimated that two tons of $^1O_2$ per year were used in this reaction for the perfume industry.[4] The singlet oxygen 'ene' reaction yields hydroperoxides as shown in Figure A2.1.

To our knowledge, the NBD chromophore has not previous'y been used as a singlet oxygen sensitizer. It is not surprising, however, that it could so function. While the quantum yield of intersystem

Figure A2.1: Illustration of the singlet oxygen 'ene' reaction. Electronically excited singlet oxygen abstracts a proton from a neighboring CH bond as it oxidizes the double bond.

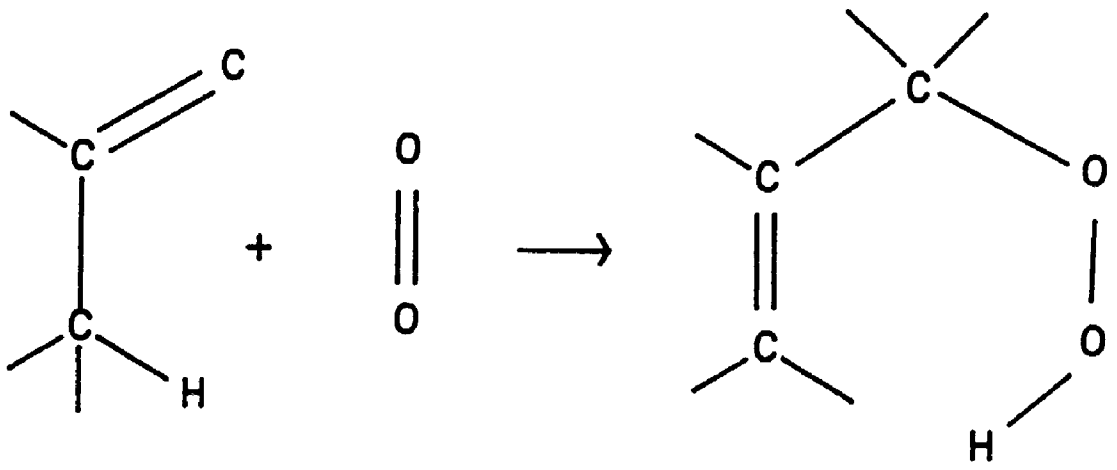
C
C
C
H
+
O
O
C
C
C
O
O
H

crossing is unknown for NBD, the low quantum yield of fluorescence (only five percent[5]) suggests there could be substantial production of triplet state NBD.

The singlet oxygen 'ene' reaction has a very low activation energy and little direct solvent dependence.[1] There is an indirect solvent dependence, however, due to the widely variant lifetimes of singlet oxygen in solution.[1] The lifetime is very long in halogenated or deuterated solvents and thus singlet oxygen is very reactive in these environments. Hydroxyl or hydrocarbon solvents yield much shorter singlet oxygen lifetimes. Therefore singlet oxygen is much less reactive in these solvents.

The solvent lifetime effect was observed qualitatively with NBD-citronellol. Exposure of NBD-citronellol in ethanol (τ = 20 μsec),[6] to intense light in an oxygen rich environment resulted in no oxidation. Samples of NBD-citronellol in $CDCl_3$ (τ = 300 μsec)[6] invariably degraded quite quickly.

The kinetics of the singlet oxygen 'ene' reaction, with NBD-citronellol as the substrate, have been examined by time dependent HPLC analysis[7,8] (480 nm) of samples irradiated with a xenon lamp. Based on the methodology developed in this thesis, these experiments revealed several significant, quantitative features of the reaction. (1) The reaction was zero order with respect to NBD-citronellol.[7,8] This was interpreted to mean the reaction observed was intramolecular. (2) A one-to-one correspondence was observed between NBD-citronellol loss (480 nm) and oxidized NBD-citronellol production.[7,8] This showed the NBD chromophore was unaltered in the transformation. (3) The ratio of the reaction rates for NBD-citronellol in acetonitrile and

methylene chloride is simply the ratio of their respective singlet oxygen lifetimes.[7] This quantitatively confirmed the singlet oxygen lifetime effect mentioned above.

^{1}H NMR of the light exposed and reacted NBD-citronellol supports the $^1O_2$ oxidation mechanism. The light reacted material was difficult to purify; ^{1}H NMR of the crude product, however, showed a disruption of the isoprene double bond structure. This is most evident from the disappearance of the terminal methyl singlets (δ = 1.68 and 1.60 ppm) α to the double bond in the original citronellol.

A2.4 Discussion

To the best of our knowledge this is the first direct observation of singlet oxygen sensitized by the NBD chromophore. The pseudo-intramolecular reaction of NBD-citronellol is an intriguing model system. It is pseudo-intramolecular because the generator site (NBD) and the target site (double bond) interact only through the transient, mobile, singlet oxygen species. As discussed in Appendix One, the presence, and relative stability, of the NBD chromophore result in facile kinetics experiments.

The rate equation for the reaction (Equation A2.1) may be written in terms of the rate of photon absorbance (I_A), the quantum yield of intersystem crossing (Φ_{isc}), and the quantum yield of singlet oxygen production (Φ_{O_2}).

$$\frac{d\,[\text{NBD-cit}]}{dt} = - I_A \Phi_{isc} \Phi_{O_2} \left(\frac{k_1}{k_0 + k_1} \right) \qquad \text{(A2.1)}$$

Equation A2.1 also relates the rate of reaction of the NBD linked citronellol to the rate constant, k_0, for relaxation of $^1O_2$ to the ground state $^3O_2$. The rate constant k_1 is the bimolecular rate constant for intramolecular reaction. We have incorporated the local concentration of the double bond into this rate constant, making it pseudo first order. If k_0 is much faster than k_1, then the rate will be simply proportional to the lifetime of $^1O_2$ in the solvent under study. This has been confirmed experimentally.[7] It suggests there is little solvent effect on Φ_{isc} and Φ_{O_2}.

The form of the rate constant k_1 is non-trivial. It must incorporate the non-homogeneity of the singlet concentration about the sensitizer and it must also allow for the concentration of the double bond. Since the reaction is zero order with respect to NBD-citronellol, the intramolecular nature of the reaction obscures these details.

If one presumes the rate constant k_1 is proportional to the local concentration of $^1O_2$ in the region of the double bond, the form of k_1 may be examined in more detail. At low concentrations the intermolecular reaction of NBD-citronellol will be suppressed and the rate of reaction will be dependent on the average distance of the double bond from the NBD sensitizer.

The concentration gradient of $^1O_2$ about individual NBD chromophores may be expressed in terms of the oxygen diffusion coefficient (D) and the singlet oxygen lifetime (τ).

$$\frac{\partial C}{\partial t} = D \nabla^2 C - \tau^{-1} C \qquad \text{(A2.2)}$$

The gradient operator ∇^2 in Equation A2.2 is the Laplacian in three dimensions with spherical symmetry. The spherical symmetry of the system means that the concentration, C, is a function only of the distance, r, from the sensitizer. In the steady state, $\partial C/\partial t = 0$, Equation A2.2 may be rewritten as shown in Equation A2.3.

$$D\ 1/r^2 \frac{d}{dr}\left(r^2 \frac{dC}{dr}\right) - \tau^{-1}C = 0 \qquad \text{(A2.3)}$$

Equation A2.3 is a second order linear differential equation, homogeneous, with variable coefficients. Rearranged to the standard form of Equation A2.4, the system may be solved using the method of supressing the first derivative.[9]

$$\frac{\partial^2 C}{\partial r^2} + (2/r)\ \partial C/\partial r - \Gamma C = 0 \qquad \text{(A2.4)}$$

In Equation A2.4, Γ combines the diffusion coefficient D and the lifetime τ as $(\tau D)^{-1}$.

The concentration of $^1O_2$ as a function of r, with the appropriate boundary conditions, is expressed by Equation A2.5.

$$C = (1/r)\ (C_o\ R \exp(\sqrt{\Gamma}\ R))\ \exp(-\sqrt{\Gamma}\ r) \qquad \text{(A2.5)}$$

In Equation A2.5, R is the finite radius of the sensitizer and C_o is the concentration of singlet oxygen at R. Realistic values of the oxygen diffusion coefficient in organic solvents ($2 \times 10^{-9}\ m^2 s^{-1}$)[10] and the lifetime of singlet oxygen in a typical organic solvent

(58 μsec)[11] show that the concentration profile of Equation A2.5 is determined almost entirely by the 1/r term. In physical terms, this suggests the decrease in the singlet oxygen concentration as a function r is due to the effect of dilution at larger r rather than the finite lifetime τ.

Figure A2.2 shows the normalized concentration plotted as a function of radial distance from the sensitizer of radius R. Citronellol has been conjugated with an NBD bearing acid analogous to Figure 4.1a but with eleven, rather than five, methylenes separating the carboxylic acid function from the amine. Under identical reaction conditions, the longer citronellol ester decays only half as fast as the shorter (five methylenes) NBD-citronellol. Molecular mechanics studies of the NBD conjugated esters are underway. The goal is to relate the observed rate of reaction to the average separation of the NBD chromophore and the isoprene double bond. The separation distance predicted by Equation A2.5 should closely approximate that determined through molecular mechanics simulation if k_1 is proportional to the local concentration of $^1O_2$.

A2.5 Conclusion

The NBD-citronellol system represents an intriguing example of an unusual intramolecular reaction. Singlet oxygen will oxidize the isoprene double bond in NBD-citronellol when exposed to direct sunlight or a high intensity xenon lamp in solvents which have a long singlet oxygen lifetime. The singlet oxygen is likely produced by triplet-triplet annihilation of triplet state NBD and ground state

Figure A2.2: Normalized concentration profile of $^1O_2$ about the NBD sensitizer. This profile is calculated according to Equation A2.5 with the finite sensitizer radius chosen to be 10 Å. The oxygen diffusion coefficient is 2×10^{-9} m^2s^{-1}. The singlet oxygen lifetime was chosen to be 58 μsec.

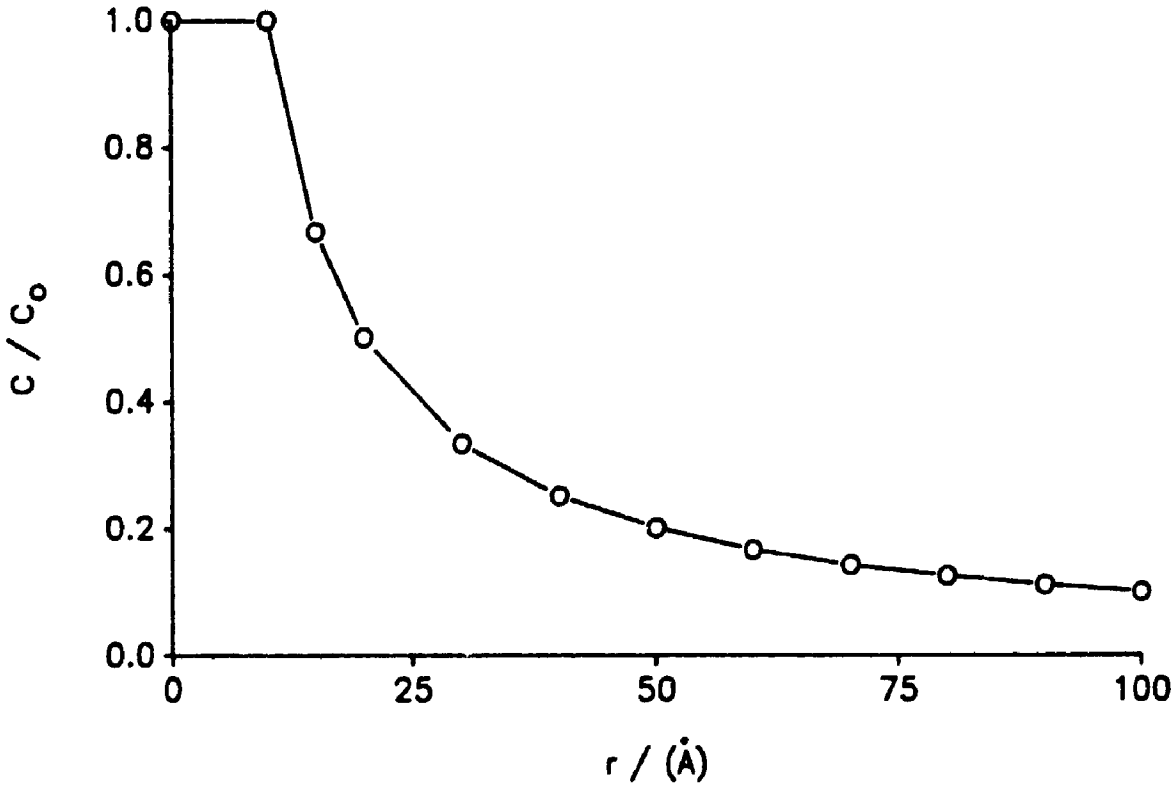
1.0
0.8
0.6
0.4
0.2
0.0
c / c$_o$
0
25
50
75
100
r / (Å)

oxygen. The short singlet oxygen lifetimes in water and hydrocarbons, plus the feeble intensity of the monitor beam, probably means the singlet oxygen reaction is unlikely to be a problem in FPR. During the bleach pulse, however, there will almost certainly be significant singlet oxygen production.

REFERENCES

(1) Frimer, A. A.; Stephenson, L. M. In *Singlet O_2*; Frimer, A. A., Ed.; CRC Press: Boca Raton, FL, 1985; Vol. 2, pp 67, 91.

(2) Straight, R. C.; Spikes, J. D. In *Singlet O_2*; Frimer, A. A., Ed.; CRC Press: Boca Raton, FL, 1985; Vol. 4, pp 91, 143.

(3) Chaineaux, J.; Tanielian, C. In *Singlet Oxygen*; Ranby, B.; Rabek, J. F., Eds.; Wiley: New York, 1978; pp 164, 173.

(4) Ohloff, G. *Pure Appl. Chem.* **1975**, *43*, 481.

(5) Petersen, N. O.; Elson, E. L. In *Methods in Enzymology*; Hirs, G. H.; Timasheff, S. N., Eds.; Academic: New York, 1986; Vol. 130, pp 454, 484.

(6) Wilkinson, F. In *Singlet Oxygen*; Ranby, B.; Rabek, J. F. Eds.; Wiley: New York, 1978; pp 27, 35.

(7) Stubble, Lou Ann, B. Sc. Thesis, The University of Western Ontario, 1989.

(8) Kogon, Aaron, B. Sc. Thesis, The University of Western Ontario, 1988.

(9) Pearson, C. E., Ed. *Handbook of Applied Mathematics*; Van Nostrand: New York, 1974; pp 290, 291.

(10) Cussler, E. L. *Diffusion*; Cambridge: New York; 1985, p 117.

(11) Jenny, T. A.; Turro, N. J. *Tetrahedron Lett.* **1982**, *23*, 2923.

APPENDIX THREE

MONOLAYER STUDIES - TRIESTERS OF *CIS,CIS*-1,3,5-CYCLOHEXANETRIOL

A3.1 Introduction

The radially symmetric triesters considered in Chapter Four were designed to be surfactant molecules. They have the required amphiphilic structure because of their three closely spaced ester functions and long alkyl chains. The potential usefulness of these symmetric novel surfactants and the importance of their orientation for interpreting FPR experiments, prompted a more detailed examination of their surfactant nature.

A3.2 Experimental

Qualitative monolayer spreading experiments were undertaken with four surfactant probes. They were 6C monomer, 8C monomer, 11C monomer, and *cis,cis*-1,3,5-(tristearoyl)-cyclohexanetriol. Stock solutions of the four triesters were prepared at concentrations of 1 mg/mL in chloroform (BDH, spectroscopic grade). The qualitative spreading behavior was examined by depositing 10, 20, and 30 μL aliquots of each test solution on the aqueous surface of a Langmuir trough lightly dusted with talcum powder or ground pepper. The Langmuir trough, 14 cm x 49 cm, was made from stainless steel and filled with triply distilled water. The surface area of the Langmuir trough was controlled by a movable teflon coated barrier and a teflon

float attached to a torsion balance. Qualitative experiments were performed at room temperature.

Quantitative pressure-area isotherms were measured using the four surfactant probes mentioned above. Professor J. Bolton of this Department kindly provided the Langmuir trough located in his laboratory for these studies. The trough (13 cm x 60 cm), machined from a solid block of teflon, was mounted on a vibration isolation table and operated under partial computer control. The surface area of the monolayer was regulated by a computer controlled, teflon-wrapped, square iron bar which rode along the top of the sides of the trough. The surface pressure was monitored by a teflon float, installed at one end of the trough, which is sealed to the sides of the trough by teflon tape. The float is attached to the lower arms of a torsion balance. The core from a linear transducer is hung from a horizontal arm of the balance and extends into the core of the transducer. Changing the surface pressure of the monolayer will move the float and thereby, through the torsion balance, change the depth of the metal core in the transducer. This alters the output voltage of the transducer and provides a very sensitive measure of the surface pressure. The subphase of this system was also triply distilled water. The apparatus and computer interfacing have recently been described in more detail.[1]

Small aliquots (10, 20, 40 μL) of the test solutions were applied to the surface of the subphase with a syringe, maintaining a minimum of three seconds between drops. Compression of the monolayer, at room temperature, began several minutes after deposition.

A3.3 Results

The qualitative tests of surface spreading indicate that all four molecules examined are surfactants. Adding a small drop of stock solution to the aqueous surface results in a rapid displacement and agitation of the talcum powder or pepper on the surface. This behavior is characteristic of surfactants.[2] A non-surfactant added to the aqueous phase, in the same manner, will form a static lens or drop on the surface without displacement of the surrounding powder.

The behavior amongst the four molecules tested, however, was not uniform. Upon addition to the surface, the tristearoyl derivative spread and formed a stable layer from which all the talcum powder or pepper was excluded. All three of the terminal bromine triesters spread but did not form a stable layer. The cleared area reached a maximum dilation, then seemed to fragment as fingers of talcum powder or pepper surged back into the cleared area. The origin of this 'breathing mode' is uncertain but may be related to the fact that all three are oils, in the pure state, at room temperature. In the case of 11C monomer, the oil is a metastable state. By contrast, the tristearoyl derivative is a solid as the pure substance.

Quantitative pressure-area curves were measured for all four probes. The terminal bromine triesters did not form a stable monolayer, however, and compression of a spread layer did not result in an observable lateral pressure. The stearic acid derivative formed stable monolayers from which reproducible pressure-area isotherms were measured, Figure A3.1. The stearic acid derivative was applied at very low densities due to the large area of the fully

Figure A3.1: Compression curve, lateral pressure versus molecular area, recorded for the stearic acid derivative of *cis,cis*-1,3,5-cyclohexanetriol on a Langmuir trough. The sharp drop at approximately 10 Å per molecule represents the end of the data record. This drop has no experimental significance.

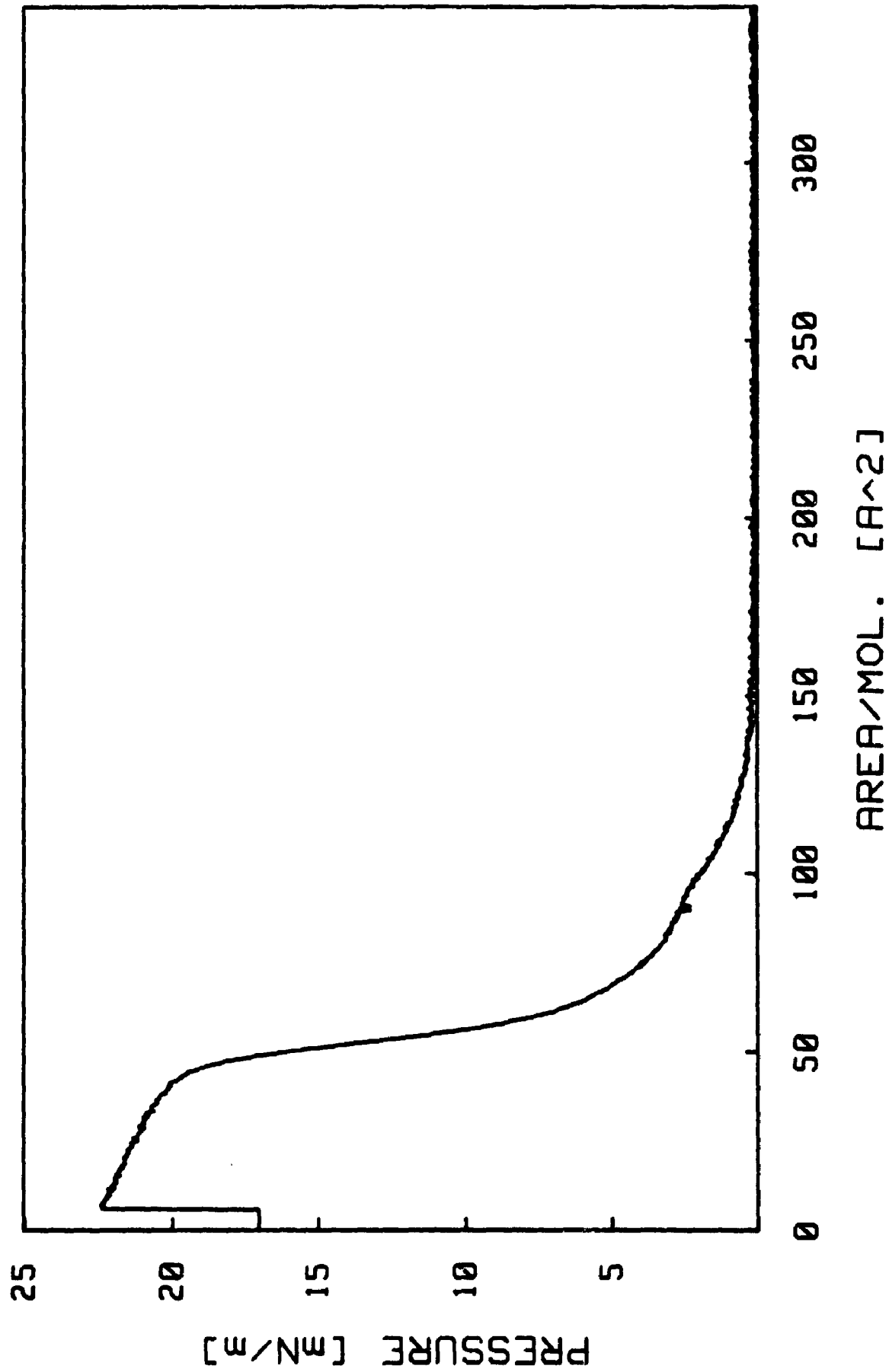
PRESSURE [mN/m]
25
20
15
10
5
0
50
100
150
200
250
300
AREA/MOL. [A^2]

extended triester. Figure A3.1 is notable from several respects. There is a phase transition at approximately 100 $Å^2$ per molecule which has a very low plateau (≈ 3 mN/m). The close-packed area per molecule is approximately 60 $Å^2$. Further compression of the monolayer results in a collapse of the surface structure at approximately 23 mN/m. Molecular models of the headgroup show that an all equatorial conformation will have a projected area of approximately 100 $Å^2$. Significantly, a conformation of the cyclohexane ring with all three esters axial will have a projected area of approximately 60 $Å^2$. ^1H NMR indicates that, at least in solution, the triesters adopt a conformation with all three chains in the equatorial position.

A3.4 Discussion

Observation of a reproducible pressure-area isotherm for the stearic acid derivative confirms the novel surfactant structure of the cyclic triester headgroup. The fatty acid triesters are an interesting system worthy of further study for at least two reasons. The first concerns the lateral asymmetry of the ring. *A priori* it is difficult to assign an orientational preference of the fully extended triester upon deposition. Energetically, is there a significant difference between the molecule deposited with one side of the ring at the water interface versus the other side? Certainly one side is distinct from the other, due to the all cis substitution. Further, it is difficult to imagine interconversion between the two orientations occurring readily. The distinction becomes apparent as the layer is compressed. Only one ring orientation will permit an equatorial to

axial conformational change of the ester functions in the headgroup (Figure A3.2) without exposing the cyclohexane ring to the aqueous phase. That such a conformational change must occur is shown by area calculations based on molecular models. The triester must be all axial to reach a close packed area of 60 $Å^2$ per molecule. Further monolayer studies are planned to examine this behavior in detail.

The origin of the phase change observed at 100 $Å^2$ per molecule is open to interpretation. The conventional liquid expanded to liquid condensed transition frequently observed in monolayer studies[3,4] has a structure very similar to that observed here. Nevertheless, the experimental results suggest a conformational change in the headgroup that closely approximates the observed areas. Further studies are also planned to examine this phenomena.

Malthete et. al.[5] have recently observed compression isotherms from a monolayer of crown ether based surfactants with radial symmetry. They do not, however, observe the phase behavior examined here.

Small angle X-ray scattering studies are in progress to determine the depth, in a model membrane system, of the terminal bromines for each of the monomer triester species. These studies, in collaboration with Professor Robert Stinson of The University of Guelph, should show different electron density profiles for the membrane depending on the presence of the triester.[6] Membranes containing the 11C monomer will possess relatively more electron density in the interior of the membrane than the corresponding 6C monomer if they orient as expected.

Figure A3.2: The molecular structures, a) and b), represent the two possible triester ring orientations possible at the aqueous interface in a monolayer experiment. Only conformation a) can undergo the equatorial to axial transition without submerging the cyclohexane ring in the aqueous phase. The hydrocarbon tails are represented by the symbol R.

a

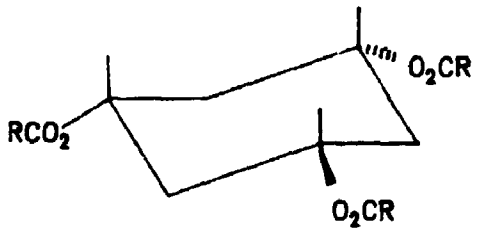

b

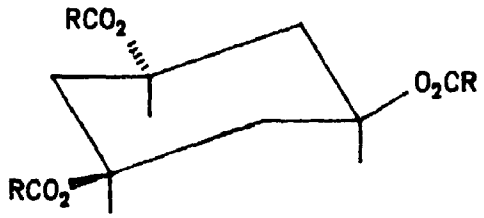

A3.5 Conclusion

The novel structure of our triesters suggests several new avenues of fruitful investigation. There is also, however, clear relevance to the diffusion measurements discussed in the body of this thesis.

While the terminal bromine triesters examined here do not form stable monolayers, they possess the triester headgroup in common with the stearic acid derivative. Information on the headgroup area of the stearic acid triester may be used for the other lipids as well. The bilayer 'equivalent' surface pressure in a monolayer is approximately 50 mN/m.[7] The collapse pressure of the monolayer (23 mN/m) is less than this figure. The collapse pressure, however, is a measure of the collective instability of the monolayer, not the orientation of individual molecules. The collapse pressure for long chain triglycerides in the liquid state (14 mN/m)[8] and α-tocopherol (23 mN/m)[9] are both less than the 'equivalent' bilayer pressure, yet they are known to incorporate into phospholipid bilayers with their polar head groups near the aqueous interface.[10,11] Similar results are anticipated for our triester probes.

At the 'bil yer equivalent pressure' the triester will be forced to undergo the equatorial to axial transition. Therefore the close packed area of our triesters in the bilayer will be approximately 60 $Å^2$ per molecule. This is approximately the close packed area assigned to phospholipids (65 $Å^2$ per molecule) in a bilayer.[3,7]

The triesters considered here are surfactants and will orient in the bilayer. Energetic considerations alone suggest this. The surface tension of a liquid crystal phase bilayer has been estimated to be

18 mN/m.[7] The free energy penalty for opening a void of 60 $Å^2$ in such a bilayer may be approximated by the product of the surface tension and the area. The free energy is approximately 6.5 kcal/mole. Although the calculation neglects the line tension of the void, this is roughly a factor of ten less than the free energy penalty for submerging the triester headgroup of a triglyceride in the hydrocarbon portion of a bilayer.[12] The similarity, discussed in Chapter Four, between triglycerides and our triesters suggest this is probably an accurate estimate for our triesters as well, and they will therefore orient in a bilayer. Similar considerations apply for the dimer and tetramer moieties.

REFERENCES

(1) Dick, Harold, Ph. D. Dissertation, The University of Western Ontario, 1988.

(2) Small, D. M. *The Physical Chemistry of Lipids*; Plenum: New York, 1986; p 73.

(3) Cadenhead, D. A. In *Structure and Properties of Cell Membranes*; Benga, G., Ed.; CRC Press: Boca Raton, FL, 1985; Vol. 3, pp 21, 62.

(4) Cantor, R. S. *Langmuir* **1986**, *2*, 331.

(5) Malthete, J.; Poupinet, D.; Vilanove, R.; Lehn, J. M. *J. Chem. Soc. Chem. Commun.* **1989**, 1016.

(6) Katsaras, J.; Stinson, R. H. *Biophys. J.* **1990**, *57*, 649.

(7) Nagle, J. F. *Ann. Rev. Phys. Chem.* **1980**, *31*, 157.

(8) Small, D. M. *The Physical Chemistry of Lipids*; Plenum: New York, 1986; p 374.

(9) Weitzel, G.; Fretzdorff, A. M.; Heller, S. *Hoppe-Seylers Z. Physiol. Chem.* **1956**, *303*, 14.

(10) Hamilton, J. A.; Small, D. M. *Proc. Natl. Acad. Sci.* **1981**, *78*, 6878.

(11) Aranda, F. J.; Coutinho, A.; Berberan-Santos, M. N.; Prieto, M. J.; Gomez-Fernandez, J. C. *Biochim. Biophys. Acta* **1989**, *985*, 26.

(12) Tanford, C. *Biochem. Soc. Trans.* **1987**, *15*, 1s.